ACSNANO
www.acsnano.org
REVIEW

High-Yield Functional Molecular Electronic Devices

Hyunhak Jeong,[†] Dongku Kim,[†] Dong Xiang,[‡] and Takhee Lee*[,†]

[†]Department of Physics and Astronomy, and Institute of Applied Physics, Seoul National University, Seoul 08826, Korea

[‡]Key Laboratory of Optical Information Science and Technology, Institute of Modern Optics, College of Electronic Information and Optical Engineering, Nankai University, Tianjin 300071, China

ABSTRACT: An ultimate goal of molecular electronics, which seeks to incorporate molecular components into electronic circuit units, is to generate functional molecular electronic devices using individual or ensemble molecules to fulfill the increasing technical demands of the miniaturization of traditional silicon-based electronics. This review article presents a summary of recent efforts to pursue this ultimate aim, covering the development of reliable device platforms for high-yield ensemble molecular junctions and their utilization in functional molecular electronic devices, in which distinctive electronic functionalities are observed due to the functional molecules. In addition, other aspects pertaining to the practical application of molecular devices such as manufacturing compatibility with existing complementary metal-oxide-semiconductor technology, their integration, and flexible device applications are also discussed. These advances may contribute to a deeper understanding of charge transport characteristics through functional molecular junctions and provide a desirable roadmap for future practical molecular electronics applications.

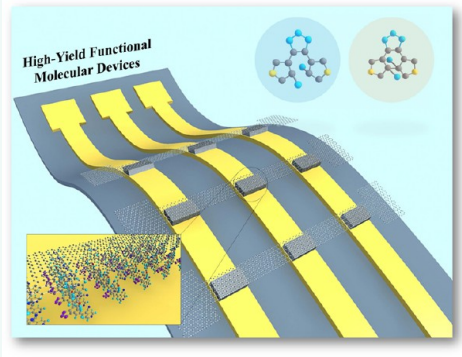

KEYWORDS: *molecular junction, functional molecular device, high device yield, charge transport characterization, self-assembled monolayer, molecular diode, molecular switch, molecular memory, flexible device*

The history of molecular electronics is generally considered to have begun with Aviram and Ratner with their early theoretical research entitled "Molecular Rectifiers" in 1974.[1] The thrilling aspect of this study was that even a single molecule, when rationally designed to resemble its silicon-based device counterpart, can exhibit preferential electronic function in the form of a two-terminal wire junction. Since then, the development of self-assembled monolayers (SAMs) and various experimental tools for investigating charge transport characteristics through molecules has been pursued.[2−6] Indeed, molecular electronics is still an active research field because it not only provides an ideal window for exploring the intrinsic properties of materials at the molecular level but also may fulfill the increasing technical demands of the miniaturization of traditional silicon-based electronics.[7]

The concept of making an ultimately downscaled single molecule device, based on numerous degrees of freedom inherent in molecular structure, has potential for the future of next-generation electrical circuit units. Instead of utilizing the single molecules for an active device component, SAMs can be incorporated into the molecular junction, while the functionalities are still exhibited in the molecular structure, using an autonomous self-assembly of molecules. The SAMs are deposited by molecules in solution, which attach themselves to a specific substrate with an anchoring group, generating a densely packed molecular monolayer.[5] The interesting nature of material self-assembly at the molecular level offers, in principle, numerous potential advantages. First, ultimately downscaling molecule size to the atomic scale may enable faster performance and high integration density with fewer heat issues. Second, the molecules' autonomous self-assembly process may reduce manufacturing production costs. Third, the great diversity of molecular structures may lead to the emergence of distinctive functionalities typically not accessible in traditional materials or approaches. These merits form a fundamental basis for attracting interdisciplinary interests to the field of molecular electronics as a promising candidate for alternative electronics, extending Moore's law beyond the foreseen limits.

For the development of this emerging technology, the fundamental physics governing the basis of charge transport must be thoroughly investigated to make significant progress. For this purpose, alkanethiolates, adopted from a pioneering study by Mann and Kuhn,[8] become a standard benchmark for various experimental testbeds in molecular electronics.[5,9−14] The alkanethiolate SAMs are known to form a well-ordered,

Received: April 29, 2017
Accepted: June 4, 2017
Published: June 4, 2017

DOI: 10.1021/acsnano.7b02967
ACS Nano 2017, 11, 6511−6548

Table 1. Summary of Fabrication Techniques for Ensemble Molecular Junctions

techniques	difficulty of fabrication	yield[a]	possibility of a massive production	ref
nanopore	straightforward	low	applicable	38
microscale *via* hole	straightforward	low	applicable	46
nanoparticles bridged	sophisticated	medium[b]	applicable	58
crosswire	sophisticated	medium[b]	inappropriate	64
liquid metal	straightforward	medium to high[b]	inappropriate	75
eutectic gallium−indium	straightforward	high	inappropriate	90
conducting polymer interlayer	straightforward	high	applicable	100, 101
carbon-based materials interlayer	straightforward	high	applicable	102, 103, 120
nanotransfer imprint	straightforward	medium[b]	applicable	142
direct metal transfer	straightforward	medium to high	applicable	153
microfluidic channel	straightforward	high	applicable	155
surface diffusion-mediated deposition	sophisticated	high	applicable	160

[a]The standards of ranges of the device yield correspond to >70%, 20−70%, and <20% for high, medium, and low, respectively. [b]We speculated the device yield by considering difficulty and addressability of each device fabrication method.

densely packed molecular layer on a metal electrode. In addition, due to a large highest occupied molecular orbital−lowest unoccupied molecular orbital (HOMO−LUMO) gap of approximately 8−10 eV,[15,16] these molecules can be regarded as insulating molecules. Consequently, the main transport mechanism is coherent tunneling, in which the tunneling current decreases exponentially as molecular length increases. Although these molecules contain no special electronic functionality in their molecular structure that can be applied to practical applications, they provide a fundamental basis for understanding the underlying physics in molecular charge transport.

In the meantime, several major issues regarding ultimately downscaled molecular junctions were observed, especially in terms of junction reliability and device yield. A primary obstacle in the development of molecular electronics is the lack of an accurate understanding of intrinsic molecular properties in the active electronic channels. Recently, various types of intrinsic molecular properties such as the change of chemical bonding, the redox process, photo- or charge-induced conformational change, and phase transition in molecular electronic devices have been widely investigated to better understand the charge transport characteristics across molecules.[17−24] However, these types of intrinsic molecular properties in molecular junctions are still under debate due to the difficulty in precise characterization. This is mainly due to the absence of reliable, high-yield device platforms for testing molecular junctions that exhibit the distinctive and intrinsic functional properties of their component molecules. The issue represents a long-standing challenge for the advancement of molecular electronics as a viable technology for practical applications.

In this context, various reliable and high-yield device platforms, especially for ensemble molecular junctions, have been recently proposed by many research groups. Because of these bodies of research, the genuine charge transport characteristics of molecular junctions can now be rigorously examined based on a statistically significant amount of collected electrical data. Furthermore, with functional molecules containing the desired functionality in the molecular structure, active research on high-yield functional molecular devices seeking a potential application for practical devices has been ongoing. Although it remains a distant goal, achieving commercially available molecular electronics is the subject of accelerated, intriguing research.

In this article, we review recent experimental efforts for pursuing high-yield functional molecular devices, in which a bundle of molecules (the contacted molecules number more than ∼1000) is contained in a junction. Several excellent reviews of the active field of molecular electronics are available pertaining to single molecule junctions or ensemble molecular junctions.[7,25−34] In contrast, the overarching aim of this review article is to provide an overview of diverse experimental efforts for realizing the practical devices of the ensemble molecular junctions apart from single molecule junctions, in which distinctive electrical features are observed with high device yield. To do so, we first summarize in detail a number of different approaches for achieving high-yield ensemble molecular junctions and discuss the practical applicability and suitability as a reliable practical device platform. To provide a thorough review and comparison, traditional testbeds for the ensemble molecular junction, which usually lead to low device yield, are also mentioned. We then address primary advances in building functional molecular devices with desired functionalities based on the high-yield molecular junction platforms with programmed functional molecules. For example, the potential applications of molecular diodes, photoswitching devices, memory and optoelectronic devices are highlighted. With those functionalities, other considerations for real-life applications such as devices on flexible substrates and integration of the devices are discussed, aspects often neglected in previous reviews. Finally, at the end of the review, we note the key issues critical to the success of the next-generation high-yield functional molecular device. The overview aims to provide a better understanding of the current status of the rapid progress in the field of molecular electronics for the realization of commercially available functional molecular devices, which might be of crucial importance for the development of alternative electronics.

APPROACHES TO THE REALIZATION OF HIGH-YIELD MOLECULAR ELECTRONIC JUNCTIONS

In the field of molecular electronics, extensive research has been performed to achieve reliable molecular junctions due to the fundamental difficulty of fabrication resulting from the ultimate scale of a molecule. Each approach to the realization of a reliable molecular junction can be distinguished primarily depending on how many molecules can be characterized in the junction, and these approaches have their own advantages as well as disadvantages. For instance, although a few molecular

DOI: 10.1021/acsnano.7b02967
ACS Nano 2017, 11, 6511−6548

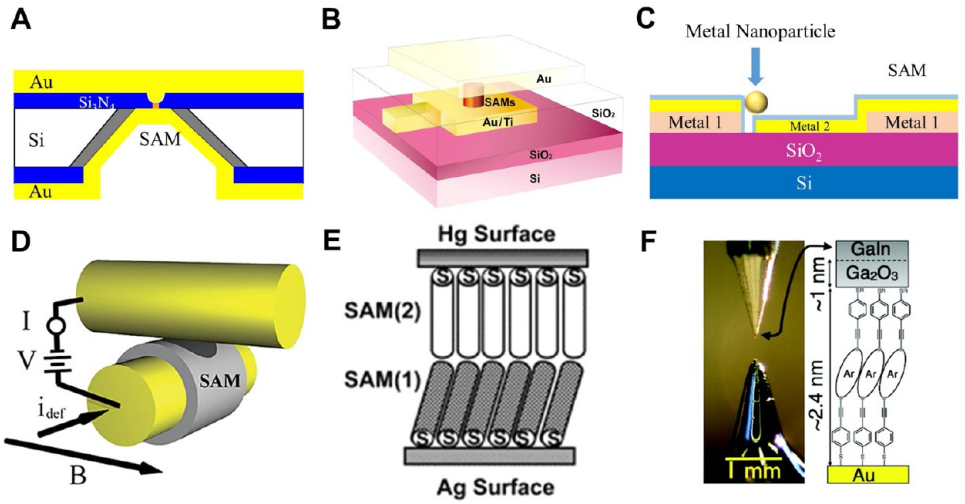

Figure 1. Examples of ensemble molecular junction platforms. (A) Nanopore. Reproduced with permission from ref 38. Copyright 2003, American Physical Society. (B) Microscale *via* hole. Reproduced with permission from ref 46. Copyright 2007, American Physical Society. (C) Nanoparticles bridged. (D) Crosswire. Reproduced with permission from ref 64. Copyright 2003, American Chemical Society. (E) Hg liquid metal. Reproduced with permission from ref 75. Copyright 2002, American Chemical Society. (F) Eutectic gallium–indium based. Reproduced with permission from ref 90. Copyright 2011, American Chemical Society.

junction techniques, including the fabrication of a single molecule junction, can provide a platform for characterizing electronic properties of an individual molecule, it is a laborious task to utilize those techniques for practical application because these junctions are usually very delicate and show a low device yield. However, ensemble molecular junctions (the contacted molecules are more than ~1000) based on SAMs show a relatively better device yield and can be used for practical applications based on a solid-state device platform. In this context, first we will discuss the development of various techniques for achieving ensemble molecular junctions in terms of the possibility of practical applications, for example, the device yield and manufacturability of a massive production based on a solid-state device platform. Table 1 depicts the summary of the typical methods, which will be mentioned in this section.

General Experimental Testbeds for Ensemble Molecular Junctions. To manifest the electronic transport characteristics of ensemble molecular junctions, two-terminal junction structures based on a metal–molecule–metal architecture have been widely adapted.[2−6] Especially in early days, many research groups have focused on a fundamental understanding of the electronic properties of molecules based on architecture rather than practical device application as a field of alternative electronics. Therefore, various techniques for fabricating ensemble molecular junctions have been proposed in many studies, but they were not suitable for practical applications due to extrinsic obstacles such as (i) low device yield, (ii) difficulty related to the fabrication of junctions (mostly due to poor addressability of molecules into gap electrodes), and (iii) low applicability for a massively parallel production of devices based on conventional lithography techniques such as the solid-state device platform. The schematics of these kinds of junctions are shown in Figure 1. Here, we will discuss these techniques from the perspective of potential device application.

Introducing an atomically thin molecular layer, which exhibits the transport characteristics of an active device component, into gap electrodes is a very challenging task due to the ultimate scale of the molecules. When SAMs of interest are deposited on metal-bottom electrodes, a prime way to sandwich the SAMs between two metallic contacts is the direct evaporation of metal electrodes. Nanopore and microscale *via* hole techniques adopt this simple principle incorporated with a solid-state device platform based on conventional lithography. Figure 1A,B shows schematics of each method. The Tour group first introduced the ensemble molecular junctions employing the nanopore and microscale *via* hole techniques.[35−37] The creation of a nanopore junction is performed in an insulating material like SiO_2 or Si_3N_4.[35,37−42] After deposition of the vertically structured insulation layer, the nanopore, in which the SAMs will be deposited, is created by local etching using electron beam lithography and plasma etching or a focused ion beam with a typical diameter between 30 and 60 nm. The remaining insulating membrane suspended over the substrate then acts as a window. By evaporating metal electrodes on both sides and depositing the SAMs on them, nanopore molecular junctions are obtained. All of the above steps can be performed using a conventional lithography-based solid-state device fabrication process. Therefore, this technique is a useful platform for massive production of the junctions and statistical determination of the intrinsic electronic transport characteristics.[35,37,43,44] In addition, the number of molecules in the junction, which is highly related to the electrical characteristics, is relatively well-defined because the junction size can be modulated accurately by a fine lithographic technique and confirmed using microscopic tools.[38,39] This reproducibility is one of the most important aspects for massive production of a device with uniform device performance. Similar to the nanopore strategy, the microscale *via* hole technique utilizes a direct metal evaporation method on bottom electrodes modified with SAMs.[45−48] The only difference between the two approaches is that the conventional photolithography technique is applied to define microscale *via* hole structures resulting in a larger junction size than the nanopore junctions. Therefore, this technique also provides the advantages of the nanopore method. Because of direct bombardment of the evaporated metal atoms with high kinetic energy on the SAMs, both techniques can induce mechanical damage, defects, or

DOI: 10.1021/acsnano.7b02967
ACS Nano 2017, 11, 6511−6548

even filamentary paths in the SAMs, resulting in poor device yield (~2%).[25,45,49−54] To resolve this critical problem for practical applications of the molecular junctions, various countermeasures have been proposed, for example, (i) cooling of the evaporator stage during which the substrate is mounted; (ii) release of most of the kinetic energy of the metal atoms in collisions with inert gas atoms while the substrate is facing away from the boat; and (iii) maintenance of a very low evaporation rate.[35−37,43,55] Despite these measures, improvement of the device yield has remained doubtful.

Instead of direct evaporation of the metal atoms on the molecular layer resulting in poor device yield, one can deposit the electrodes by generating soft contacts on the SAMs. Conceptually, this strategy involves a mechanical placement of preconfined electrodes on the molecular layer, which is free from atomic defects caused by the metal evaporation. One example of this strategy is the fabrication of nanoparticle-bridged molecular junctions. The conceptual schematic of this junction is depicted in Figure 1C. In this technique, a small gap between two metal electrodes is first fabricated using electromigration,[56] electron beam lithography,[57] or the angled metal evaporation method.[58] Self-assembly of the molecular layer is then performed on the electrodes. Additionally, by trapping the nanoparticles in the gap, an electrical pathway consisting of metal−SAMs−nanoparticles−SAMs−metal is generated. Here, several methods can be applied to trap the metal nanoparticles in the gap, for example, (i) the application of an AC electric field between the electrodes to pull in the nanoparticles;[57] (ii) the application of a local magnetic field to ferromagnetic nanobeads coated with metal;[59,60] or simply (iii) the dispersal of the nanoparticles from solution.[58] Because this technique excludes the direct metal evaporation process, the device yield can be improved compared with the techniques mentioned in the previous paragraph. In addition, the fabrication procedure is compatible with solid-state device fabrication processes. However, this technique may have several disadvantages in other aspects of device applications. First, precise control of the nanoparticles with a specific size and number at a well-defined location is quite challenging (*i.e.*, the number of molecules connected by the nanoparticles at each electrode is variable), such that the charge transport characteristics of each molecular junction fabricated in a batch may seriously differ. Second, because this technique involves the nanoparticles between each molecular layer on both electrodes, the junctions are actually a double junction, wherein the charge transport characteristics may greatly be affected by the physical properties of the nanoparticles.[56] These issues may hinder the molecular junction manufactured by the nanoparticle-bridged technique to create a viable platform for the practical application of molecular devices.

Another kind of soft contact method, evaporation-free on SAMs, is a crosswire technique. A schematic of the crosswire molecular junction is shown in Figure 1D. Because the fabrication technique utilizes externally prepared long metal wires as the electrodes and makes a soft contact on SAMs similar to the nanoparticle-bridged junctions, it can prevent the unfavorable potential of metal atom penetration or defects associated with the monolayer during the device fabrication process, which result in an improved device yield compared with metal-evaporated molecular junctions.[61] In detail, this technique consists of two 10 μm-diameter metal wires, one modified with SAMs of interest, mounted onto a stage with the wires in a crossed geometry and with one wire perpendicular to the applied magnetic field.[62−66] To control the junction separation, a small DC current (<5 mA) flows through the wire generating the Lorentz force in the magnetic field. The deflection current is then slowly increased to bring the wires together, forming a junction at the point contact. In this technique, various molecules, end groups, and metal wires can be incorporated because of the relative simplicity of the junction formation.[67] Furthermore, this technique enables the observation of a linear conductance scaling of molecules *via* the sensitive modulation of the number of contacted molecules varied by the deflection current.[64,68] However, exact control of the number of contacted molecules is hard to achieve, and the orientation of the SAMs on the wire is not well-defined because of the round curvature of the metal wire. This poor addressability of molecules may hinder a reliable and stable attainment of charge transport characteristics of the molecular junction ensemble when this technique is applied for molecular device fabrication. In addition, this technique is inadequate for massive production of the devices based on the solid-state device platform because of the requirement of the external magnetic field for the formation of the junctions despite the improved device yield compared with the metal evaporated molecular junctions.

Similar to the crosswire technique, the prevention of metal atom penetration or related defects in SAMs, which will improve the device yield, can be accomplished by the liquid metal contact. This technique takes advantage of the metal or alloy having a low melting point that enables mechanical manipulation of the top electrode *via* a soft contact on the bottom electrode modified with the SAMs. Among the candidate materials, Race *et al.* first introduced a clean mercury (Hg) drop modified with SAMs as the top and bottom electrodes.[69] Figure 1E depicts a schematic of the Hg−SAMs−SAMs−metal junctions. In their experiment, the Hg drop as a top electrode is suspended from an amalgamated copper rod that can be lowered by a micrometer screw to make contact with the substrates containing barium, cadmium, calcium, copper, and lead, on which the SAMs are formed on a microscope stage. This simple principle can be applied to generate the ensemble molecular junctions based on both the monolayer and the bilayer SAMs by preparing the bottom electrodes with various metals, semiconductors, and molecules.[70−79] There are several advantages of using the Hg drop as the electrodes.[76] First, because the liquid Hg drop has no structural features, such as edges, terraces, and pits, it is less likely to result in defects in the absorbed SAMs. Therefore, it can conform to the topography of solid surfaces, thus forming a conformal contact with SAMs on the surfaces. Second, this technique allows the exploration of the electrical properties of a wide range of organic/organometallic functionalities by diversifying the junction compounds. Finally, it is easy to assemble the junction over a large number of sites, which can generate several replicate experiments to collect a statistically large data set number. However, this technique also has some drawbacks.[76,80,81] First, Hg is toxic, having harmful effects on the health of the user. Second, the junction stability is unsatisfactory, especially under the applied bias required for the electrical measurements originating from the intrinsic properties of Hg itself: high vapor pressure, easy to electromigrate, changes in shape under the applied potential, and amalgamate with the bottom electrodes.[82−85] Thus, the junction yield is not dramatically improved compared with metal-evaporated junctions (<25%). Third, this technique

DOI: 10.1021/acsnano.7b02967
ACS Nano 2017, 11, 6511−6548

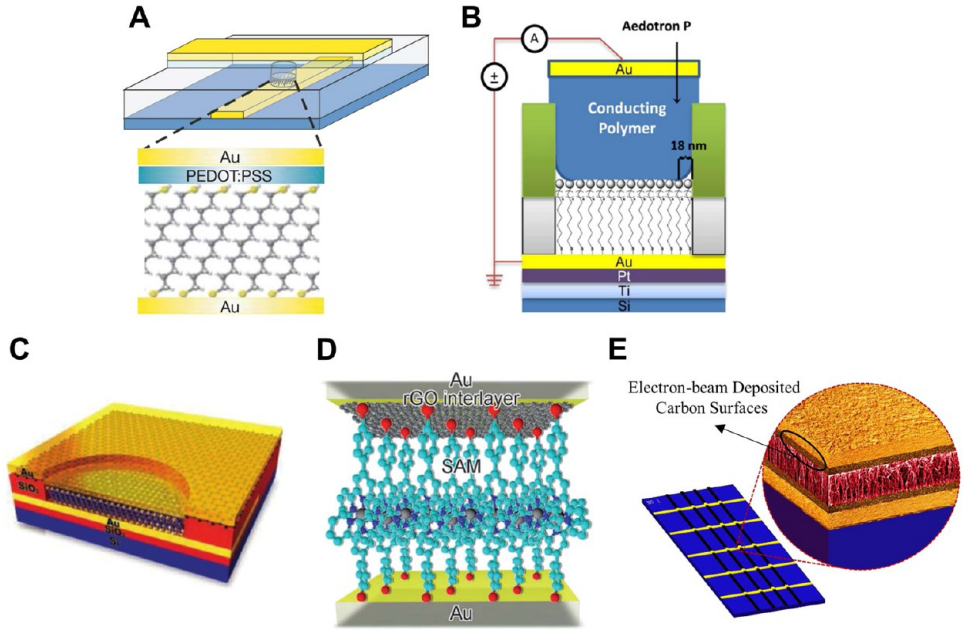

Figure 2. Approaches for high-yield solid-state-based ensemble molecular junctions; conducting interlayer-based junctions. (A) Conducting polymer PEDOT:PSS. Reproduced with permission from ref 100. Copyright 2006, Nature Publishing Group. (B) Conducting polymer Aedotron P. Reproduced with permission from ref 101. Copyright 2012, American Chemical Society. (C) Graphene. Reproduced with permission from ref 102. Copyright 2011, Wiley-VCH. (D) Reduced graphene oxide. Reproduced with permission from ref 120. Copyright 2012, Wiley-VCH. (E) Electron beam deposited carbon. Adapted with permission from ref 103. Copyright 2016, American Chemical Society.

requires external equipment such as a microscope, syringe, and micromanipulator for formation of the molecular junctions, and the measurements must be performed under a solvent bath, which is undesirable for functional molecular device applications.

Instead of Hg, stable and nonharmful liquid alloy electrodes may be beneficial to overcome the issues related to the above-mentioned Hg electrodes. Whitesides group initially introduced an idea consisting of conformal electrodes from non-Newtonian fluid metal,[86] eutectic gallium–indium (EGaIn), and their use for studying charge transport characteristics across ensemble molecular junctions.[81,87–89] Figure 1F shows a microscopic and schematic image of the EGaIn-based molecular junction. In this technique, an EGaIn drop suspended from the needle of a syringe was brought into contact with the bare Ag surface, and the syringe was then retracted slowly until the EGaIn bifurcated on each side into conical tips. Because the conical tip protruding from the needle did not retract into a semispherical droplet (as would Hg), the contact area can be considerably reduced. Finally, using the micromanipulator, the EGaIn tip is brought into contact with the SAMs. The Ga_2O_3 interlayer (1–2 nm), which is formed by oxidation of EGaIn on the surface, is beneficial for the stability of the molecular junction as a protective layer leading to a high device yield (<90%). Nevertheless, the resistance of the interlayer is estimated to be low, which is enough to characterize the electrical characteristics of the molecular junctions. Typically, incorporated with a template striped bottom electrode modified with SAMs, diverse physical and chemical characteristics in the molecular junctions have been investigated.[90–96] There are several advantages when EGaIn electrodes are used for the molecular junctions instead of Hg electrodes: (i) unlike Hg, EGaIn does not flow until it experiences a critical surface stress, (ii) makes conformal, nondamaging contacts at room temperature, (iii) can be molded into nonspherical shapes with micrometer-scale (or larger) dimensions, (iv) has a low vapor pressure, and (v) is nontoxic. In addition, the work function of EGaIn (4.1–4.2 eV) is close to that of Hg (4.5 eV), but EGaIn does not form an alloy with many metals.[97,98] Thus, EGaIn could be an ideal replacement for Hg. However, there are some disadvantages related to the technique, impeding its suitability as a junction platform for practical device applications, for example, (i) although EGaIn exhibits better material properties than Hg as an electrode, the fabrication method for the molecular junctions still requires external equipment like the Hg electrode-based technique; (ii) defining a reproducible junction size that determines the electrical characteristics of the junction remains uncertain; and (iii) the interfacial properties between the Ga_2O_3 layer and SAMs are ill-defined with respect to morphology and resistivity.[35–37] These disadvantages may hamper the viability of the liquid metal/alloy electrode technique for the practical application of molecule devices. It is noteworthy, however, that this technique can be improved with a distinctive approach designed to resolve some of these issues, which will be detailed in a later section.

As a promising future candidate of alternative electronics against conventional Si-based electronics, which approaches its scalable limit, the realization of high-yield and stable molecular junctions has been a long-standing challenge in the field of molecular electronics, and it is an essential prerequisite for practical device applications. Although enormous efforts have been made by many research groups to develop reliable testbeds for the investigation of the fundamental transport characteristics, mentioned above, some critical disadvantages of the techniques still hinder their utilization for practical device platforms. Therefore, in the following section, we will discuss high-yield ensemble molecular junction fabrication techniques that may overcome these obstacles and be applicable not only for examining the fundamental charge transport characteristics of molecular junctions but also potential device applications.

DOI: 10.1021/acsnano.7b02967
ACS Nano 2017, 11, 6511–6548

Realization of High-Yield Ensemble Molecular Junctions. As mentioned in the previous section, some of ensemble molecular junction fabrication techniques may be useful for investigating the electrical characteristics of the molecular layer, but they have the following limitations in terms of future device applications: (i) low device yield, (ii) junction fabrication difficulties, and (iii) low applicability for massive device production based on conventional lithography techniques like the solid-state device platform. In the following section, we will discuss alternative techniques for fabricating the molecular junctions that have been presented by various research groups to address these problems.

Interlayer Techniques. The low device yield problem of the metal-evaporated molecular junctions, which mostly resulted from metal atom penetration into the molecular layer, can be resolved by adhering to a simple idea: the introduction of a protective interlayer before evaporation of the top electrodes. Based on this strategy, various materials have been proposed for the interlayer, such as thin oxide,[99] conducting polymer,[100,101] and carbon-based materials.[102,103]

The schematics of the conducting polymer-based junction architectures are shown in Figure 2A,B. To our knowledge, the Boer group first introduced the conducting polymer interlayer technique to manufacture high-yield large-area molecular junctions.[26,100,104−106] In this technique, they basically followed a similar fabrication process for the microscale *via* hole technique except they incorporated a commercially available water-based suspension of poly(3,4-ethylenedioxythiophene) stabilized with poly(4-styrenesulfonic acid) (PEDOT:PSS) as a top electrode on the SAMs and used a photoresist matrix as an insulating wall. While depositing the PEDOT:PSS interlayer, the SAMs can be protected from the formation of a filamentary path or contaminants under ambient conditions because the layer can be spin-coated on them. Moreover, each grain size of the macromolecules of the PEDOT:PSS is too large to penetrate the densely packed molecular layer, and the difference in water affinity between the PEDOT:PSS layer and the backbone of the SAMs makes them microscopically repulsive.[26] Based on this structural stability, large-area molecular junctions could be fabricated with a junction size ranging from 10 to 100 μm. Additionally, the aging effect on molecular junctions was confirmed to be minimal for at least several months in air, and there was no visible degradation upon sweeping. Most importantly, a large collection of molecular junctions can be easily manufactured with standard integrated device fabrication processes with a yield of working devices of ∼100%. Using the PEDOT:PSS interlayer technique, the possibility of functional molecular electronic device applications, such as on the molecular diode photoswitching device, was investigated both on rigid and flexible substrates.[107−110] The details concerning these applications will be discussed in later sections.

Figure 2B shows a device schematic of an 1% poly(3,4-ethylenedioxythiophene)-*block*-poly(ethylene glycol) (Aedotron P) interlayer-based molecular junction.[101] Using this technique, they modified the fabrication process proposed by Boer group by replacing the photoresistant insulating layer with an inorganic dielectric (alumina and silicon nitride), which was deposited using conformal coating methods and the PEDOT:PSS interlayer with a commercially available Aedotron P dispersed in an organic solvent. The particular Aedotron blend is a block copolymer of PEDOT and polyethylene glycol dissolved in nitromethane and doped with *p*-toluene sulfonate. Although the Aedotron P interlayer shows higher resistivity than PEDOT:PSS, submicrometer scaling of the molecular junctions was possible because of the better wetting properties and low viscosity of nitromethane on a conformal inorganic insulating wall. These properties allow the deposition of the interlayer into pores as small as 100 nm in diameter and 50 nm deep. This aggressive scaling of the junction fabrication technique to the limits of conventional lithographic methods may enable the realization of high-yield, low variation-integrated molecular junctions. Nevertheless, some issues regarding the use of the conducting polymer interlayer contact remain to be addressed. (i) The interface characteristics between the interlayer and SAMs are not fully understood. Moreover, the interlayer may dominate the charge transport characteristics in the junctions, especially when the resistivity of the interlayer is comparable with that of the molecular layer.[26,100,101,106,111] (ii) The intrinsic material properties of the conducting layer may limit the variety use of species of molecules due to their compatibility. Thus, there is still a plenty of room to improve the interlayer materials for the realization of robust ensemble molecular junctions.

Carbon-based materials ranging from activated carbons to carbon nanotubes and graphene have attracted a large amount of interest as the most promising electrodes because of their desirable physical and chemical properties. These properties include robust electronic transport characteristics, low cost, a variety of forms (powders, fibers, aerogels, composites, sheets, monoliths, and tubes, among others), ease of processability, a relatively inert electrochemistry, controllable porosity, and electrocatalytic active sites for a variety of redox reactions.[112−114] In particular, there have recently been comprehensive investigations of graphene in various research fields.[115,116] Among these, graphene is a two-dimensional array of carbon atoms arranged in a honeycomb lattice. Each carbon atom is sp^2-hybridized and is bound to its three neighbors.[115,116] Especially because of its outstanding material properties such as high conductivity, transparency, chemical stability, and mechanical strength, graphene is considered a future candidate for optoelectronic device applications.[117,118] Regarding high-yield molecular junctions, Wang *et al.* first suggested the use of the multilayer graphene electrode for manufacturing high-yield ensemble molecular junctions. In their study, they transferred a multilayer graphene sheet, synthesized by chemical vapor deposition on a Ni substrate, onto the SAMs as the buffer layer instead of spin coating the conducting polymer, as shown in Figure 2C.[102] The prepared multilayer graphene films produce a typical sheet resistance of ∼600 Ω/sq and a transmittance of ∼90% in the visible wavelength range. After the transfer of the multilayer graphene sheet on SAMs, a metal layer was evaporated on top of the graphene films to reduce the contact resistance of the graphene films during electrical probing. Using this graphene interlayer before the deposition of the top metal electrodes prevents the formation of filamentary paths that result in a low device yield. In this case, the device yield have been found to be > ∼90%, regardless of the properties of the isolating layer and contact groups (hydrophobic *vs* hydrophilic). Compared with earlier conducting polymer-based molecular devices, graphene interlayer-based devices may have potential advantages in terms of better charge transport characteristics due to a low contact resistance with a wide range of variable molecular lengths and different contacts. In particular, the demonstrated graphene interlayer-based molecular junctions show good durability,

DOI: 10.1021/acsnano.7b02967
ACS Nano 2017, 11, 6511−6548

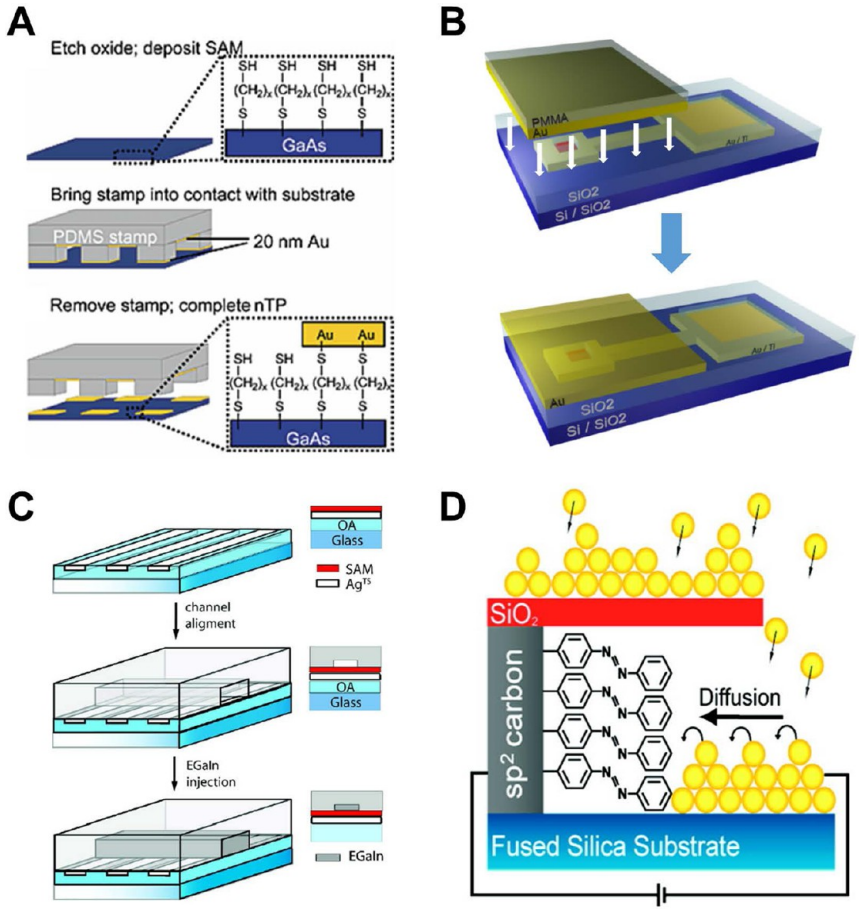

Figure 3. Approaches for high-yield solid-state-based ensemble molecular junctions; distinctive fabrication techniques. (A) Nanotransfer imprint. Reproduced with permission from ref 142. Copyright 2003, American Chemical Society. (B) Direct metal transfer. Reproduced with permission ref 153. Copyright 2015, IOP Publishing. (C) PDMS-based microfluidic channel. Reproduced with permission from ref 155. Copyright 2010, American Chemical Society. (D) Surface diffusion-mediated deposition. Reproduced with permission from ref 160. Copyright 2011, American Chemical Society.

thermal and operational stability, and device lifetimes, all of which are crucial for the practical application of molecular devices. Based on these type of molecular junctions, inelastic electron tunneling spectroscopy measurements have been performed to observe the vibrational modes of molecules even on flexible substrates.[119]

One disadvantage of graphene interlayer-based molecular junctions is that the prepared graphene film should be transferred onto the SAMs using a mechanical method because graphene is atomically thin and chemically stable. To resolve this issue, the use as the top layer of reduced graphene oxide (rGO), which can be achieved from chemically exfoliated graphene oxide (GO), has been suggested.[108,109,120,121] GO consists of atomically thin flakes of oxidized graphite that is dispersible in various solutions and can produce dispersible rGO by chemical reduction.[122,123] The resistivity of the rGO is comparable to that of single-welled carbon nanotubes[124,125] and can be improved by thermal treatment.[126,127] Because rGO is dispersible in organic solvents compared with graphene, one advantage of the use of rGO as electrodes is solution processability. For example, an rGO film electrode can be easily spin- and spray-coated directly onto a substrate or generated by vapor reduction of spin-coated GO film.[128,129] Seo *et al.* first introduced the use of rGO as an interlayer electrode in molecular junctions, as shown in Figure 2D.[120] In their study, they prepared the solvent-dispersed rGO sheets by reduction of GO sheets dispersed in water using a chemical reduction process. The conductivity of the rGO film was approximately 7600 ± 200 S/m, having much higher conductivities than that of highly doped PEDOT:PSS. After the formation of the rGO interlayer by a spin-coating process onto the SAMs-modified gold bottom electrodes, gold top electrodes were evaporated onto the rGO film at a low deposition rate. It has been demonstrated that there is no hysteresis or electrical short conduction in the current−voltage characteristics, indicating a high-device yield (>99%). In addition, the fabricated molecular junctions exhibited no noticeable degradation under vacuum conditions for 30 days. Not only the high device yield but also the good stability and accessible processability of rGO interlayer-based molecular junctions enable this fabrication technique to be applicable for functional molecular electronic device applications. For example, there have been various rGO-based functional molecular device applications even on flexible substrates, such as a nonvolatile memory, photoswitching device.[108,109,121]

Other uses of sp^2-hybridized carbon material family members for molecular junctions, such as pyrolyzed photoresist films (PPF) and electron-beam deposited carbon films (eC), have been introduced by McCreery group.[103,130−135] PPF is disordered and partially graphitic carbon with a relatively low

DOI: 10.1021/acsnano.7b02967
ACS Nano 2017, 11, 6511−6548

resistivity (~0.006 Ω cm) that is prepared by pyrolyzing patterned photoresistant stripes under a reducing atmosphere (5% H_2 and 95% N_2) at 1000 °C for 1 h.[130,136,137] This material is patternable by photolithography, which is thermally stable, and it is not subject to electromigration-like metals. Additionally, electrochemical reduction of diazonium reagents on PPF provides an irreversible bond of the molecular layers to sp^2 carbon surfaces with a C−C bond,[103,138,139] and the surface of PPF is flat, with a root-mean-square (rms) roughness value similar to that of the substrate upon which it is formed. However, PPF has a relatively poor conductivity (~200 S/cm) compared with graphene or conducting polymers, and the requirement for slow pyrolysis at an extremely high temperature in forming gas is not readily amenable for use as the buffer interlayer for molecular junctions because the buffer layer is usually generated after the deposition of the molecular layer. Therefore, the high conductivity and partial transparency of thin metal films must be combined with the flatness and surface modification chemistry of PPF while also avoiding high-temperature processing. Instead of PPF, eC has been described previously for conducting the carbon interlayer, resulting in a partially transparent electrode. Figure 2E shows a schematic image of the molecular junctions using eC interlayer electrodes. To fabricate the molecular junctions, patterned bottom electrodes composed of Cr, Au, and eC are first vapor deposited on the substrate using a shadow mask. The target source for the eC layer is high purity graphite, and the deposition rates are kept low, resulting in highly smooth surface morphology. The SAMs of molecules with diazonium moiety can then be deposited on the eC layer by electrochemical reduction of the corresponding diazonium ions retaining a covalent C−C bond. Subsequently, the eC buffer interlayer and Au top electrodes are e-beam evaporated in one vacuum cycle. The 10 nm-thick eC films have sheet resistances of 10^4−10^5 Ω/sq, yielding resistivities of 0.03−0.16 Ω cm, which is similar to that reported for the 300 nm-thick film.[140] Based on the electrical characterization of the fabricated Cr/Au/eC-SAMs//eC/Au junctions, a top contact of the eC interlayer yields molecular junctions with a high yield (>90%), good reproducibility, a long cycle life (>10^9 scans), and a wide temperature tolerance (6−600 K). Additionally, the resulting molecular junctions are compatible with conventional semiconductor device fabrication technology for massively parallel production with high device yield and excellent stability, while avoiding the high temperatures and material-transfer steps often required for graphene-based molecular junction designs.

Distinctive Fabrication Techniques. Despite the improved device yield and several advantages of interlayer-incorporated molecular junctions using various distinctive materials as mentioned above, no possible variation of the top electrode materials may restrict the manifestation of diverse molecular functionalities due to the limited interactions between the molecular layer and top electrode. In addition, no in-depth investigations of the contact properties between the SAMs and interlayer have been conducted to provide an unambiguous understanding of the charge transport characteristics of the molecular junctions. In this section, therefore, we will discuss other high-yield ensemble molecular junction fabrication techniques that can resolve the issues without the use of buffer interlayers.

Nanotransfer imprint technology where a thin metal layer is transferred from elastomeric stamps like poly(dimethylsiloxane) (PDMS) onto a designated surface[141] was first introduced by Loo *et al.* for fabricating large-area molecular junctions.[142] This technique depends on the surface chemistry of the designated target surface, to which the thin metal layer on the stamp bonds chemically and releases it from the stamp.[143,144] Thus, it results in well-defined and highly reproducible nanostructures with various contact areas. As shown in Figure 3A, the fabrication process is briefly described as follows: (i) SAMs are formed by vapor deposition on the GaAs surface, on which the native oxide layer is etched away using chemical etchants; (ii) a gold-coated elastomeric PDMS stamp with appropriate relief features is brought into contact with the substrate, and the gold on the raised part of the PDMS stamp is bonded and transferred to the SAMs-coated GaAs; (iii) removal of the stamp from the substrate completes the printing process. Because the molecules chemically bind the gold patterns to the substrate, the patterns can be anchored permanently to the substrate. Since this technique involves the transfer of the thin metal electrode prepared in advance onto the designated SAMs, the resulting structures do not suffer from filamentary path formation, which results in a low device yield of the molecular junctions, as observed for the direct evaporation of metals on the SAMs.[145−148] In addition, due to chemical bonds between the transferred metal electrode and end group of the SAMs, the contact resistance usually exhibits lower values compared with the case of the physisorbed contact.[12,147,149] It is also possible to manifest distinctive charge transport characteristics obtained by diversifying the constituent materials of the molecular junction, for example, the molecular species and the bottom and top electrode. In another sense, simultaneous fabrication of the junctions with many different junction sizes and patterns is allowed based on solid-state device fabrication processes for profitable statistics of the obtained electrical data.[142] However, one challenge is how to precisely determine the number of molecules under study because the roughness of the top electrode may generate contact vacancies when they make contact.[150] More seriously, the partial deformation and degradation on the thick PDMS mold surfaces may cause poor contact properties, which may result in a low device yield.

Instead of using the molds, in which the removal of the stamps from the top electrode is affected by surface chemistry between the top electrode and SAMs, generation of the soft contact can be achieved without the molds but by using a sacrificial layer like a polymer, which can be washed away after junction formation as the support for the thin metal layer.[151−153] Thus, this technique, which is called direct metal-transfer or the polymer-assisted lift-off (PALO) method, possesses several advantages of the nanotransfer imprint technique, namely, parallel device fabrication, nanoscale-to-centimeter device sizes, high-quality metal films, and a nondamaging deposition. Figure 3B shows a schematic of the device fabrication procedure using this technique. The details of the procedure are similar to those of the nanotransfer imprint method because the main concept of the fabrication process is introducing mechanical placement of the thin metal top electrode onto the SAMs yielding the soft contact. Briefly, as the first step, the patterned top metal electrodes are first deposited onto a dummy substrate such as a silicon substrate. The poly(methyl methacrylate) (PMMA) or poly(styrene) is spin-coated onto the dummy substrate to support the metal electrodes, which can be damaged while the electrodes are detached from the substrate. After coating, the top metal electrodes with a thin polymer layer are detached from the

DOI: 10.1021/acsnano.7b02967
ACS Nano 2017, 11, 6511−6548

dummy substrate by immersing the film into an etchant. This etchant weakens the polymer−substrate adhesion. Then, the detached transfer film is gently rinsed with deionized water and applied onto the molecular layer to yield vertical metal−molecule−metal junctions. Finally, the remaining polymer layer is removed by dipping the samples in an organic solvent. The capillary action, resulting from the surface tension of liquid on which the transfer film is floated, enables the transfer film to intimately contact the molecular layer. To facilitate intimate contact between the top electrodes and the molecular layer without wrinkles on the electrode, the proper choice of the polymer layer for the buffer liquid with consideration of their interface energies is most important.[151] A common concern related to those nanotransfer imprint-based molecular junctions is the roughness of the transferred electrodes. In this regard, the surface morphology of the electrodes follows that of the dummy substrate, exhibiting an excellent morphology profile due to the detachment of the thin metal electrode from the smooth dummy substrate on which it was deposited.[151,153,154] Using this technique, many ensemble molecular junctions have been fabricated simultaneously with various ranges of contact areas. In addition, the junctions exhibit a high device yield (~70%) without the formation of short circuits or damaging the monolayer, providing good stability, durability, and device lifetime properties, which are important factors for the practical application of molecular devices. These advantages, together with the possibility of fabricating a large number of molecular junctions in parallel, allow for rigorous statistical investigations of the electrical characteristics of molecular junctions and their future applications.

Because the mold or sacrificial polymer layer on which the top electrode is deposited greatly influences the contact properties of the molecular junctions, establishing a reliable interface is a challenge that must be overcome to obtain reproducible molecular junctions fabricated using the above techniques. One possible solution for this issue would be the use of a liquid metal electrode, as we mentioned in the General Experimental Testbeds for Ensemble Molecular Junctions section. This technique takes advantage of the metal or alloy having a low meting point that enables mechanical manipulation of the top electrode as a soft contact, so the electrode has no structural features such as edges, terraces, and pits, and it is less likely to result in defects in the absorbed SAMs. In addition, it conforms to the topography of the contacted surfaces, thus forming an intimate contact with SAMs on the surfaces. For example, the Ga_2O_3/EGaIn electrode is beneficial for the stability of the molecular junction leading to high device yield. Nevertheless, this technique requires external equipment such as a microscope, syringe, and micromanipulator for the formation of molecular junctions, which is not practical for parallel manufacturing of the functional molecular devices. Additionally, they lack the encapsulation and addressability needed to operate in a pressure- and temperature-controlled chamber.[155] To overcome this shortcoming, Nijhuis group proposed a method to create solid-state-based molecular junction arrays using the Ga_2O_3/EGaIn electrode stabilized in microfluidic channels made with an elastomeric polymer (PDMS).[98,155−157] A microfluidic channel is based on capillaries that typically have lateral dimensions of 10−1000 μm, and a simple two-dimensional channel system can be used for many applications.[158] A schematic of the fabrication process for the microfluidic channel-based molecular junction structure is shown in Figure 3C. First, the pattern of Ag electrodes was fabricated using conventional photolithography. Using a UV-curable adhesive, they then affixed a glass substrate to the pattern of the Ag electrodes. The cured optical adhesive interacts strongly with the Ag and the glass support, but not with the wafer. The Ag/adhesive/glass composite was then cleaved from the wafer by applying a lateral force between the glass substrate and the wafer. Subsequently, a microfluidic channel in PDMS was aligned perpendicular to the Ag electrodes after the formation of the SAMs. Finally, the fabrication was completed by filling the microfluidic channels with Ga_2O_3/EGaIn electrodes. The advantage of this technique is that encapsulation of the top electrodes in PDMS eliminates the instabilities associated with micromanipulators (device yield was 70−90%) such as drift or vibrations and minimizes user-to-user variations in the details of the formation of the top electrode. Due to this stability, the obtained data show high precision and replicability. These features enable the study of the electrical characteristics of the junctions over a long period of time and the various range of temperatures from 160 to 297 K. Additionally, the cone-shaped tips of EGaIn electrodes can only be prepared one at a time per setup, while the microfluidic channel technique can be performed in parallel to fabricate large numbers of junctions.[98]

Another distinctive fabrication method for a high-yield ensemble molecular junction would be the surface diffusion-mediated deposition (SDMD) technique.[159,160] This technique involves remote diffusion-mediated deposition of the metal electrode onto the molecular layer, which leads to a horizontally aligned junction architecture. Due to the indirect deposition of one metal electrode, one can resolve the low device yield problem resulting from metal atom penetration or damage in the molecular layer when a metal electrode evaporation step is included in the fabrication process. The molecular junction structure based on the SDMD technique is illustrated schematically in Figure 3D. To fabricate the molecular junctions, first PPF or carbon films were established as the bottom electrode on thermally oxidized silicon wafers. As mentioned above, electrochemical reduction of diazonium reagents on the PPF/carbon film provides irreversible bonding of the molecular layers to sp^2 carbon surfaces with a C−C bond.[103,138,139] The surface of the PPF/carbon film is also flat, having a rms roughness value similar to that of the substrate upon which it is formed. After bottom electrode formation, a patterned SiO_2 mask layer, which will be utilized as a protective layer for some parts of the PPF film, was created on the PPF films. Then, the unprotected PPF film was etched by a reactive ion etch process to yield a nearly vertical sidewall of PPF film beneath the etching mask. On the vertically aligned sidewall of PPF film, the molecular layer was electrochemically deposited *via* the covalent C−C bond. Finally, angled deposition of the metal electrode on the molecular layer was optimized to create a soft contact by a metal atom diffusion process. The remote diffusion of metal atoms instead of direct evaporation reduces the risk of penetration and damage in the molecular layer, which leads to excellent device yield (>90%) and reproducibility of the molecular junctions. In addition, the conductance steps were readily observable because the electrical contact was controlled through surface diffusion of the metal atom on individual molecules one at a time, which allows characterization of a wide range of molecular junctions containing single/several molecules to bundle molecules. However, it is somewhat challenging to control the exact number of molecules in the junction because this technology depends on a remote

DOI: 10.1021/acsnano.7b02967
ACS Nano 2017, 11, 6511−6548

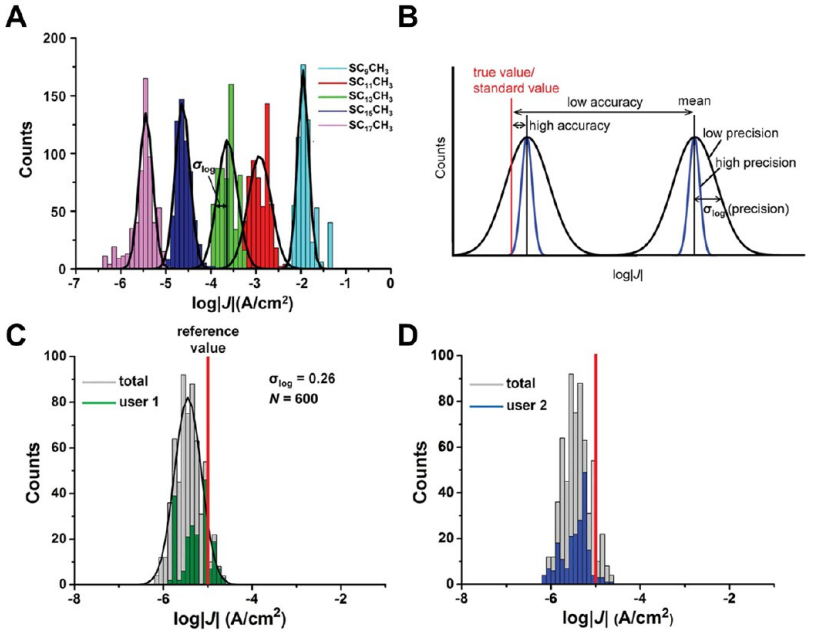

Figure 4. (A) Histograms of log|*J*| at −0.5 V for junctions with SAMs of alkanethiolates with Gaussian fits. (B) Schematic illustration of the definition of the accuracy and precision (σ_{log}) of the electrical measurements for SAM-based junctions. (C, D) Histograms of log|*J*| at −0.5 V for $SC_{17}CH_3$ obtained by two different users using microfluidic channel. Reproduced with permission from ref 98. Copyright 2014, Wiley-VCH.

diffusion process, the detailed physics of which are unknown. Additionally, possible choices of the molecule species may be limited because of the PPF bottom electrode surface. Nevertheless, the resulting molecular junctions are compatible with conventional semiconductor device fabrication technology for parallel production with high device yield and excellent reproducibility.

Statistical Analysis of High-Yield Molecular Junctions. Among various merits of fabricating high-yield molecular junctions using a solid-state device structure, one of the most remarkable advantages is the capability of mass production because the fabrication can be performed following conventional manufacturing processes. Mass production provides a statistically sufficient number of molecular devices for analysis, which enables us to distinguish the genuine transport characteristics of molecular junctions from uncertain electrical information.[45,46,98,102,156,161] Such a statistical investigation is especially beneficial to typical methods for electrical characterization of molecular electronic devices, for example, length/temperature variation, transition voltage spectroscopy (TVS), and inelastic electron tunneling spectroscopy (IETS).[110,152] Therefore, in this section, we present a review of the statistical analysis performed to characterize the charge transport properties of high-yield ensemble molecular junctions.

Figure 4A shows the statistical histograms of the values of log|*J*| for Ag^{TS}-SC_n//GaO_x/EGaIn molecular junctions with n = 10, 12, 14, 16, and 18. Generally, statistical histograms show populations of a certain characteristic in which groups of items are all related. In this case, current density J is measured to make generalizations about J for the Ag^{TS}-SC_n//GaO_x/EGaIn molecular junctions. The charge transport mechanism across SAMs of *n*-alkanethiolates is regarded as coherent tunneling,[10,162,163] and hole tunneling is theoretically more favorable than electron tunneling.[164] The rate of tunneling decreases exponentially with the width of the barrier (*i.e.*, the length of the molecule), is independent of temperature, and is usually approximated by a form of the Simmons eq (eq 1), where J_0 (A/cm^2) is a constant that depends on the system and includes contact resistance, d (Å) is the width of the tunneling barrier, and β (n_C^{-1} or Å^{-1}) is the decay constant.[165,166]

$$J = J_0 \exp(-\beta d) \quad (1)$$

These factors may have junction-to-junction variations depending on the detailed physics of a junction structure such as interface/contact properties and the impurity density in the molecular layer.[5,41,80,167−172] According to eq 1, for example, the values of log|*J*| are normally distributed when the variation in d is assumed to follow a normal distribution because J depends exponentially on d.[91,173] Thus, plotting the values of |*J*| on a log scale produces normal distributions of log|*J*|, which can be fitted as Gaussian curves by nonlinear least-squares fitting to all collected data as shown in Figure 4A. The extracted fitting parameters of each Gaussian curve, such as the log-mean, ⟨log|*J*|⟩, and the log-standard deviation, σ_{log}, can be roughly considered as representative parameters of the molecular junctions, drawing a distinction between informative and non-informative data. By determining the representative parameters, one can make generalizations about certain electrical characteristics of molecular junctions based on a specific test bed, in which measurement artifacts such as outliers may suppress the correct interpretation of charge transport properties. It should be noted that, however, the proper design of statistical tools for collecting data is critical to draw accurate conclusions from the data.[173] Based on the above method, statistical parameters in addition to J in high-yield molecular junctions can be analyzed by Gaussian fitting (*i.e.*, nonlinear least-squares fitting based on Gaussian curves) when the distribution can be assumed to be normal.[110,174,175] When adopting this statistical model, the precision of the data can be considered as the width of the distributions corresponding to the standard deviation of the Gaussian curve, and the accuracy can be considered as the closeness of the Gaussian mean value

DOI: 10.1021/acsnano.7b02967
ACS Nano 2017, 11, 6511−6548

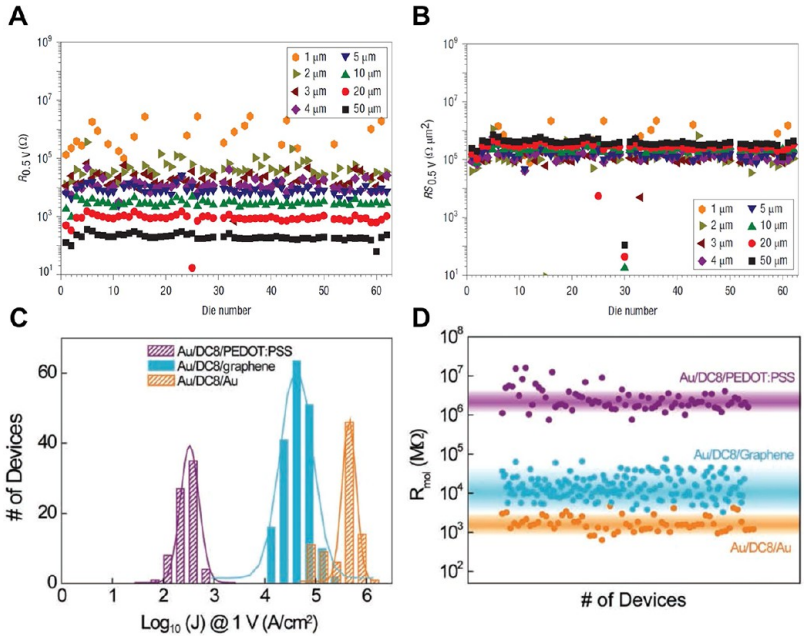

Figure 5. Statistical representation of molecular junction resistances. (A) Automatically measured resistances of $C_{18}H_{37}$-SH SAM junctions with diameter between 1 and 50 μm as a function of die number. (B) The normalized resistance (in $\Omega\ \mu m^2$) as a function of die number. Reproduced with permission from ref 106. Copyright 2008, Nature Publishing Group. (C) Histogram of logarithmic current densities at 1 V for working molecular devices according to the kind of top electrode (PEDOT:PSS, graphene, or Au). (D) The resistance per molecule R_{mol} values for these molecular junctions. Reproduced with permission from ref 102. Copyright 2011, Wiley-VCH.

of the distribution to a reference value, or standard value as shown in Figure 4B.[5,41,80,167−172] Thus, one way to compare different molecular junctions fabricated by various test beds is to compare the precision and accuracy of the statistical distributions from the electrical data. This principle can also be applied to determine the stability and easy applicability of the junction fabrication technique beyond the device yield by examining user-to-user correlations. For example, the Nijhuis group has shown that the stabilization of the EGaIn top electrode in microfluidic device minimizes the user-to-user variations in the formation of the top electrodes, the geometric area of the junctions, and the potential error associated with the vibrations and drift of the cone-shaped tip of EGaIn mounted on a micromanipulator as top electrodes resulting in precise data.[5,41,80,167−172] Figure 4C,D shows that both data sets have their log-mean value of J close to the reference value and that the precisions of both distributions are comparable.

One of the pursued virtues for high-yield molecular junctions with applicability as practical devices is replicability and reproducibility of the electrical data. From a large number of fabricated molecular junctions, each junction can show constant electrical characteristics if the test bed exhibits replicability and reproducibility. This characteristic is intimately related to high precision, which we mentioned above, but the standard deviation value that can be regarded as precision may be modulated depending on how the statistical model is applied, for example, a bin size of a histogram can affect the fitting parameters of a Gaussian curve.[176] Thus, instead of precision, inspecting all the electrical properties of each molecular junction is beneficial to determine the reproducibility of molecular junction test bed. Figure 5A,B shows a statistical representation of junction resistances from each device fabricated by PEDOT:PSS interlayer technique using alkanethiolates. The current density−voltage (J−V) characteristics have been measured for Au-alkanethiol//PEDOT:PSS/Au junctions C_nH_{2n+1}-SH with n = 8−22.[106] In the graphs of Figure 5A, the junction resistances at a low bias of $C_{18}H_{37}$-SH SAMs are presented as a function of the diameter and the die number. In a wafer, there were 62 identical die structures, and each die contained *via* hole-structured molecular junctions with diameters ranging from 1 to 50 μm, as indicated in the figure legend. The normalized resistances (in $\Omega\ \mu m^2$) are presented in Figure 5B. Excluding two dies, which were shorted due to an artifact of the automatic prober, most of dies showed a constant normalized resistance, exhibiting good reproducibility, and the device yield was almost uniform. Furthermore, the resistance which monotonically scales with contact area was as expected for a parallel ensemble of single molecule junctions. However, careful inspection of Figure 5A,B revealed a slight increase in resistance with the device area due to differences in the local electrical resistance varying over the junction.[106]

The most useful benefit of the statistical analysis is to characterize the electrical data that are informative and ignore data that are non-informative by using a proper statistical model to discriminate between the two. Therefore, to make a correct comparison of genuine electrical characteristics from each molecular junction fabricated by different fabrication methods, determination of representative electrical properties is pursued.[26,31,153,156] Figure 5C,D shows an example of a comparison of the electrical properties of molecular electronic devices produced with different top electrodes based on statistical analysis. In Figure 5C,D, the charge transport parameters (J and R_{mol}, *i.e.*, resistance per molecule) were compared for octanedithol (DC8) molecular junctions according to the different kinds of top electrode (PEDOT:PSS, graphene and Au) to demonstrate the quality of the contact properties of the graphene-based devices. In these comparisons, the authors observed that the resistance for Au/DC8/graphene was slightly higher than that for Au/DC8/Au devices by <1 order of magnitude (Figure 5D). This finding indicates that the

DOI: 10.1021/acsnano.7b02967
ACS Nano 2017, 11, 6511−6548

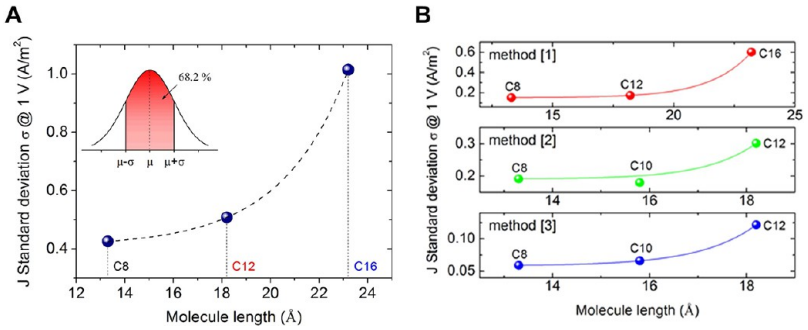

Figure 6. (A) A plot of the Gaussian standard deviation σ extracted from Gaussian fitting of the current density histograms *vs* the molecular length. Black dotted curve represents the exponential fitting results. (B) Plots of the Gaussian standard deviation σ for different device fabrication methods. Reproduced with permission from ref 179. Copyright 2016, IOP Publishing.

interfacial contact between graphene and DC8 was comparable to that between Au and DC8 (Figure 5C,D), unlike the relatively poor contact between DC8 and PEDOT:PSS with much higher resistance. This comparison can also be applied in different types of junction systems. For example, the authors observed that the R_{mol} (approximately 10 GΩ) for DC8// graphene devices was higher by 0.5−2 orders of magnitude than CP-AFM and STM measurements using the same molecular types, due to the unfavorable physisorbed contact between graphene layers and DC8 molecules.[10,26,147,177] However, the R_{mol} of the devices with PEDOT:PSS was observed[26,100] to be approximately 10^3 GΩ, which is much higher than the CP-AFM and STM measurements, by 3−5 orders of magnitude. Thus, it can be concluded that the graphene interlayer electrode may be a better candidate for ensemble molecular junctions in terms of the junction resistance because of the high vertical resistance of PEDOT:PSS itself.[178] This finding leads to difficulty in characterizing the charge transport through short molecular lengths (<2 nm) in the PEDOT:PSS-based molecular junction system because R_{mol} can be comparable to that of the PEDOT:PSS interlayer.[106] Therefore, the approach of graphene-based molecular electronic devices may be advantageous for characterizing a wider range of molecular systems.

In most cases, of statistical analysis, usually only statistically representative (*i.e.*, averaged) electrical characteristics were treated as crucial parameters, while the deviations (*i.e.*, precisions) of these characteristics from junction to junction did not attract particular attention except when determining the reproducibility of the molecular junction test bed. Nevertheless, because these deviations may stem from variations in the specific microscopic structures of the molecular layers, it can be worth investigating to gain insight into the structural states of the molecular layers for robust future electronic applications. Therefore, an investigation of the deviations in electrical characteristics by taking advantage of the high-yield junction would be beneficial for these purposes. Jeong *et al.* have performed this kind of statistical investigation using the high-yield molecular junctions fabricated by the direct metal-transfer technique.[179] In their experiment, they analyzed a large number (approximately 400) of molecular junctions, each composed of 128 junctions for octanethiol, dodecanethiol, and hexadecanethiol (C8, C12, and C16, respectively) alkanethiolate molecules. The working devices were defined and selected from all the devices based on the Gaussian distribution, and the representative $J-V$ characteristics could be derived in terms of statistically meaningful characteristics as we mentioned above. The authors also found that the degree of the distribution (the Gaussian standard deviation σ) of the logarithmic J values of each molecular junction around the statistical mean value (*i.e.*, the Gaussian mean μ) is dependent on the molecular length as shown in Figure 6A. Generally, this statistical distribution can be attributed to fluctuation factors that cause such a distribution of tunneling current densities in molecular junctions. For example, these factors can be unexpected variations (*i.e.*, fluctuations) in the molecular configurations of the molecular layers in the junction, such as the tilting angle of the SAMs on the bottom electrode, surface roughness of the bottom electrode, existence of defects or contaminants, and contact properties at the metal−electrode interface.[147,180−182] Note that such variations may stem from parameters that are controllable during the junction fabrication process, such as variations in the junction area; however, this type of fluctuation could be canceled out because all of the molecular junctions in that study were generated by single batch processes, *i.e.*, all the devices were created at the same time. Instead, variations in intrinsic parameters that are mostly uncontrollable in molecular junctions, for example, the tunneling pathway, are more likely to be the main causes of the fluctuations in the statistical distribution.[183] In their analysis, they attributed this fluctuations in the statistical distribution to the total conformational degrees of freedom of the molecules with different molecular lengths. The maximum energy of an individual molecule, for example, the alkanethiolates in their study, increases with the addition of each alkyl chain unit based on the repetitively connected spring model of a molecule in which the internal energy increases with the length d ($E \propto d^2$). Thus, the total conformational degrees of freedom of the molecule grow with the molecular length d due to the higher probability of various conformational states.[184] In this case, the molecule with a longer length can produce larger variations in the thickness of the molecular layer than shorter molecules due to intrinsic and extrinsic feature, for example, more likely incorporation of defects and contaminants in the molecular layer or substantial molecular deformation due to the thicker cross-sectional area and higher structural degrees of freedom. Therefore, the thickness (*i.e.*, the tunneling barrier width) of the molecular layer and thus the $J-V$ characteristics that depend on the thickness might be proportional to the molecular length. Based on this analysis, a similar tendency has been observed from the same types of molecular junctions fabricated by three different methods, as shown in Figure 6B.

Next, we will provide other examples of the statistical analysis of electrical characteristics obtained from high-yield ensemble molecular junctions. Figure 7A depicts the IETS data measured

DOI: 10.1021/acsnano.7b02967
ACS Nano 2017, 11, 6511−6548

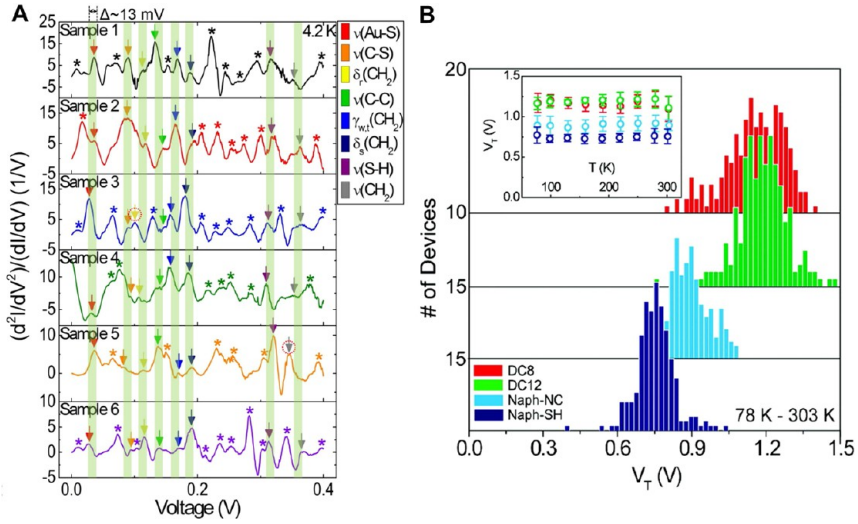

Figure 7. (A) IETS data of six C12 molecular junctions measured at 4.2 K. Each arrow indicates the corresponding molecular vibration modes of the C12 molecule. Peaks that cannot be assigned to any possible vibrational modes of the molecule are marked with asterisks. In this plot, shaded squares are used to compare each characteristic peak from device to device. Reproduced with permission from ref 152. Copyright 2015, American Physical Society. (B) Histograms of V_T data points for the DC8, DC12, Naph-NC, and Naph-SH molecular devices at 78−303 K. The insets show V_T *vs* T plots for the DC8, DC12, Naph-NC, and Naph-SH molecular devices. Reproduced with permission from ref 175. Copyright 2011, American Chemical Society.

at 4.2 K for the six C12 molecular junctions fabricated using the direct metal-transfer method. IETS, which is associated with the interaction between the tunneling charges through a small tunneling barrier and the specific molecular vibrational modes, is a primary characterization technique to identify the chemical species and provides the fingerprint information for the molecular junctions.[32,185,186] Because impurities (such as nanoparticles) in the junctions produce completely different IETS features compared to the target molecules, the IETS can provide an unambiguous determination tool for the molecular species in the molecular junction by investigating discrepancies in the signal.[152,187−189] In the study, the spectra were stable upon successive bias sweep, and the characteristic vibration peaks of the alkanethiolates were observed (shaded squares in Figure 7A) repetitively for different molecular junctions. In addition to these peaks, however, unexpected features in the IETS characteristics were also observed; some peaks could not be assigned to any possible molecular vibration modes (marked as asterisks in Figure 7A) and dips.[40,190,191] Additionally, the overall trajectories of each signal and normalized intensity of peaks ($(d^2I/dV^2)/(dI/dV)$) exhibited different behaviors from device to device despite having similar $J-V$ characteristics. In some cases, especially for ensemble molecular junctions, it is known that an incorporation of defects, such as metal nanoparticles, into molecular junctions can introduce a hybrid metal particle-molecule electronic resonance state that can result in substantial modification of the intensity and line shape of the IETS signal, such as negative values or dips.[187−189] The molecular conformations and contact geometry induced by the interaction between the electrode metal and molecular layer also play an important role in the substantial modification of the IETS characteristics.[192−194] Theoretical investigations based on the resonance model also predicted that depending on the energetic parameters of the system, the contribution from the elastic component may be negative and, furthermore, may outweigh the positive contribution of the inelastic component, resulting in dips in the IETS characteristics.[188,195] This is a second-order effect in electron-vibration coupling, which may be related to reabsorption of molecular vibration by the elastic current component.[196] In their study, defect-induced arbitrary changes in the molecular conformations in the SAMs of each molecular junction were attributed to the device-to-device variations of the IETS characteristics. This can be a typical example of the statistical investigation of the electrical characteristics obtained from high-yield molecular junctions.

As another example of the statistical analysis, Wang *et al.* have performed a statistical investigation regarding TVS. The TVS technique is a spectroscopic skill that can estimate the energy level alignment with respect to the Fermi levels (E_F) of the electrodes and the frontier molecular orbitals in the molecular junctions.[66] Based on the Fowler−Nordheim (F-N) tunneling model,[197] an inflection position in a plot of $\ln(I/V^2)$ *vs* $1/V$ (F-N plot), which can be indicated as a transition voltage (V_T), correlates to an effective barrier height (*i.e.*, $|E_F - (E_{HOMO}$ or $E_{LUMO})|$, where E_{HOMO} is the energy level of the highest occupied molecular orbital and E_{LUMO} is the energy level of the lowest unoccupied molecular orbital). This point can be considered a transition point from direct tunneling to F-N tunneling and is usually exhibited as a minimum point in the F-N plot. Therefore, it is the great advantage of the TVS technique to estimate the effective barrier height, which is of crucial importance for determining their electronic charge transport properties,[3,15,198,199] by simple modulation of the current−voltage characteristics of the molecular junctions. However, an important precedent for the actual application of the TVS technique is that the $J-V$ characteristics of the molecular junctions should not be noisy because the V_T corresponds to the local minimum point of the F-N plot. Thus, it would be beneficial to perform the statistical analysis on the TVS technique, especially when the $J-V$ characteristics are unstable. Figure 7B shows the statistical histograms of V_T values (total 883 data) for the four types of molecular junctions determined from $J-V$ data measured at different temperatures ranging from 78 to 303 K. The junctions were fabricated using the PEDOT:PSS interlayer, and each molecule consists octanedithol (DC8), dodecanedithiol (DC12), naphthalene-

DOI: 10.1021/acsnano.7b02967
ACS Nano 2017, 11, 6511−6548

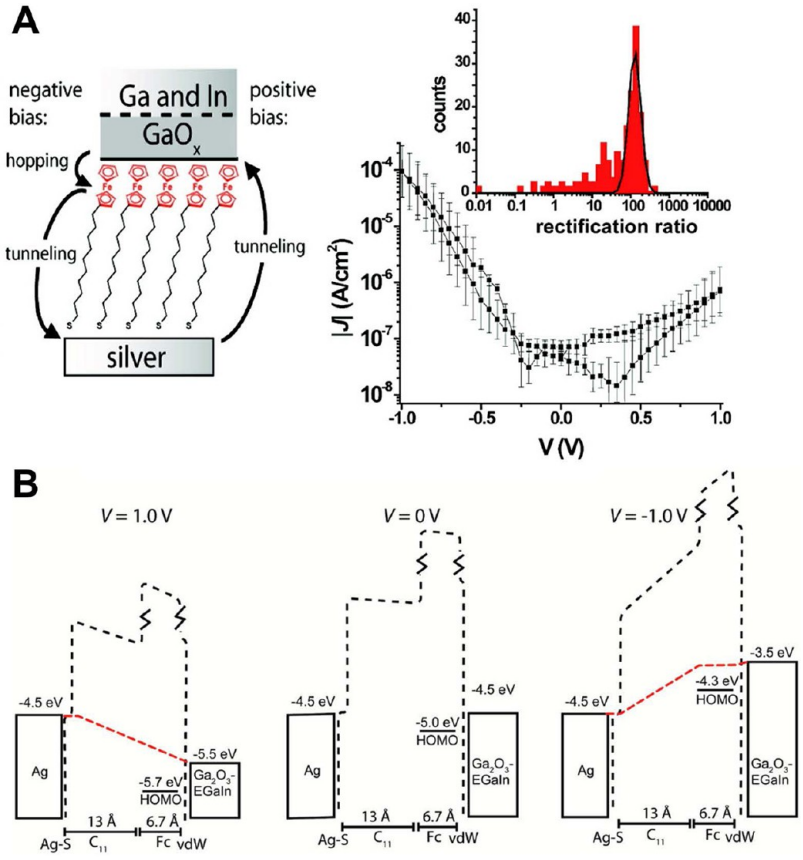

Figure 8. (A) Left: A schematic image of the molecular diode junction consist of Ag^{TS}-$SC_{11}Fc$//Ga_2O_3/EGaIn. Right: A semilog plot of the average absolute value of the current density *vs* the voltage of the junctions. The error bars indicate the log-standard deviation. Inset shows the histogram of the rectification ratios with a Gaussian fit to this histogram. Reproduced with permission from ref 155. Copyright 2010, American Chemical Society. (B) Proposed schematic representation of the energy level diagrams (with respect to vacuum) of the molecular junctions at +1.0 V (left), 0 V (middle), and −1.0 V (right) bias. The Ga_2O_3/EGaIn top electrode was biased. Reproduced with permission from ref 172. Copyright 2010, American Chemical Society.

isocyanide (Naph-NC), and naphthalene-thiol (Naph-SH). From the representative V_T values, it was found that V_T did not depend on the length of alkyl molecules based on the statistical analysis, which is in good agreement with previous experimental and theoretical results.[3,31,200] Additionally, more effective coupling between the HOMO level of oligoacene-SH and electronic energy states of the metal electrode was observed than that of oligoacene-NC as the smaller representative V_T value. This result was consistent with the report that the E_{HOMO} value of oligoacene-SH series lies closer to E_F of gold than that of the oligoacene-NC series by 0.7−1.3 eV based on ultraviolet photoelectron spectroscopy.[201]

HIGH-YIELD FUNCTIONAL MOLECULAR ELECTRONIC DEVICES

Molecular Diodes. The diode or rectifier, which conducts a much larger current in one biased polarity (forward) than the other (reverse), is one of key components in modern integrated electronic circuits. In conventional semiconductor-based electronics, this feature can usually be implemented by joining oppositely doped (p-type and n-type) semiconductors to each other.[197] The first theoretical proposal regarding the use of a single molecule as part of a molecular rectifier was introduced by Aviram and Ratner in the 1970s.[1] In their proposal, the basic principle to facilitate the rectifying features is borrowed from the conventional semiconductor diode, in which the organic molecule contains an electron-donating moiety (donor) and an electron-withdrawing moiety (acceptor) joined by the σ bridge that electrically separates each part. Since then, tremendous experimental efforts to realize the distinctive features in the two-terminal molecular junctions have been pursued.[94,132,172,202] Most of these studies have been conducted primarily on single molecule junctions for a deeper understanding of the charge transport characteristics of the molecular diodes rather than for practical applications. In addition to the experimental efforts, there were further theoretical investigations of the rectification mechanism in the molecular junctions that could be classified as three mechanisms, that is, the Aviram−Ratner[1] model, Kornilovitch−Bratkovsky−Williams[203] model, and Datta−Paulsson[204] model.[205] In this section, we review the development and progress of the molecular diodes that are realized by high-yield ensemble molecular junction fabrication techniques, as we mentioned above, and their applicability in terms of electronic circuit applications.

To date, the molecular rectification phenomenon in the two-terminal junction using the SAMs of molecules has been extensively studied by Whitesides and Nijhuis groups.[94,95,155,157,172,206] Figure 8 shows an example of their study of the molecular diodes. In their experiments, the junctions comprised SAMs of 11-(ferrocenyl)-1-undecanethiol ($SC_{11}Fc$) on the surface of template-stripped silver (Ag^{TS}) bottom electrodes, with eutectic liquid metal (EGaIn) top

DOI: 10.1021/acsnano.7b02967
ACS Nano 2017, 11, 6511−6548

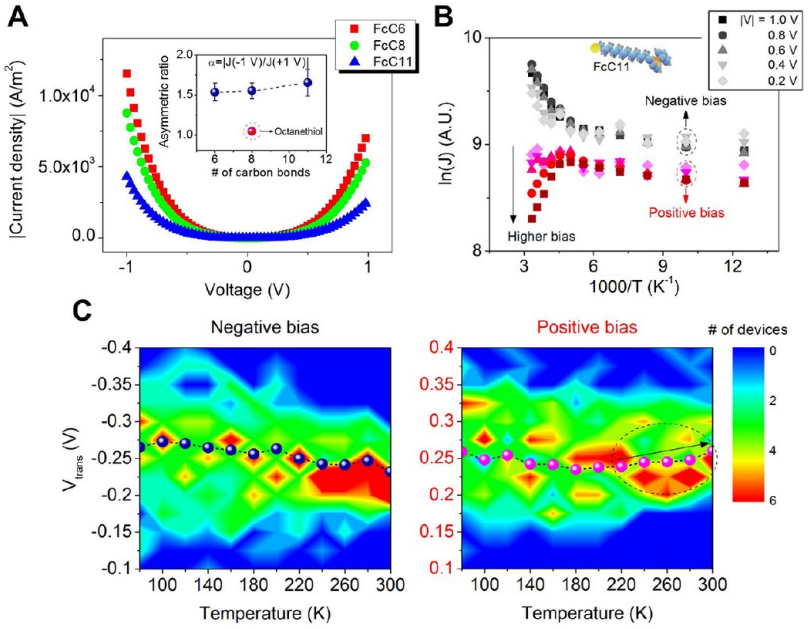

Figure 9. (A) Representative electrical characteristics of the FcC molecular devices. Inset shows the asymmetric ratio of the molecular junctions. The asymmetric ratio of a control junction using octanethiol was also depicted in the plot. (B) Normalized Arrhenius plots for an FcC11 molecular device under different applied voltages from ±0.2 to ±1.0 V with a ± 0.2 V interval at each voltage polarity. (C) Contour plots of statistical histograms of the V_{trans} values *vs* the temperatures at each voltage polarity. In the plots, the averaged values are depicted as data points and dotted lines. Reproduced with permission from ref 110. Copyright 2016, American Chemical Society.

electrodes stabilized in microfluidic channels in an elastomeric polymer (PDMS) for a high-yield molecular junction platform as shown in Figure 8A (left image). By using the microfluidic channels, they could construct arrays of SAMs-based molecular diodes that (i) are mechanically stable, (ii) do not incorporate direct metal deposition onto SAMs, (iii) do not require external equipment for measurements, and (iv) are relatively free from defects in SAMs.[80] The device yield of the junctions generated using this method was sufficiently high (70−90%), and the junctions rectified currents with large rectification ratios (R) of ∼130 were defined as

$$R = |J(-V)|/|J(+V)| \quad (2)$$

Figure 8B shows a semilog plot of the representative absolute value of the J *vs* V of the junctions, and the inset shows the histogram of the R with a Gaussian fit to this histogram. They used a procedure for the statistical analysis of the data (N = 300−800 obtained from two to five devices) in which all data were fitted to single Gaussian functions using a nonlinear least-squares fitting procedure to obtain the log-mean value of J for each measured potential and its log-standard deviation.[81] To interpret the molecular rectification, schematic illustrations of energy level diagram across the molecular junction are presented in Figure 8B. In all the experiments, the Ga_2O_3/EGaIn top electrode was biased, and the Ag^{TS} bottom electrode was grounded. The HOMO level of the ferrocene moiety (Fc) couples more strongly to the Ga_2O_3/EGaIn top electrode than to the Ag electrode since it is in close proximity to the former and separated from the latter by the SC_{11} group. At a negative bias, the Fermi level of the Ga_2O_3/EGaIn electrode increases, and, consequently, the HOMO level of the Fc rises into the window between the Fermi levels of the two electrodes (Figure 8B, right) and can participate in charge transport as a resonant tunneling state. At a positive bias, the Fermi level of the Ga_2O_3/EGaIn electrode decreases, and the HOMO level of the Fc falls with it (Figure 8B, left). Because the HOMO level remains below the Fermi levels of both electrodes, in the range of positive voltages applied, charges (holes or electrons) cannot classically flow through the HOMO. Instead, the charges must tunnel through not only the SC_{11} group but also the Fc. At a positive (reverse) bias, therefore, the width of the tunneling barrier increases by the length of the Fc over the width of the tunneling barrier at negative (forward) bias.[172] This mechanism can be generalized according to the Kornilovitch−Bratkovsky−Williams model, in which asymmetric tunneling barriers result in an asymmetric potential drop across the junction leading to the current rectification.[203] Since this pioneering realization of the ensemble molecular junction-based diode, there have been tremendous in-depth studies regarding the molecular diodes using the SC_{11}Fc molecular layer, for example, (i) the even−odd effect,[94] (ii) role of a binding group and purity of the precursors, and surface topology of bottom electrodes in the performance of molecular diodes,[95,207] and (iii) enhancement of the rectification ratio by rational design of the molecule.[208]

Using the SC_nFc molecules possessing structural and electronic asymmetry, another attempt to fabricate a large number of molecular didoes was undertaken by Jeong *et al.* using polymer interlayer-based microscale *via* hole junctions.[107,110] They facilitated the PEDOT:PSS layer with the SAMs of 6-ferrocenyl-1-hexanethiol, 8-ferrocenyl-1-octanethiol, and 11-ferrocenyl-1-undecanethiol (denoted as FcC6, FcC8, and FcC11, respectively, in their study) for ∼50 each molecular device to be analyzed, and the device yield was found to be ∼50%. The representative electrical characteristics of the molecular junctions are shown in Figure 9A, and the inset represents their asymmetric ratio (α, which equals the rectification ratio R). They found that the molecular devices also showed asymmetric electrical characteristics, as described the studies presented in the above paragraph; however, the representative α was found to be low, consistently ranging from

DOI: 10.1021/acsnano.7b02967
ACS Nano 2017, 11, 6511−6548

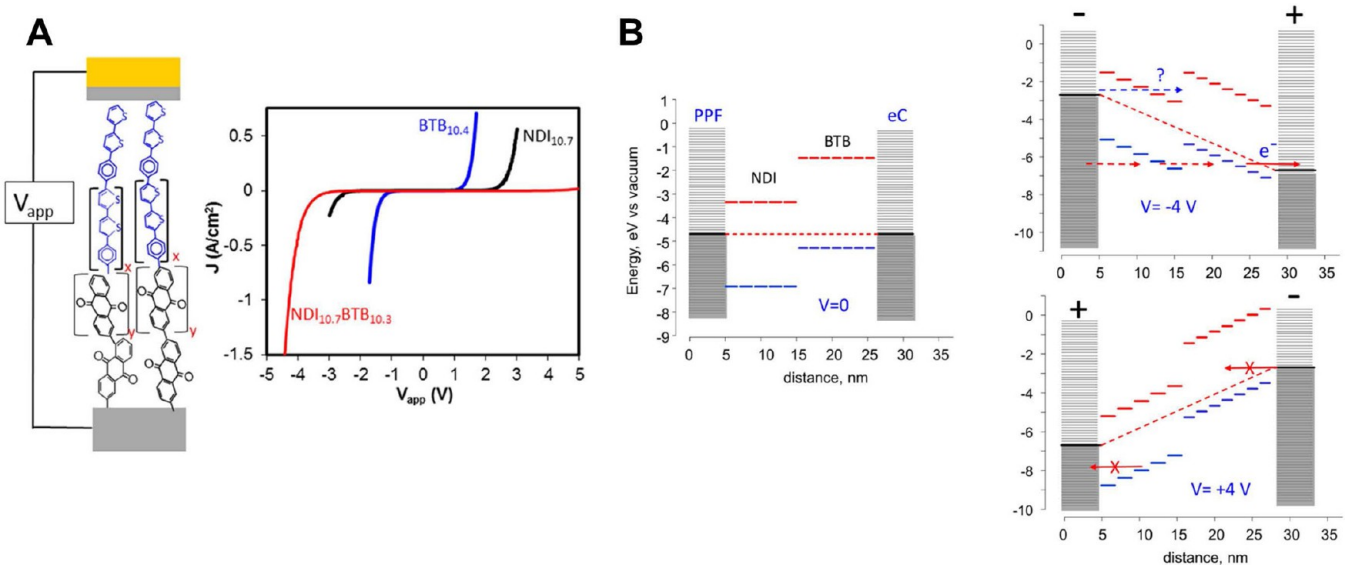

Figure 10. (A) Left: Schematic illustration of a bilayer molecular junction with an initial layer of anthraquinone (AQ) on pyrolyzed photoresist film (PPF), followed by a second layer of bis-thienyl benzene (BTB), and *x* and *y* indicate varying lengths of oligomers. Right: Current density *vs* bias voltage (*J*−*V*) curves of NDI/BTB, NDI-only, and BTB-only junctions. (B) Energy level diagram for a bilayer junction of five NDI molecules and seven BTB molecules, to approximate the $NDI_{10.7}BTB_{10.3}$ bilayer junction at zero bias (left panel), the same diagram with a −4 V bias (upper right panel), and +4 V bias (lower right panel), assuming a linear potential profile through the molecular layers. Arrows indicate possible electron transfers between contacts and molecular layers. Adapted with permission from ref 132. Copyright 2016, American Chemical Society.

∼1.6. The reason for the low α was attributed to the contribution of the HOMO of Fc to the tunneling transport in both voltage polarity regimes, resulting in similar current densities at each voltage polarity adopting the similar analysis method of Nijhuis *et al.* Therefore, it is crucial that careful engineering of the contact properties between the molecular layers and the electrodes be ensured to achieve a large number of molecular diodes with a high asymmetric ratio. However, an interesting temperature- and bias-dependent feature in the electrical characteristics was observed such that the *J* values decreased slightly for increasing temperatures over high temperatures (≥ ∼220 K) and a high bias voltage (≥ ∼0.6 V), as shown in Figure 9B. Normally, current through a molecular junction (or other types of junctions) is dependent on temperature in such a way that current increases with increasing temperature when thermionic conduction or defect-mediate conduction mechanisms are dominant.[5] The origin of this distinctive behavior was attributed to the redox-induced conformational changes in the ferrocene-alkanethiolate molecules.[94,209] To confirm the validity of the mechanisms, the authors performed a temperature-dependent TVS analysis based on a multibarrier tunneling model, as shown in Figure 9C.[46] In their analysis, two possible conformational changes of the ferrocene-alkanethiolate were confirmed as a barrier-raising effect of both the alkyl chain and Fc. This study suggested the significance of consideration of the macroscopic structural organization of the molecular junction as well as the intrinsic molecular properties to facilitate ferrocene-alkanethiolate-based molecular diodes.

Recently, McCreery group reported molecular rectification using a PPF-molecule//eC/Au high-yield molecular junction structure to examine molecular bilayers with thicknesses totaling more than 5 nm,[131,210] to introduce structural asymmetry into the molecular junction interior. The molecular bilayers using bis-thienyl benzene (BTB), 2-anthraquinone (AQ), fluorine (FL), nitroazobenzene (NAB), and a derivative of phenyl naphthalene di-imide (NDI) were deposited by successive electrochemical reduction of diazonium precursors on PPF bottom electrodes and an eC/Au top contact deposited on them as shown in the left panel of Figure 10A. Their corresponding *J*−*V* characteristics for molecular junctions containing only one molecular species are also shown in the right panel of Figure 10A in the case of ∼10.5 nm-thick films of BTB and NDI (the subscripts in the graph represent the thickness of each SAMs, and each film thickness corresponds to consecutively linked seven and five individual molecules of BTB and NDI, respectively). From the graph, it can be observed that curves for junctions containing only one molecular component are symmetric with respect to polarity. The graph also shows the *J*−*V* characteristics for a bilayer made by sequential electrochemical reduction of BTB and NDI diazonium precursors, yielding a thickness comparable to the sum of the two individual layers. The *J* decreases significantly for the thicker bilayer film but very asymmetrically with respect to polarity, for which the *R* increases from ∼82 at ±3.5 V to 190 at ±4.5 V for the NDI/BTB bilayer. To understand the mechanism underlying the effect of orbital energies on the *J*−*V* asymmetry, the energy band diagram was considered as shown in Figure 10B, which shows the Fermi levels and orbital energies for a NDI/BTB bilayer junction containing five NDI molecules and seven BTB molecules. The potential profile across the junction assumed to be the simplest case of a constant electric field across a dielectric material under bias is indicated as a dashed red line. As shown in the upper right panel of Figure 10B, the high electric field under bias (∼2 MV/cm for $V = -4$ V) is predicted to cause significant shifts in orbital energies due to the linear potential profile altering the local electrostatic potential of each molecule in the bilayer. Under a bias of −4 V (here, PPF is biased), the HOMO energies of molecules are raised close to the eC contact, and the

DOI: 10.1021/acsnano.7b02967
ACS Nano 2017, 11, 6511−6548

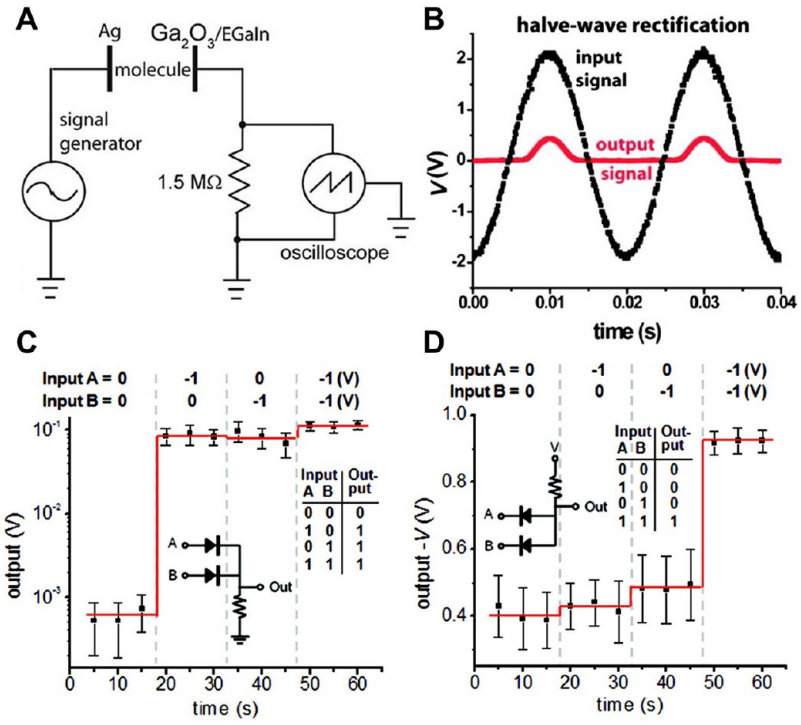

Figure 11. (A) A schematic illustration of Ag^{TS}-$SC_{11}Fc$//Ga_2O_3/EGaIn junction-based half-wave rectifier. (B) Sinusoidal input signals (V_{in}, black) with the corresponding output signal (V_{out}, red) of the half-wave rectifier circuit depicted in (A). Reproduced with permission from ref 206. Copyright 2011, American Chemical Society. (C, D) Schematic drawing of the electronic circuits and the experimentally measured truth tables for (C) OR and (D) AND logic gates formed by arrays of junctions with molecular diodes incorporated in the device. The inputs (A and B) are indicated at the top of the graphs. The red line is a guide to the eye for the measured output voltage. Insets show the configurations of the circuits and the measured truth tables. Reproduced with permission from ref 157. Copyright 2015, RSC Publishing.

charge transport is permitted from a HOMO into empty eC orbitals, as indicated by the solid red arrow in the upper right panel of Figure 10B. One possibility for continued transport is shown by the dashed red arrows, in which the current can flow fluently from PPF to eC through the molecular HOMOs. Meanwhile, the opposite bias of +4 V, as shown in the lower right panel of Figure 10B, indicates a very different situation such that electrons in the NDI HOMO cannot be transferred into the filled PPF orbitals nor can the electrons in eC reach the empty BTB orbitals, which results in weak current flow. Due to these different energy level alignment conditions under each bias polarity, large R values could be obtained in the molecular bilayer-based molecular junctions.

To date, the molecular diodes have mainly been studied with a focus on how to achieve reliable and stable molecular rectification rather than their possible applications. As an example of practical application of the molecular diodes, Figure 11 shows two examples of electronic circuit applications using SAMs with Fc termini-based molecular diodes, as studied by Nijhuis group. Figure 11A shows a schematic image of the molecular half-wave rectifier circuit with the molecular diode in series with a resistor (1.5 MΩ) and an AC signal generator. Here, molecular diodes with a form of Ag^{TS}-$SC_{11}Fc_m$//Ga_2O_3/EGaIn (m = 1 or 2) were used, and the top electrodes of cone-shaped tips were facilitated for high-yield ensemble molecular junctions. As mentioned in the previous section, the cone-shaped tips of Ga_2O_3/EGaIn usually require external equipment to complete the two-terminal junction structure, but they can be applied for the massive production of molecular devices by using different fabrication methods like microfluidic channel because of the robust stability and liquid alloy properties of Ga_2O_3/EGaIn top electrodes.[98,155] AC measurements have three advantages over DC measurements for investigating molecular rectification: (i) Using AC can minimize the formation of filaments by electromigration because electromigration of metal atoms may occur in high electrical fields.[211,212] (ii) Using AC makes it possible to collect data rapidly: recording a J−V curve by incrementally applying a DC bias usually takes several minutes, while recording the same curve with, for instance, an AC signal at 50 Hz takes 20 ms. (iii) Using AC makes it possible to incorporate a resistor in series with the molecular tunneling junction and effectively places an upper bound on the potential drop across the junction and protects against breakdown. Based on the AC measurements, the J−V characteristics of the half-wave rectifier using Ag^{TS}-$SC_{11}Fc$//Ga_2O_3/EGaIn molecular diodes are shown in Figure 11B. In the plot, the measured input voltage, V_{in} (black line; 50 Hz sinusoidal signal with a peak voltage of 2.1 V), and the corresponding measured output voltage across the 1.5 MΩ resistor, V_{out} (red line), are depicted. The V_{out} signal showed desirable half-wave rectification properties and was not detectably phase-shifted relative to V_{in}, but the values of V_{out} were significantly lower than the values of V_{in}. The proposed circuit application using molecular diodes, however, could not fulfill the robust characteristics of commercial inorganic diode-based circuits because of (i) low rectification, (ii) high internal resistance at a forward bias, (iii) a relatively short lifetime, and (iv) a small operational bias window. Nevertheless, this study offers the possibility of using functional molecular electronic junctions for practical circuit applications.

Another example of the implementation of molecular diodes for practical circuit applications is depicted in Figure 11C,D. In

DOI: 10.1021/acsnano.7b02967
ACS Nano 2017, 11, 6511−6548

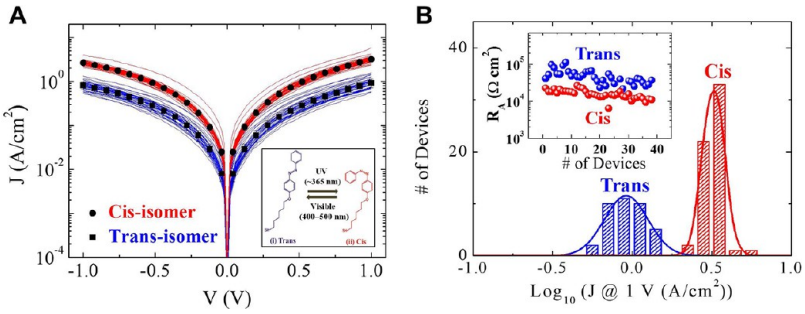

Figure 12. (A) *J*–*V* curves on a logarithmic scale for *trans*-isomer (blue) and *cis*-isomer (red). The symbols and error bars represent the average and standard deviation of the current density for all the measured devices (50 devices for each isomer case), respectively. Inset shows photoisomerization process of azobenzenethiolate used in the study. (B) A histogram of *J* at 1 V for the *trans*- and *cis*-isomers. The solid lines are Gaussian fitting curves. The inset shows the distribution of the resistance-area products (R_A) for the *trans*- and *cis*-isomers. Reproduced with permission from ref 161. Copyright 2011, Elsevier.

that study, they presented a technique to fabricate an EGaIn top electrode that generates arrays of SAMs-based junctions using a microfluidic PDMS channel with a device yield of ~80% and applied this technique to arrays of molecular diode-based logic. This method required no patterning of the bottom electrode and is compatible with ultraflat and clean template-stripped electrodes, which are readily available in ordinary laboratory conditions.[213,214] A Boolean function-based logic gate is used to perform a digital logic operation with one or more inputs and generates a single output and can be generated by utilizing diodes or transistors.[215−217] By using molecular diodes with arrays of (1-(3-(3′-ferrocenylpropyl)-diphenylacetylene))methanethiol ($HSCH_2PhCCPh(CH_2)_3Fc$) ensemble molecular junctions, two-input OR and AND logic gates were configured as shown in the insets of Figure 11C,D. Here, the authors applied DC voltages of 0 and −1 V as low and high inputs and measured the output as the voltage across a 10 MΩ resistor. Figure 11C shows the truth table of the OR gate measured experimentally representing a low output (logic 0) when both input voltages were low (0 V) and a high output (logic 1) when either or both of the input voltages were high (−1 V). This is because when one of the inputs was high, one of the diodes conducted and most of the voltage drop occurred across the constant resistor. Additionally, when both inputs were set to be high, both diodes allowed current to pass through the junctions, and the output voltage with two high inputs was the same as the one with only one high input voltage (logic 1) since the diodes were connected in parallel. The difference between the high and low state voltages was found to be around 2 orders of magnitude, reflecting the *R* of ~100. In the case of the AND gate, as shown in Figure 11D, a low output (logic 0) was observed when either one or both of the inputs were low (0 V), as indicated in the truth table. However, when both inputs were high (−1 V), both diodes were reverse-biased with resistances that were larger than the 10 MΩ resistor, causing a small voltage drop across the resistor and, hence, a high output voltage (logic 1). These examples show the potential applicability of high-yield functional molecular junctions for practical purposes.

Molecular Photoswitches. An electronic switch device, in which the conductance is controllably tuned on and off by external stimuli (*e.g.*, electric, magnetic field, light, or heat, among others), is a key component of modern computer circuits because the fundamental operation is based on digital processing. In recent years, a large amount of studies have been conducted to address the molecular switching phenomenon stimulated by electric field,[4,120,121,218−220] magnetic field,[221,222] photon,[24,161,223−229] or chemical processes.[230,231] To exploit this property, the molecules should have at least two stable isomer states between which transition is allowed. Molecular photoswitches exhibit such a switching phenomenon by using a photochromic molecule with a moiety that reacts with a specific light and changes the isomer states. In the following section, we will review the research on molecular photoswitching devices, which were performed based on functional SAMs and high-yield molecular junction fabrication techniques.

Among various photochromic molecules, azobenzene- and diarylethene-derivative molecules are the most frequently studied candidates for photoswitching molecular junctions. Azobenzene is composed of two phenyl rings linked by a N═N double bond, in which the photoisomerization of *trans* and *cis* isomers is possible when light of particular wavelengths is shed: ultraviolet light, which corresponds to the energy gap of the $\pi-\pi^*$ (S_2 state) transition, for *trans*-to-*cis* conversion, and blue light, which is equivalent to that of the $n-\pi^*$ (S_1 state) transition, for *cis*-to-*trans* isomerization.[232] Due to physical and chemical changes resulting from photoisomerization, the electronic characteristics of the azobenzene-derivatives may also change in response to light illumination. Kim *et al.* reported the conductance switching properties of azobenzene-derivative ((4-(phenylazo)phenoxy)hexane-1-thiol) molecular junctions in terms of their molecular configurations with a high-yield vertical junction structure as solid-state device platform. The junctions were fabricated using the PEDOT:PSS interlayer as a top electrode. These azobenzene-derivative molecules have two distinct isomers: a *trans*- (extended form) and a *cis*-isomer (compact form), depending on the wavelength of irradiating light (365/400−500 nm for *cis*/*trans*), as shown in the inset of Figure 12A. Generally, this kind of transition can be characterized by two distinct band peaks consisting of an intense band peak near 350 nm and a weak band peak between 400 and 450 nm in the UV−vis absorption spectrum.[233] In their research, they could observe a transition of the absorption spectra and water contact angle on the Au surface from each isomer state. Figure 12A shows the *J*–*V* characteristics of the molecular junctions of each isomer state. In each plot, the *J*–*V* curves for ~50 molecular junctions are depicted. The important point is that the representative current densities of the *cis*-isomer junctions were higher than those of the *trans*-isomer junctions. To identify this conductance difference numerically, statistical histograms of the logarithmic current densities (log *J*) at 1 V were plotted for both isomers, as shown in Figure 12B.

DOI: 10.1021/acsnano.7b02967
ACS Nano 2017, 11, 6511−6548

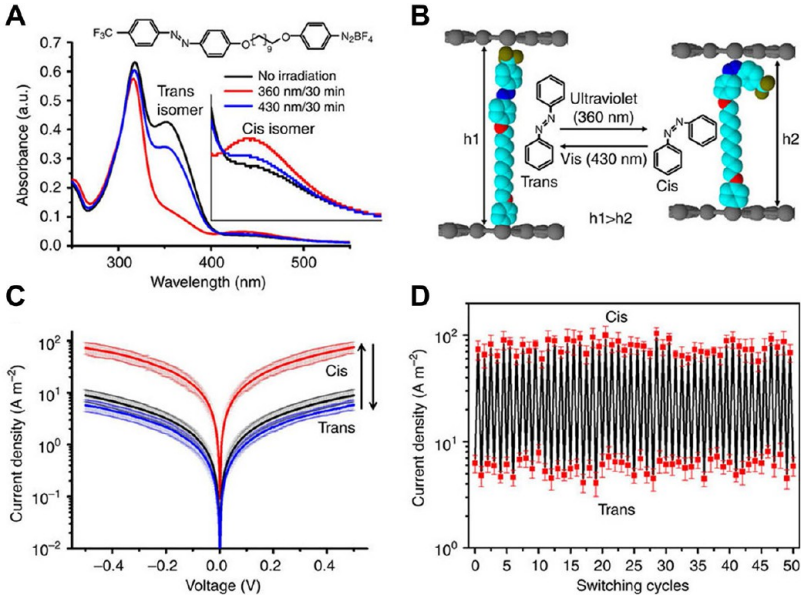

Figure 13. (A) Chemical structure of aryl azobenzene and UV−vis spectra in solution regarding ultraviolet/vis irradiation. Inset shows the zoomed-in spectra at a range from 400 to 550 nm. (B) Molecular tunneling barriers (with h1 and h2 being the vertical distance between the two graphene electrodes) corresponding to conformational changes in aryl azobenzene molecules with light irradiation. (C) Photoinduced current density−voltage plots on a log scale over a low-voltage range for the graphene-aryl azobenzene monolayer-graphene devices. (D) Current density plots for each isomer state over 50 cycles of reversible photoswitching (induced by ultraviolet/vis irradiation per 45 min); the plots were generated from average values obtained at 0.3 V from over five devices (the error bars denote the standard deviation values obtained from over 20 data points for each state). Reproduced with permission from ref 229. Copyright 2013, Nature Publishing Group.

From the histograms, the representative current densities were determined as the mean values of the Gaussian fittings of the histograms and were found to be 0.93 and 3.21 A/cm^2 for the *trans*-isomer and *cis*-isomer junctions, respectively. To elucidate the conductance switching phenomenon of the junctions, the authors performed a temperature-variable characterization and ultraviolet photoelectron spectroscopy (UPS) measurements. From the temperature-variable characterization, the overall conduction mechanism of each isomer junction was found to potentially be a direct tunneling-based phenomenon because there were no significant changes in the slopes of the Arrhenius curves as the temperature was varied.[38,165,166] They also observed no significant differences between the HOMO levels of the *trans*- and *cis*-isomers on an Au substrate based on the UPS measurements, which indicates that the main origin of the higher conductance of the *cis*-isomer may be the difference in the molecular tunneling distance resulting from the photoisomerization of the molecules.[226,227] In this study, however, the conductance switching phenomenon could not be observed through real-time light irradiation because the device was fabricated with a molecule with two isomer states that were predefined before top electrode deposition, and the top electrodes block efficient illumination of light onto the SAMs after junction formation.

Since the molecular photoswitching phenomenon occurs as a transition of isomer states based on photon energy, using a transparent substrate and electrode for the two-terminal molecular junctions such that light can be efficiently incident (*i.e.*, less absorbed or reflected) on the molecular layer may enhance the quantum efficiency of the devices. Among the candidate materials for this purpose, graphene electrodes may provide suitable characteristics for a chemically stable, optically transparent, mechanically flexible, and molecularly compatible junction. Graphene is allowed for the one-sided grafting of aryl diazonium molecules *via* a dediazonization process for sp^2 carbon network materials.[234,235] Figure 13A shows an example of aryl azobenzene-derivative with the diazonium moiety ((*E*)-4-(10-(4-((4-(trifluoromethyl)-phenyl)diazenyl)phenoxy)-decyloxy)benzenediazonium tetrafluoroborate; abbreviated as PhC10AB) and its UV−vis spectroscopy characteristics studied by Seo *et al.* Upon successive irradiation of light, the absorption spectra of the molecules in solution showed the transition near peaks of the wavelength for 360 and 430 nm as expected. The corresponding molecular junction structure, which was fabricated using graphene as top and bottom electrodes on a transparent plastic substrate, is schematically depicted in Figure 13B with *trans*-/*cis*-isomer conformations of the PhC10AB molecules. The fabricated molecular junctions depicted a high device yield due to soft contacts at the top electrode interface. Because the *cis*-isomer involves short-distance tunneling transport compared with the *trans*-isomer (h1 > h2 in Figure 13B), the *J*−*V* characteristics exhibited transition from the low-conductance state to high-conductance state under UV light irradiation, as shown in Figure 13C.[226,227] In addition, the reversible photoinduced conformational changes in the aryl azobenzene SAMs were repeatedly observed with the change in current density with respect to the switching number (Figure 13D). Over more than 50 cycles of reversible photoswitching, the two conductance states were stably obtained without significant degradation, indicating that highly stable photoswitchable molecular monolayer devices could be achieved using the graphene electrodes. In addition to photoinduced conductance switching, the authors found that applied voltages can induce the transition of two molecular conductance states of the aryl azobenzene SAMs in the junctions.[236,237] From these results, it is noted that making use of graphene electrodes, a compound that is transparent and highly conductive, enables the operation and transmission of photoinduced changes in the

DOI: 10.1021/acsnano.7b02967
ACS Nano 2017, 11, 6511−6548

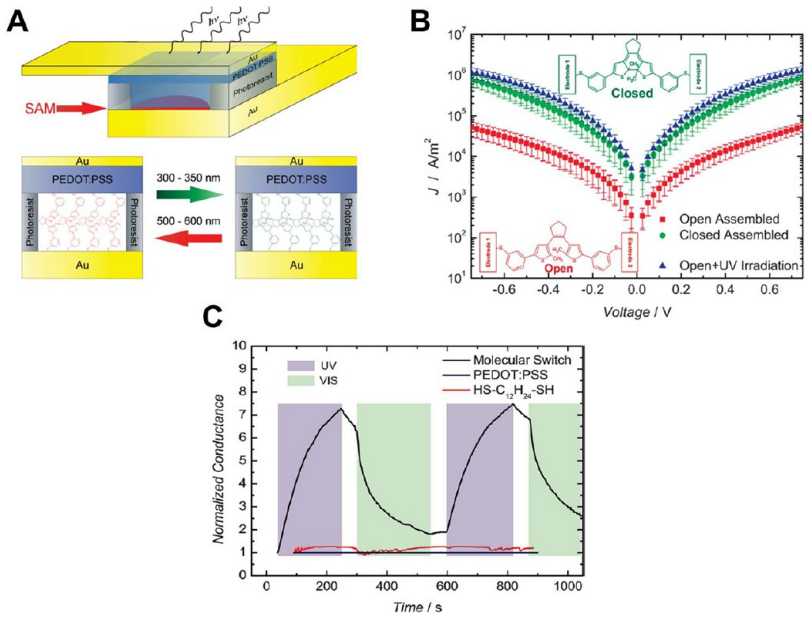

Figure 14. (A) Schematic cross-section of the device layout of a large-area molecular junction in which the diarylethene is sandwiched between Au and PEDOT:PSS/Au. Using UV (312 nm) illumination the open, nonconjugated isomer (in red) can be converted to the closed, conjugated isomer (in green). Visible irradiation of 532 nm reverses the photoisomerization process. (B) *J*−*V* characteristics of the closed (green) and open (red) isomers as self-assembled in the molecular junctions, and *J*−*V* characteristics of the junctions with the open isomer self-assembled and subsequently photoisomerized to the closed isomer with UV irradiation (blue). Averaged data (at least 35 devices) from devices with diameters of 10−100 μm. Error bars denote standard deviation. (C) Comparison of the normalized conductance data from the molecular diarylethene switches with *in situ* measurements on junctions with nonswitchable 1,12-dodecanedithiol and with PEDOT:PSS only. Reproduced with permission ref 24. Copyright 2008, Wiley-VCH.

molecular conformational length of aryl azobenzene-derivatives, which would be a suitable material choice for highly sensitive molecular photoswitch devices.

Another well-known class of photochromic molecules is diarylethene derivatives.[17,223,225,228] These molecular switches have two distinct isomers like the azobenzene-derivatives: the ring-closed form is conjugated, and the ring-open form is nonconjugated. The ring-closed form of the diarylethene derivatives is achieved under irradiation in the UV region (λ = 300−350 nm), and the ring-open form is under irradiation in the visible region (λ = 500−600 nm). It is expected that both isomers show different conductance because the conjugation is changed.[24,223−225,238,239] This is a somewhat different type of photoisomerization process compared with the azobenzene derivatives because the main origin of the different conductance for *trans*- and *cis*- isomers of azobenzene derivatives is usually attributed to the different tunneling distance. Figure 14A shows a schematic image of the diarylethene derivative (inset in Figure 14B) molecular photoswitch structure using PEDOT:PSS interlayers and the microscale *via* hole technique developed by Kronemeijer *et al.* This large-area molecular junction incorporated a 90 nm-thick PEDOT:PSS electrode, and an auxiliary semitransparent 20 nm-top gold contact was thermally evaporated onto the junctions, resulting in a high device yield. The 20 nm thickness of the gold top electrode ensured sufficient optical transmission through the layers of PEDOT:PSS (90 nm) and Au (20 nm) of approximately 20−50% in the 300−350 nm and 500−600 nm regimes, respectively, for illumination of the SAMs inside the devices. The as-assembled open (OFF) and closed (ON) forms determine the lower and higher limits of possible current density, respectively, as shown in Figure 14B. This different conductance is due to the lowering of a HOMO−LUMO gap when π-conjugation is extended (closed state) to the diarylethene derivatives.[24,223−225,238,239] Additionally, the *J*−*V* characteristics of the converted open-state isomer after UV irradiation from a closed-state isomer showed the conductance increase through the molecular layer, as expected from the as-assembled devices with a closed isomer state. To further elucidate the bidirectional switching, the authors performed multiple *in situ* illumination cycles as shown in Figure 14C. As can be observed in the plot, modulation of the current density through the devices by consecutive irradiation sequences was successfully demonstrated. As a control experiment, *in situ* measurements were also performed on devices without any molecular layer (Au/PEDOT:PSS/Au) and with 1,12-dodecanedithiol as the SAMs. Based on the results, there were no substantial changes in the conductance upon irradiation of these devices, indicating an absence of any form of photoconduction in these devices. However, the conductance in the high-conductance state was observed to slowly decrease after switching off the UV light, in contrast to devices with the assembled closed state. Based on the observation that an applied voltage may also induce molecular switching in addition to the light irradiation,[236,237] the decrease may arise from the presence of a constant voltage bias stress over the samples during these *in situ* measurements. The implementation of diarylethene-derivative-based molecular photoswitches processed by conventional fabrication techniques shows clear progress toward functional molecular electronic applications and circuit integration.

In the two-terminal vertical molecular junction structure, the reversible switching behavior of molecular photoswitches is often quenched for several reasons, such as (i) low transmittance of the top electrode layer, (ii) a strong electronic interaction between the SAMs and bottom electrode, and (iii) a

DOI: 10.1021/acsnano.7b02967
ACS Nano 2017, 11, 6511−6548

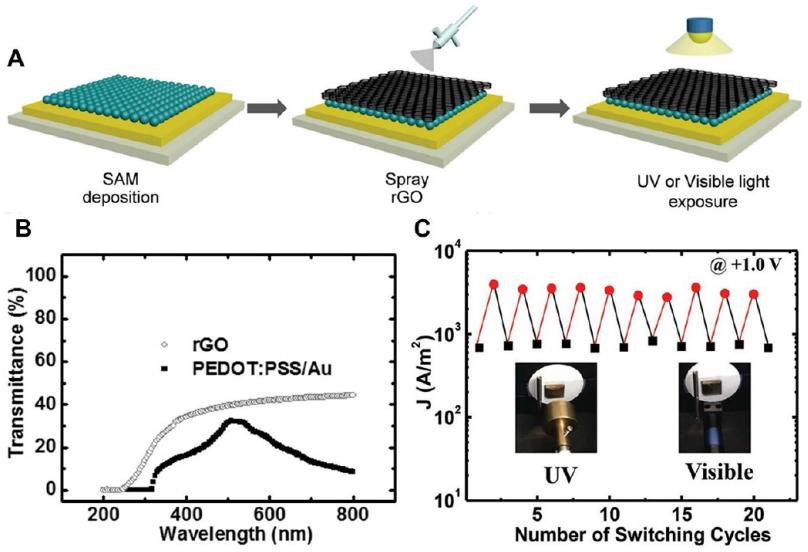

Figure 15. (A) Schematics illustrating the device fabrication processes for diarylethene-based photoswitching molecular devices with rGO top electrode. (B) The transmittance of rGO and PEDOT:PSS/Au films on glass substrates. (C) The reversible photoswitching phenomenon repeated 20 times by alternating UV and visible light irradiation. Reproduced with permission from ref 109. Copyright 2015, Wiley-VCH.

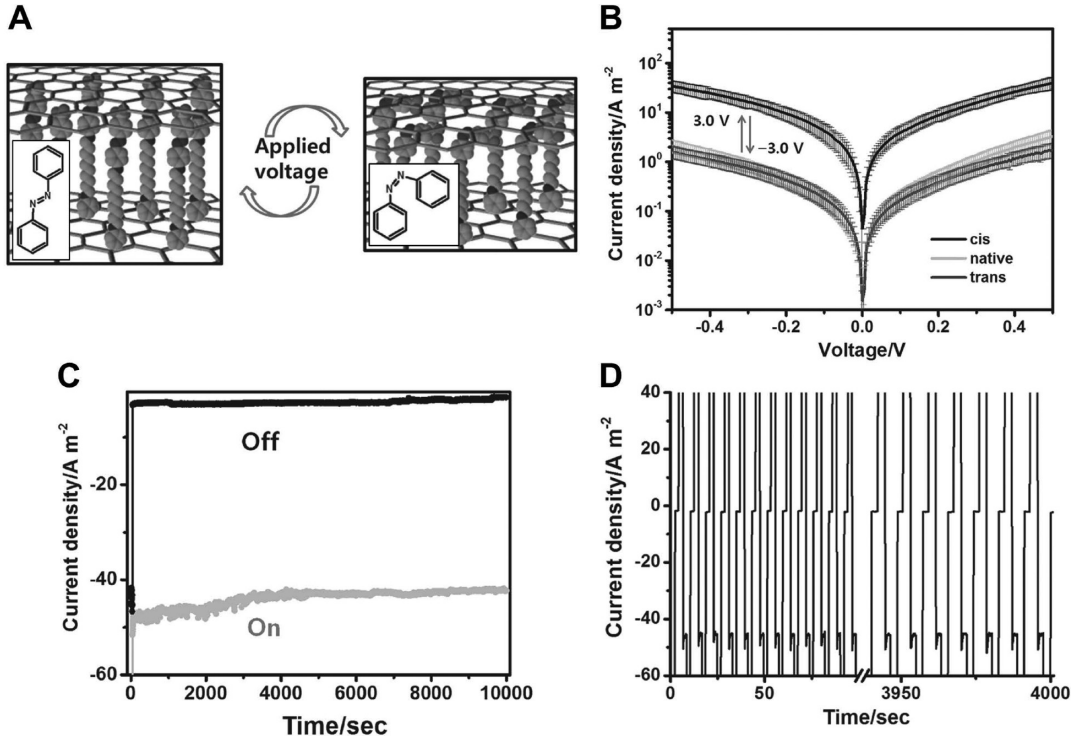

Figure 16. (A) Illustration of voltage-induced conductance switching between the two conductance states of the conformational isomers of the azobenzene (PhC10AB) molecules in a monolayer. (B) Current−voltage characteristics for voltage-driven reversible conductance switching of rGO-PhC10AB SAMs//rGO devices corresponding to two conformational states. The voltages were swept from −0.5 to +0.5 V after applying voltages of +3 and −3 V to induce conformational changes from *trans*−*cis* isomers and *cis*−*trans* isomers, respectively. (C) Memory retention performances of the ON state and the OFF state at −1 V after applying voltages of +3 and −3 V, respectively. (D) WRER performances at +3, −1, −3, and −1 V (with 2 s of pulse width time). Adapted with permission from ref 121. Copyright 2013, Wiley-VCH.

lack of free volume for a conformational change in the molecules.[108,161,223,240] Therefore, the most fundamental approach to enable the reversible switching phenomenon is to enhance the quantum efficiency of the photochromic molecules by increasing the light transmittance of the material to be used as the top electrode, which is the pathway for the light. As previously described, for example, the introduction of a PEDOT:PSS interlayer, and in particular a gold top electrode that is an excellent blocker of light, may disturb the light to be effectively transmitted. To resolve this issue, an rGO electrode, which is transparent and a conductive two-dimensional carbon-based material, can be utilized as the top electrode for the molecular photoswitch junctions. Figure 15A shows a schematic illustration of fabrication process for rGO interlayer-based

DOI: 10.1021/acsnano.7b02967
ACS Nano 2017, 11, 6511−6548

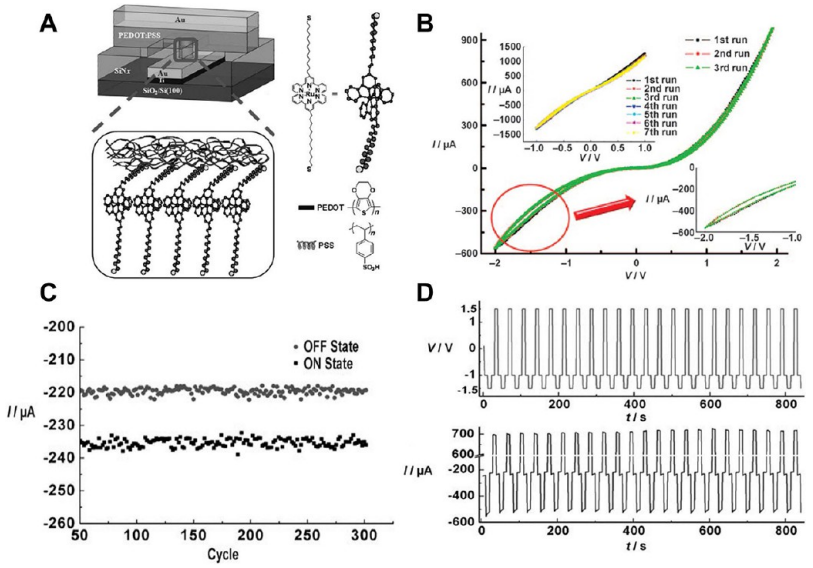

Figure 17. (A) Schematic representation of the device layout of a conducting polymer (PEDOT:PSS) on the ruthenium complex SAMs. (B) Hysteretic *I*−*V* characteristics of the molecular device (Au-ruthenium complex SAMs//PEDOT:PSS/Au). The *I*−*V* characteristics of the device were recorded by scanning the applied voltage from 0 to +2 V and then to −2 V, followed by a reverse scan from −2 to +2 V. Top inset shows a control experiment using PEDOT:PSS without ruthenium SAMs between the top and bottom electrodes. Bottom inset shows magnification of the hysteretic *I*−*V* curve. (C) Current in the ON state and OFF states as a function of the number of WRER cycles. (D) Write−multiple read−erase−multiple read (WRER) cycles of a molecular device containing Ru^{II} complex for a rewritable data storage application. The writing, reading, erasing, and reading voltages were −1.5, −1, + 1.5, and −1 V, respectively. Reproduced with permission from ref 219. Copyright 2009, Wiley-VCH.

molecular photoswitch junctions. In this fabrication process, the formation of the rGO top electrodes on the diarylethene-derivative molecular layer was conducted by spraying highly transparent and conductive rGO flakes, which were dispersed in dimethylformamide (DMF), enabling soft contact without significant damage or contaminants on the SAMs. The corresponding transmittance characteristics of the rGO film are presented in Figure 15B with those of a PEDOT:PSS/Au film for comparison. The results showed that the enhanced transmittance of the rGO film compared with the PEDOT:PSS/Au film over all ranges of wavelength facilitates pronounced reversible switching behavior, which was not shown in the case of the PEDOT:PSS/Au top electrodes.[108] Figure 15C shows the reversible photoswitching phenomenon successively observed by consecutive conductance transformation over 20 times upon alternating UV (360 nm) and visible (520 nm) light irradiation. These results demonstrated that diarylethene-derivative molecular devices with an rGO top electrode could exhibit a reliable and reversible photoswitching phenomenon in response to light illumination.

Molecular Memories. Molecular memory is a data storage device that uses molecular species as the data storage element performed by any of several mechanisms, including charge storage, photochromism, or changes in conductance.[241] In principle, the fabrication of this molecular memory junction requires the integration of molecular switches, in which the intrinsic properties of the molecular layer transform in response to external stimuli because independently stable states can encode the information as "ON" and "OFF".[218,242,243] However, an additional feature that should be possessed by molecular memories for real implementation is that these independent states should retain their information without spontaneous degradation, especially while reading the information. To achieve this goal, the rational design of molecular species and suitable choices of junction structure and materials are critical to achieve stable and high-yield ensemble molecular layer-based nonvolatile memories. Moreover, in terms of practical applications of molecular memories, the two-dimensional array or crossbar geometry is a promising architecture for the nanoelectric circuitry for several reasons:[244−249] (i) Due to the simple two-dimensional structure, crossbars may be fabricated using a wide variety of techniques including conventional lithography;[250−252] (ii) it can exhibit excellent scaling and integration density depending on the wire configuration;[253] and (iii) the crossbar structure is defect tolerant. Thus, the crossbar-type molecular memories may be served as a primary prototype of the molecular memory architecture. For example, nanoscale molecular random access memory composed of a [2]rotaxane monolayer with a crossbar architecture has been reported as a prototype of molecular memory.[254] Min *et al.* proposed the solution-processed fabrication of an azobenzene derivative (PhC10AB) molecular layer-based nonvolatile memory device on an rGO electrode with the crossbar structure, as shown in Figure 16A. In this junction structure, a GO film spin coated onto an ITO coated plastic substrate was chemically reduced to rGO, which results in a nucleophilic surface that can provide electrons to the electrophilic azobenzene diazonium molecules. The top rGO contacting the vertically aligned crossbar structure was then facilitated by spray coating using rGO solution diluted in DMF on the SAMs, showing a device yield of ∼60%. The schematics in Figure 16A show the concept of voltage-induced *trans*−*cis* isomerization of PhC10AB molecules, in which a specific bias voltage applied between two electrodes in a molecular junction can allow the transition of the isomer states by electron transmission between an electrode and molecules.[237] In the previous section, the authors showed that reversible voltage-controlled isomerization of azobenzene-derivatives is available

DOI: 10.1021/acsnano.7b02967
ACS Nano 2017, 11, 6511−6548

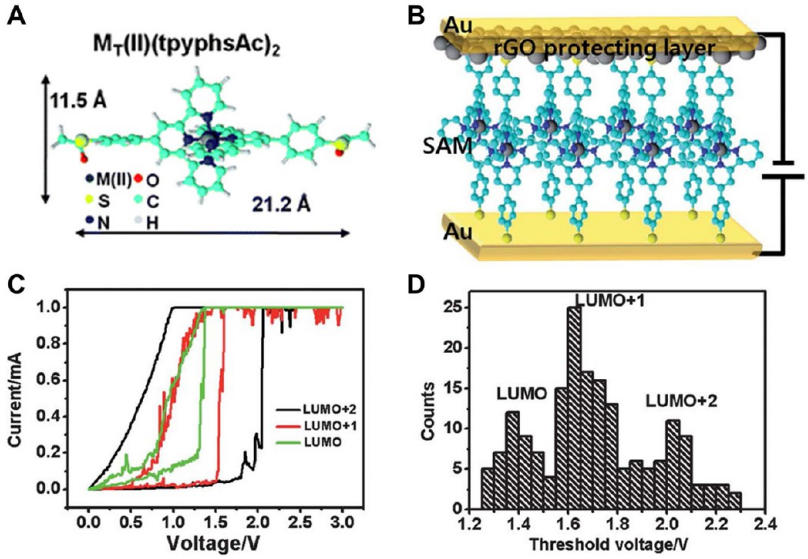

Figure 18. (A) Structure of transition-metal(II) bis-acetylthiophenylterpyridine (*i.e.*, $M_T^{II}(tpyphs)_2$) complexes. (B) Illustration of an Au/rGO contact for an Au-SAMs//rGO film/Au device. (C) *I*−*V* curves and (D) statistical distributions of the threshold voltage in Au-$Fe^{II}(tpyphs)_2$ SAMs//rGO film/Au devices, showing three distinguishable conductance states. Reproduced with permission from ref 220. Copyright 2012, RSC Publishing.

with a change in the junction distance in rGO-PhC10AB//rGO devices that will lead to a rewritable nonvolatile memory effect. In contrast to *trans*−*cis* photoisomerization of azobenzene derivatives in monolayers or in solution, this electric field (or electron)-induced isomerization occurs in a few seconds,[237,255] which takes from a few to several tens of minutes in the case of photoisomerization.[256,257] Figure 16B shows plots of *J*−*V* characteristics for the molecular memory junctions in different conformations after application of +3 V or −3 V biased voltages, respectively (+3 V for *trans* to *cis* transformation and −3 V for *cis* to *trans* transformation, and the top rGO electrode was biased). The height change upon the transition of isomer states in their SAMs was estimated to be approximately 6.45 Å, resulting in a significant change in the tunneling resistance value between the two isomer states and showing a large difference of over 15 times in the *J*−*V* plots. Based on this conductance switching phenomenon, the reversible *trans*−*cis* isomerization controlled by a voltage pulse of +3 V and −3 V with −1 V of reading voltage was exploited for application in a nonvolatile memory device, as shown in Figure 16C,D. At the reading voltage, the current value of the ON state was approximately 20 times larger than that of the OFF state, which the ON/OFF ratio was maintained for a retention time of >10000 s (Figure 16C). The nonvolatile molecular memory performances of write−read−erase−read (WRER) were stable for over 400 cycles and preserved after six months of storage, demonstrating the excellent stability and durability of the molecular junctions (Figure 16D). This study shows a clear example of the utilization of molecular isomerization for molecular memory applications with a conventional molecular junction fabrication technique.

Rather than utilizing an isomerization process in a molecule, a redox-active molecule, with reversible electron-transfer behavior, in the metal complex by oxidation and reduction processes, involves an attractive feature that shows hysteric electrical characteristics, which can be used for nonvolatile memory applications.[258−263] Lee *et al.* reported a nonvolatile memory effect in ensemble molecular junctions using alkylthiolates with Ru^{II} terpyridine complexes. Figure 17A depicts a schematic illustration of the cross-section of the junction structure with a PEDOT:PSS interlayer on the Ru^{II} complex-based SAMs. Long alkyl chains on both sides of the Ru^{II} complexes effectively prevented penetration of PEDOT:PSS onto the SAMs, resulting in a high device yield of ∼80%. The corresponding *J*−*V* characteristics of Au−Ru^{II} complex alkylthiolate SAMs//PEDOT:PSS/Au junctions are shown in Figure 17B. In the negatively biased region when the top electrode was biased, reproducible hysteric *J*−*V* characteristics were observed, in which charging/uncharging of the Ru^{II} complexes in the SAMs were attributed to represent the origin of the hysteresis.[260,264] In addition, the endurance and WRER properties upon a successive voltage pulse sequence of +1.5 V and −1.5 V with −1.0 V reading bias voltage were investigated as shown in Figure 17C,D, and the results showed stable conductance switching behavior in excess of 300 cycles.

Depending on the species of central metal and ligand in the redox-active complexes, multilevel conductance switching, which results from multiple electron-accepting states in the molecule, can be probed by energy band alignments between the Fermi level of the contact metal and HOMO or LUMO levels of the molecule. For example, metal complexes with conjugated polypyridine ligands, such as terpyridine, are known to have multiple electron states that can undergo localized multiple reduction steps in the metal complexes, suggesting the possibility of multilevel molecular memory components.[265] An example of this kind of molecule having a metal complex core with conjugated ligands (bis[4′-(4-thioacetylphenyl)-2,2′:6′,2″-terpyridinyl]$M_T^{II}(PF_6)_2$, M_T = Fe, Ru, and Co, denoted as $M_T^{II}(tpyphsAc)_2$) is schematically shown in Figure 18A. Using the molecules, the electron affinity levels were obtained in solid-state-based junctions with an rGO top electrode (Figure 18B). The corresponding hysteric *J*−*V* characteristics were observed in ensemble molecular junctions of the Fe^{II} complex SAMs, as shown in Figure 18C. In terms of the bias voltages at which the conductance switching behavior occurred, the junctions exhibited three different threshold voltages based

DOI: 10.1021/acsnano.7b02967
ACS Nano 2017, 11, 6511−6548

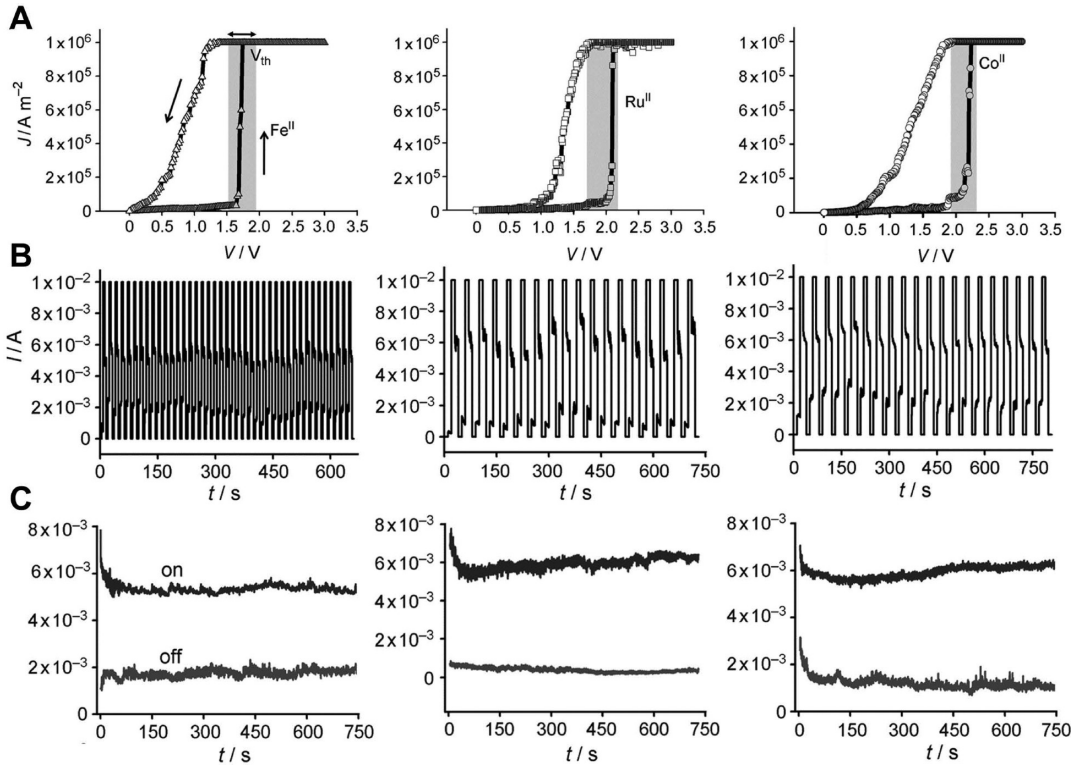

Figure 19. Nonvolatile molecular memory properties of $Ru^{II}(tpyphsAc)_2$, $Fe^{II}(tpyphsAc)_2$, and $Co^{II}(tpyphsAc)_2$, respectively. (A) J–V characteristics on a linear scale for Au-$M_T^{II}(tpyphsAc)_2$ SAMs//rGO/Au junctions show conductance switching. The threshold conductance voltages observed in each molecular junction from 50 devices are indicated as V_{th} in each J–V curve. (B) Memory effect of Au-$M_T^{II}(tpyphsAc)_2$ SAMs//rGO/Au devices. Write–multiple read–erase–multiple read operations are shown. (C) Corresponding ON and OFF retentions are shown. Adapted with permission from ref 120. Copyright 2012, Wiley-VCH.

on the statistical histograms (Figure 18D). This result indicates that the resonant tunneling through the molecular junction involved in the redox processes occurred by aligning each intrinsic electronic level of the molecule to the Fermi level of the electrodes.[266,267] The threshold voltages were also dependent on the central metal atoms of $M_T^{II}(tpyphsAc)_2$. The representative J–V curves of Au-$M_T^{II}(tpyphsAc)_2$//rGO/Au junctions for each Fe, Ru, and Co metal atom complexes are shown in Figure 19A. From the results of the statistical analysis, it was found that each threshold voltage value depicts 1.5–1.9 V for Fe, 1.7–2.1 V for Ru, and 1.9–2.3 V for Co, respectively. The threshold conductance voltages of each $M_T^{II}(tpyphsAc)_2$ were in good agreement with the energy gaps between the Au Fermi level and the electron affinity level of each metal complex. Based on the conductance switching operation, nonvolatile molecular memory characteristics of Au-$M_T^{II}(tpyphsAc)_2$//rGO/Au junctions are shown in Figure 19B,C. The WRER operations were performed in the following manner: Reading the current density at +1.5 V after pulsing voltages for 1.5 s at +3.0 V for the ON state and 0.0 V for the OFF state (Figure 19B). Each WRER cycle was conducted more than 20 times for one test set, and good reproducibility was observed with an ON/OFF ratio of approximately 5. The molecular memory junctions also showed good retention characteristics such that each ON and OFF state was sustained for at least 10 min as shown in Figure 19C. Although the ON/OFF ratio of the above nonvolatile molecular memory was not satisfactorily compared with conventional bulk organic memory devices showing 4–5 orders of magnitude,[268,269] these nanoscaled molecular memories possess some good device characteristics in terms of high switching speed, low power consumption, high integration density, and a possibility of large array fabrication, which may be a potential alternative for future memory applications.

Molecular Devices on Flexible Substrates. Recently, flexible electronics, which is an emerging technology for fabricating electronic circuits on flexible plastic substrates, such as polyimide (PI), polyethylene terephthalate (PET), and polyethylene naphthalate (PEN), has attracted great attention from many research groups due to its potential applicability to wearable electronics.[270,271] Based on a rapid advance in materials for flexible circuit applications, various electronic applications have been developed, such as light-emitting diodes,[272] electronic circuits,[273,274] memory devices,[275] sensors,[276,277] displays,[278,279] solar cells,[280] and bioelectronic devices.[281] One of the most noticeable advantages of using molecular layers as an active device component for electronic devices is that ultimate scaling is feasible because the molecular layers can be considered as extremely thin organic films. This thin-film property also makes the molecular layers a suitable channel material for flexible electronics applications.[282] Thus, with an adequate selection of materials and architectures for molecular junctions, high-yield flexible molecular devices may provide a clear example for practical applications of the molecular junctions.

Figure 20 presents the first realization of high-yield flexible molecular devices. Here, PI was used as the flexible substrate for two reasons: (i) It has a relatively high thermal stability (up to 520 K), which prevents substrate deformation during the thermal treatment used to make the isolating layer (photo-

DOI: 10.1021/acsnano.7b02967
ACS Nano 2017, 11, 6511–6548

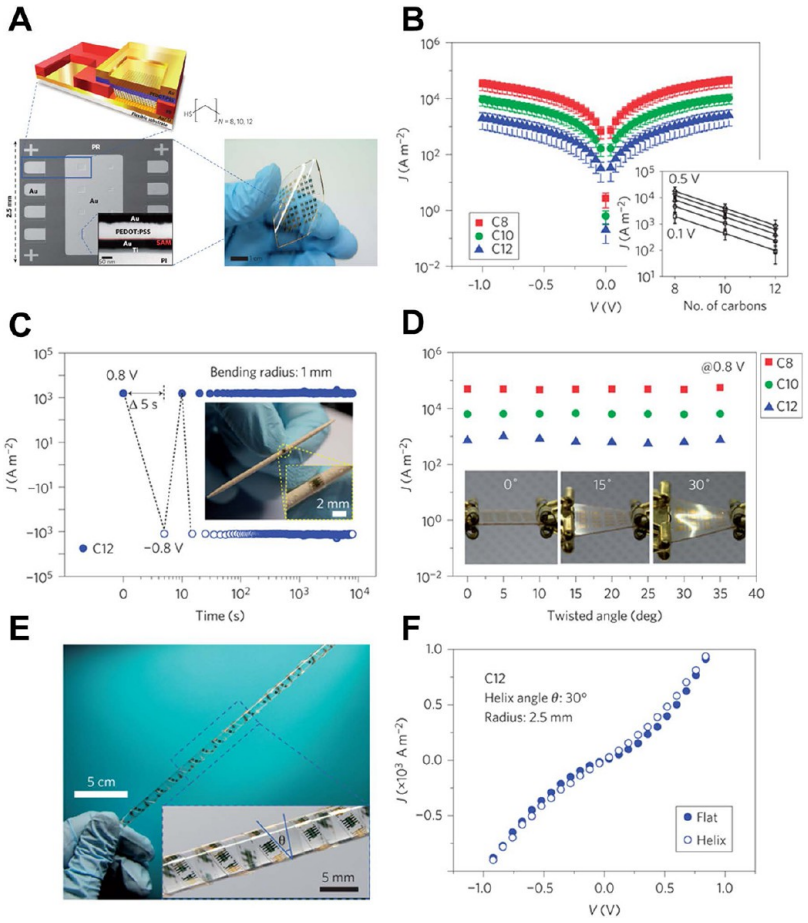

Figure 20. (A) Upper left image: Schematic of a flexible molecular device. The layers (from bottom to top) are a flexible substrate, a bottom Au/Ti electrode, a molecular layer or photoresist (PR) for electrical isolation, a PEDOT:PSS layer, and a top gold electrode. Lower left image: SEM image of a molecular device. Inset: high-resolution cross-sectional TEM image of a molecular device. Lower right image: Photograph of completed device under bent condition. (B) Current density *J* (on a log scale) *vs* voltage *V* for octanethiol (C8), decanethiol (C10), and dodecanethiol (C12) molecular devices under flat conditions at 300 K. Inset: *J* (on a log scale) *vs* number of carbon atoms. Error bars denote standard deviation of individual measurements for several devices. (C) Current density *J* *vs* time (both on log scales) for a C12 device being bent around a toothpick (bending radius, $r \approx 1$ mm, shown in inset). The voltage was stepped between +0.8 V and −0.8 V, and *J* was measured every 5 s for 10,000 s. (D) Values of *J* measured at 0.8 V for C8, C10, and C12 devices as a function of twist angle. Insets: Photographs taken at three different angles. (E) Photograph of flexible devices rolled over a tube (radius, 2.5 mm; $\theta = 30°$) under helical structural conditions. (F) Plot of *J* (on a linear scale) *vs* *V* for a C12 device under flat (solid circles) and helical (open circles) conditions. Reproduced with permission from ref 282. Copyright 2012, Nature Publishing Group.

resist) insoluble in ethanol for the self-assembly process performed on the bottom gold electrode;[100] and (ii) the low surface roughness of PI reduces the defect density of the SAMs in the junction. To prevent electrical shorts due to penetration of the top metal layer during deposition, the PEDOT:PSS interlayer was introduced between the top metal layer and the SAMs (Figure 20A). Nevertheless, changes in the electrical resistance of PEDOT:PSS films on flexible substrates were negligible, and defects or cracks in the PEDOT:PSS/substrate were not observed, even when the substrate was bent to a radius of 5 mm. Figure 20B shows the representative exponential length-dependent current densities of alkanethiolates (C8, C10, and C12) molecular junctions under flat conditions, which are indicative of tunneling through a molecular tunnel barrier with a β of ~0.8 n_C^{-1} (inset in Figure 20B). The error bars in Figure 20B represent the standard deviation of many junctions (more than ~20 devices for each molecular type). To ensure a practical device platform, the stability and durability of the molecular junctions must be determined.[75,100,218] Figure 20C shows the *J* values of the flexible molecular devices that were maintained when bent over a toothpick (bending radius ≈1 mm) for 1×10^4 s, indicating excellent durability and operational stability under extreme bending conditions. These results also suggest that there were no significant changes in the structure and phase of SAM molecules in the molecular junctions when the device was severely bent. To further elucidate the mechanical stability of the molecular junctions, Figure 20D presents the *J*−*V* characteristics and operational stability of C8, C10, and C12 flexible molecular devices under twist conditions. The results demonstrated no noticeable degradation as the twist angle was varied from 0° to 35° (in steps of 5°). Figure 20E shows a photographic image of the flexible molecular device (a strip with dimensions of 0.25 cm × 40 cm containing 1024 molecular junctions) rolled over a tube (radius = 2.5 mm) in a helical configuration ($\theta = 30°$). The corresponding *J*−*V* characteristics of a C12 device under helical and flat conditions are shown in Figure 20F. Despite the severe deformation of the molecular junctions, pronounced changes in these characteristics were not observed under helical structural conditions. In

DOI: 10.1021/acsnano.7b02967
ACS Nano 2017, 11, 6511−6548

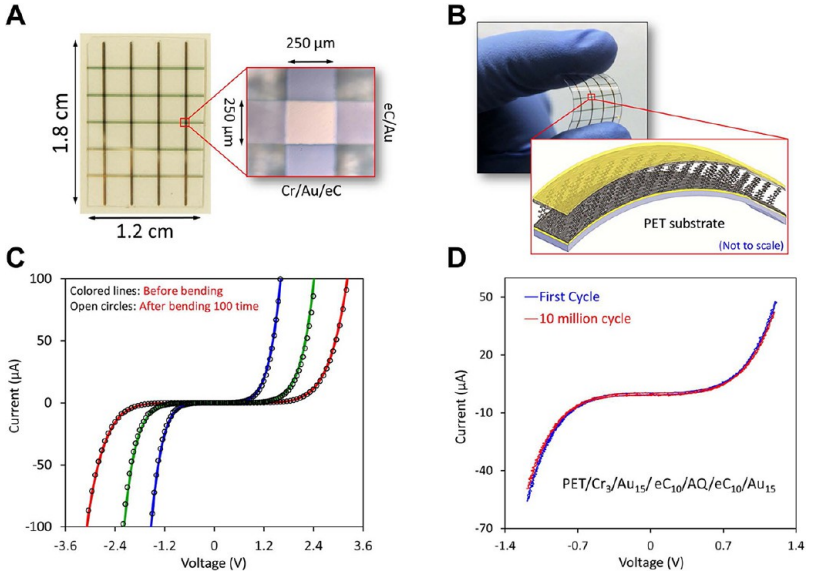

Figure 21. (A) Optical image of Cr/Au/eC-AQ SAMs//eC/Au devices deposited on transparency film (PET). Magnification shows an individual junction. (B) Optical image of the fabricated device on PET substrate while bent. (C) $J-V$ curves of junctions fabricated on flexible PET substrate before (lines) and after (points) being bent 100 times to the degree shown in (B), which reduced the 1.8 cm dimension in (A) to ~1.4 cm. (D) Overlay of $J-V$ curve of freshly fabricated AQ junction on flexible PET substrate before (blue) and after (red) 10 million $J-V$ cycles to ±1.3 V in air. Reproduced with permission from ref 103. Copyright 2016, American Chemical Society.

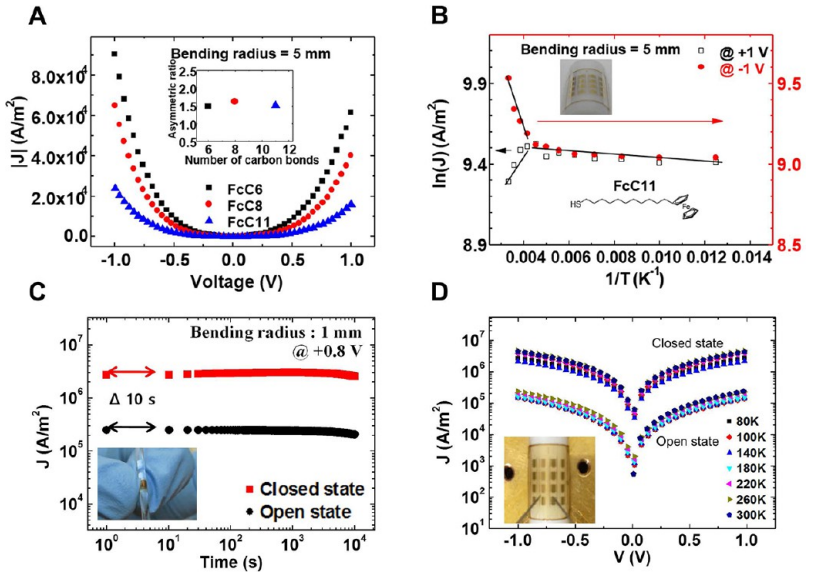

Figure 22. (A) $J-V$ characteristics of FcC6, FcC8, and FcC11 molecular devices fabricated on flexible substrates. The data were measured under bending conditions with a bending radius of 5 mm. The inset displays the asymmetric ratios of the devices under the same bending conditions. (B) Arrhenius plot for a flexible FcC11 molecular device under bending conditions with a bending radius of 5 mm. Reproduced with permission from ref 107. Copyright 2014, Wiley-VCH. (C) Arrhenius plot of J *vs* the inverse of the temperature ($1/T$) for the molecular junctions bent around a toothpick (bending radius, $r \approx 1$ mm, shown in inset). (D) Temperature-variable current density–voltage results for photoswitching molecular junctions on the closed and open states when subjected to bending (bending radius = 5 mm). The inset shows a real device being measured. Reproduced with permission from ref 108. Copyright 2014, Wiley-VCH.

addition, by modeling the mechanical stress on the molecular layer and electrodes under the bent condition, the authors suggested that ultrathin SAMs-based devices are reliably operational when bent, twisted, or deformed into helical structures. Among the various approaches for generating high-yield molecular junctions, as mentioned in the previous section, the interlayer technique, which incorporate the protective layers in contact with the SAMs to prevent direct filamentary path formation during top metal electrode deposition, is a promising candidate method for fabricating flexible molecular electronic devices. Due to efficient flexibility of the organic materials for the interlayer, such as PEDOT:PSS,[283] these high-yield molecular junctions can maintain their electrical characteristics even under severe mechanical deformation.

Another kind of flexible material candidates for the interlayer in high-yield molecular junctions are carbon-based materials. Because these materials such as graphene,[284] rGO,[285] and eC[286] are conductive, transparent, and most importantly tolerant of

DOI: 10.1021/acsnano.7b02967
ACS Nano 2017, 11, 6511–6548

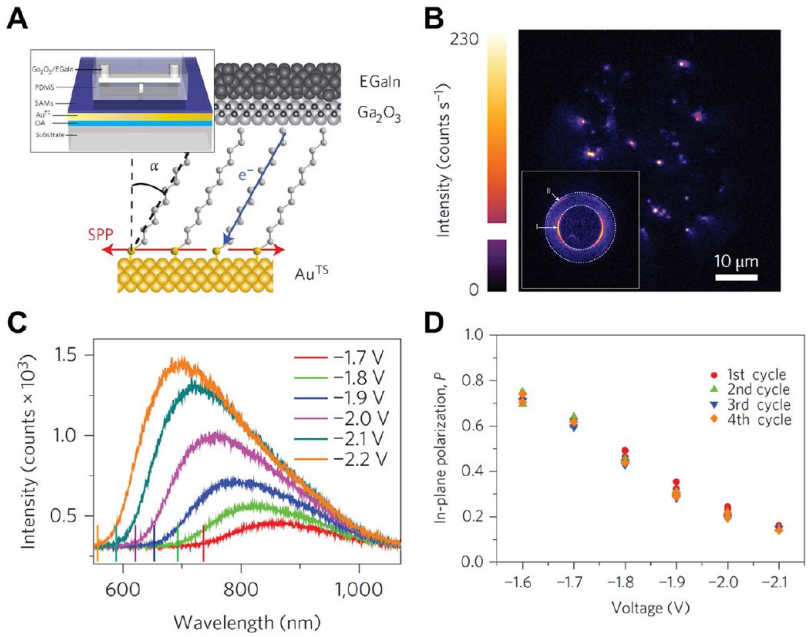

Figure 23. (A) Schematics of the molecular junction with the Ga_2O_3/EGaIn top electrode constrained in PDMS and an ultraflat Au^{TS} bottom electrode supporting SAMs of SC_n. (B) Real plane and back focal plane (inset) images of plasmons excited in an molecular junction with a SC_{12} SAM on a 50 nm Au^{TS} film at −1.8 V. Modes I and II indicate SPP modes with wave vectors k = 1.01 and k = 1.47, respectively. (C) Corresponding spectra of plasmons excited under the same conditions as in (B) with varied bias voltage. Vertical lines indicate the corresponding wavelength with energy eV_{bias}. (D) Voltage dependency of in-plane polarization *P* during four voltage cycles. Adapted with permission from ref 287. Copyright 2016, Nature Publishing Group.

mechanical stress in thin film structures, they can serve as the protective layer for flexible (even transparent) ensemble molecular junctions with a high device yield. For example, Najarian *et al.* facilitated eC electrodes for this purpose and obtained semitransparent and high-yield flexible molecular junctions. Figure 21A shows optical images of $Cr_3/Au_{15}/eC_{10}$-AQ//eC_{10}/Au_{15} devices on PET substrates. The detailed fabrication procedure is mentioned in the Interlayer Techniques section. The *J*−*V* characteristics for three different AQ thicknesses are shown in Figure 21C, in which the points superimposed on the plots are the *J*−*V* characteristics for each device after being bent 100 times to the extent shown in Figure 21B. Because the eC layer is an amorphous thin carbon film, which is tolerant of mechanical deformation, no observable degradation was observed in the curves. Additionally, the total molecular junctions thickness of ∼60 nm is much less than the bending radius, and the strain on the molecular junction is small. Therefore, when strong bonding between eC and the molecular layer is guaranteed, the mechanical robustness of the eC layer provides stable junctions with identical *J*−*V* response before and after bending. Based on the mechanical stability, the *J*−*V* cycle was performed after 10^7 times of biasing to ±1.5 V, and the *J*−*V* characteristics were indistinguishable, indicating excellent flexible device stability. It is also noteworthy that similar investigations of flexible molecular junctions fabricated using graphene[119] and rGO[109,120,121,129] electrodes have been performed, and like the eC electrodes, the molecular junctions with carbon-based materials exhibited excellent mechanical stability under various mechanical deformations.

As an example of the practical application of flexible molecular electronic devices, functional molecular devices fabricated on flexible plastic substrates have been investigated because of their distinctive features under mechanical stress conditions. Figure 22 depicts two examples of functional molecular devices on the flexible substrates showing (i) asymmetric electrical characteristics (*i.e.*, rectifying) and (ii) photoswitching characteristics. From each plot, it can be observed that even under severe mechanical deformations (Figure 22A,C), the distinctive features of the functional molecular devices were still maintained without significant degradation of their device performance. Additionally, the junctions exhibited excellent retention and endurance properties similar to that observed for the rigid devices. Furthermore, the flexible plastic substrates (PI) were stable and reliable as a device platform for investigating the electrical characteristics of the flexible molecular junctions at low temperatures down to ∼80 K (Figure 22B,D). These results indicate that the distinctive electrical characteristics of the functional molecular junctions are intrinsic molecular properties that are irrelevant to external conditions such as the substrate type or mechanical stress.

Other Applications of Functional Molecular Devices. Another kind of functional molecular device could be a molecular optoelectronic device. Nijhuis group have extensively studied the potential applicability of molecular optoelectronic devices.[287,288] Surface plasmon polaritons (SPPs) are confined and enhanced local electromagnetic waves at infrared or visible frequencies that propagate along a metal−dielectric interface, thereby providing a nanofabricated system for optoelectronic circuit applications.[289,290] To excite the surface plasmons, external light sources are usually utilized for this purpose.[291−293] Instead of the light-driven excitation of the surface plasmons, tunneling electrons in metal−insulator−metal junctions can also directly excite the surface plasmons in a manner such that the tunneling electrons inelastically couple to a plasmon mode.[294−297] The tunneling electron-driven plasmonic source is attractive because there is no interference by background light and the response is fast. Especially in

DOI: 10.1021/acsnano.7b02967
ACS Nano 2017, 11, 6511−6548

molecular electronic junctions, tunneling behavior can be carefully controlled by tuning the chemistry of the molecule, which enables adjustment of the properties of the plasmons. In addition, due to an ultimately miniaturized scale of the molecular length, the molecular electronic plasmon sources are smaller than the conventional plasmon sources. The schematics of the ensemble molecular junction-based plasmonic source are shown in Figure 23A. The junctions were fabricated using the Ga_2O_3/EGaIn top electrode constrained in PDMS on the solid-state device platform showing a high device yield, and the SAMs consisted of alkanethiolates (SC_n, n = 10, 12, 14, 16, and 18) or (4-((4-(ferrocenyl)phenyl)ethynyl)-phenyl)methanethiol. Figure 23B shows the real plane and back focal plane image of plasmons excited by tunneling electrons in a molecular junction with SC_{12} SAMs biased with −1.8 V with an Au^{TS} thickness of 50 nm. Each bright spot corresponds to localized or propagating surface plasmons, which was spatially inhomogeneous. Furthermore, the arcs in the inset of Figure 23B with wave vectors $\mathbf{k}$ = 1.01 (mode I) and $\mathbf{k}$ = 1.47 (mode II) were explained based on the results of the dispersion calculations, indicating that they corresponds to leakage radiation from SPPs propagating along the Au^{TS}−SAMs−air interface and the Au^{TS}−SAMs−PDMS interface, respectively. By tuning the molecular electronic properties of the junctions, the properties of the plasmons can be controlled. Figure 23C presents spectra of plasmons with varied bias voltages across the junctions. As shown in the plots, the blueshift spectra increase with the bias voltage, and thereby the peak wavelength decreases. The intensity of the plasmon emission from the junction could also be controlled by changing the value of n for the SC_n SAMs. Another plasmonic parameter that can be controlled by the molecular junctions is the polarization of the plasmon sources. Figure 23D depicts the in-plane polarization P (defined as $P(V) = \frac{I_1(V) - I_2(V)}{I_1(V) + I_2(V)}$, where I_1 and I_2 are the photon counts for two orthogonal polarization channels) *vs* the bias voltage plots in a SC_{12} SAMs molecular junction. From the plots, it was found that P is voltage dependent and fully reversible, indicating that bias-induced control of the polarization of the plasmonic sources is feasible. The authors attributed the origin of polarization change to electric field-induced conformational change against the bottom surface. These results clearly show the molecular electronic control over the plasmon source. Using these properties, a high-performance and ultimately miniaturized molecular plasmonic source could be realized.

The major goal of molecular electronics is to combine the different types of functional molecules into integrated circuits through an autonomous self-assembly process.[106] One of the most remarkable advantage of the massively parallel lithographic fabrication of high-yield molecular junctions is that it may allow molecular junctions to be integrated with commercially viable microelectronics.[31] The integration of individual molecular junctions, however, requires additional processes like wiring interconnects, which may be limited depending on the molecular junctions architecture or processing window.[106] Thus, reliable, stable and high-yield molecular junctions with a suitable junction architecture are accompanied for integrated molecular circuits. For example, Hal *et al.* demonstrated the integration of large-area molecular junctions in strings where up to 200 devices are connected in series. The fabrication process involved the PEDOT:PSS interlayer with microscale *via* hole architecture, which was fully amenable to conventional lithographic technology. In addition, this process comprises patterned interconnections in both top and bottom electrode layers, and strings can be fabricated in which a large number of molecular junctions are connected in series. Figure 24A shows a schematic cross-section

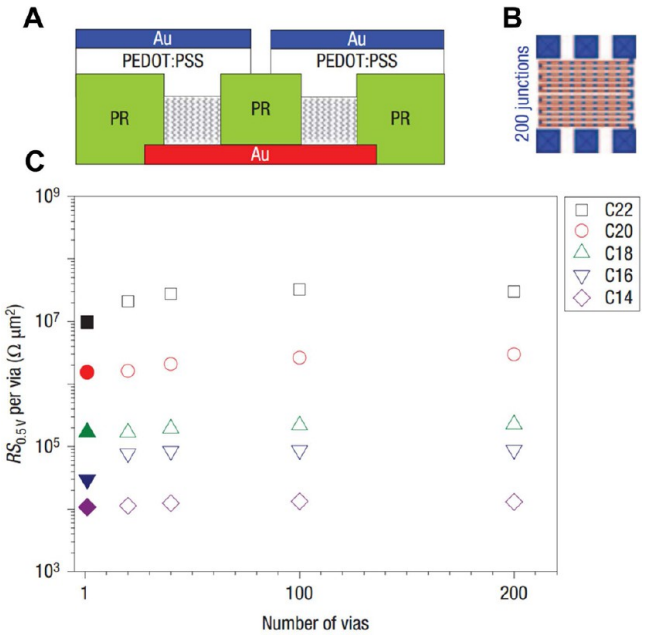

Figure 24. (A) Schematic cross-section of a part of a string showing two connected junctions. (B) Layout of strings in which a number of molecular junctions are connected in series. Each section contains two junctions. The red and blue colors represent the bottom and top gold layers, respectively. (C) The normalized resistance of alkane-monothiol C_nH_{2n+1}-SH SAM junctions with n = 14−22, integrated in strings using the default process flowchart. The junctions are 5 μm in diameter. The normalized resistance per *via* is presented as a function of the number of junctions. Values for discrete single junctions are included as solid symbols for comparison. Reproduced with permission from ref 106. Copyright 2008, Nature Publishing Group.

image of a portion of string connecting two molecular junctions. The layout of the strings, as presented in Figure 24B, shows that up to 200 devices could be integrated in series with a yield of unity. In addition, owing to the reproducible electrical characteristics, the normalized resistance per junction was independent of the number of interconnected junctions, as shown in Figure 24C.

To the best of our knowledge, the first practical application for the commercial production of large-area molecular junctions was introduced by Bergren *et al.* as a discrete component in analog clipping circuit. The audio clipping circuits often utilize electronic components with nonlinear current−voltage characteristics (*e.g.*, semiconductor diodes) to distort the input signal waveforms. Because the molecular junctions exhibit distinctive and tunable nonlinear electrical characteristics, differences in the electrical performance of the molecular junctions enable the wide range of sounds in electronic music. The molecular junctions were composed of PPF/molecule/eC layers arranged in a cross-junction format with a high device yield (> ∼95%), as shown at the top of Figure 25A. The fabrication technique was amenable to manufacturing and integration with conventional circuitry, the details of which are provided in the Interlayer Techniques section. Figure 25A also shows photographs of a

DOI: 10.1021/acsnano.7b02967
ACS Nano 2017, 11, 6511−6548

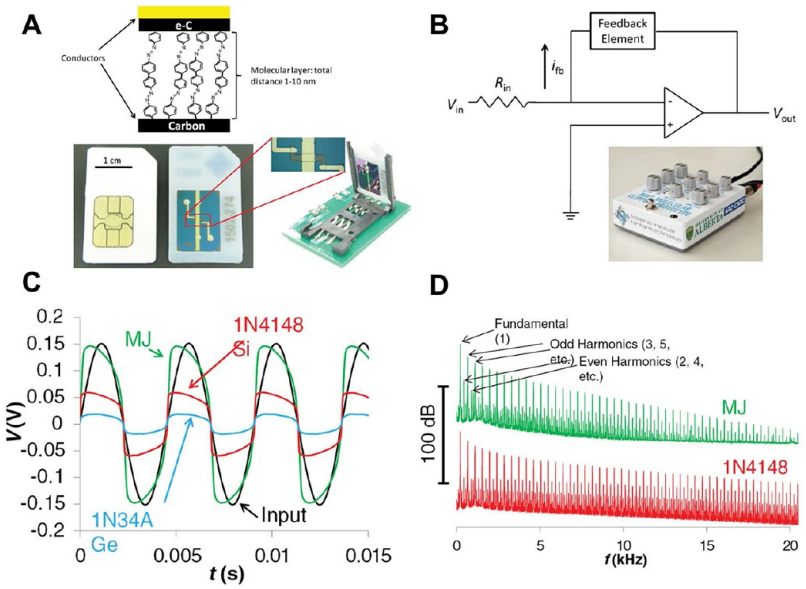

Figure 25. (A) Upper image shows cross-sectional schematic of an idealized molecular junction structure, showing organic molecules sandwiched between two conducting contacts, in this case consisting of a carbon bottom contact and electron-beam evaporated carbon and Au as the top contact. Lower images show photograph of the molecular junctions fabricated using a SIM-card pin−out (with a conventional SIM card shown for comparison) to simplify testing and integration into analog circuits, as shown at right. (B) Simplified schematic showing the clipping amplifier section of the circuit employed in the prototype for the op-amp clipping gain stage. The photograph at bottom shows the actual prototype. (C) The input sine wave (black curve) is shown below the output resulting from using the molecular junction clipper (green curve) or Si diode pair clipper (red curve) and Ge diode pair clipper (blue), where the amplitude results from the clipping device characteristics shown in (B). (D) The power spectra for the Si and molecular junction waveforms in (C) with odd and even harmonics labeled. Reproduced with permission from ref 133. Copyright 2016, IOP Publishing.

molecular junction mounted on the SIM (subscriber identification module) card holder, which connects the device to the external circuitry. A common analog distortion circuit that utilizes voltage waveform clipping using the operational amplifier is shown in Figure 25B with a photographic image of the actual prototype. Feedback clipping operates to distort the input signal using a feedback component with nonlinear current voltage characteristics. The output signal of the feedback clipping circuit for a sinusoidal input is shown in Figure 25C. The plots demonstrated that the molecular junctions yield a distortion response similar to the diode clippers. Power spectra for the clipped waveforms in Figure 25C are shown in Figure 25D, which depict the distribution of the harmonics. The molecular junctions provided a different power response in comparison to the Si diode clippers, and they could be tuned by adjusting molecular layer thickness resulting in different nonlinear current−voltage characteristics. Finally, this fascinating study presented a representative example of a real-world application of high-yield functional molecular junctions and the feasibility of manufacturing molecular junctions for use in commercial applications.

SUMMARY AND OUTLOOK

Since the genesis of the research field of molecular electronics, tremendous progress has been achieved both theoretically and experimentally by scientists and engineers who were fascinated by intriguing physical, chemical phenomena, and potential device applications of molecular junctions. Many different paradigms, especially for ensemble molecular junctions, have been explored to acquire an improved understanding of many features of molecular junctions, including molecular design, molecule−electrode interface engineering, and junction architectures. Particularly, from the perspective of practical applications, two-terminal devices have emerged as the most feasible architectures for molecular electronic devices as the future of next-generation electrical circuit units with a higher integration density and speed and lower fabrication cost, power, and consumption.[31,298−300] However, the ambiguousness of grafting the ultimately downscaled molecules into the nanogap electrodes intrinsically hinders the development of the stable devices. Prior to pursuing this goal, fabrication techniques for reliable and reproducible molecular junctions compatible with conventional microelectronics enabling massively parallel manufacturing with a high device yield should be accomplished. In this review, we presented recent developments in different fabrication techniques for high-yield molecular junctions as well as their prospective for future electronic device platforms. Each technique has its own advantages and drawbacks, from which one can carefully choose for one's own purpose. By taking advantage of the high device yield, statistical investigations of the electrical characteristics of the molecular junctions were thoroughly conducted to distinguish genuine transport characteristics from uncertain information. Moreover, we highlighted the significant advancements in high-yield molecular functional devices toward practical applications. All the functional features originating from the rationally designed molecules or their interactions with contact electrodes would certainly be interesting and promising for distinctive results in the field of molecular electronics. Note that all the topics regarding functional molecular devices beyond our discussion in this review were not addressed due to our limited knowledge and scope. For example, molecular sensors,[301−304] molecular field-effect devices,[302,305−309] molecular light-emitting diodes,[310−313] and molecular spectroscopic devices for molecular fingerprinting and DNA sequencing[314−316] can be potential applications utilizing the high-yield ensemble molecular

DOI: 10.1021/acsnano.7b02967
ACS Nano 2017, 11, 6511−6548

junction platform. In addition, the frequency response of two-terminal molecular junctions based on an equivalent circuit model has been proposed.[317−320] All these prospective studies provide a solid basis for advancing the commercial applicability of the ensemble molecular junctions.

Furthermore, some challenges remain, which are inherently related to the intrinsic nature of the molecules, to be resolved for enhancing microelectronics applications with functional molecular components. Although other crucial issues should be resolved, we believe the following issues are likely to be the most essential for realizing the long-term goal. (i) Rational design for ready accessibility: The functional features of the molecular junction structure may stem from various factors like electronic functionality in the molecule itself or in the molecule/electrode contact interaction. Therefore, the rational design of both the molecule and the junction architecture for making them readily accessible (*i.e.*, easy to synthesize the molecular species and fewer fabrication steps) is highly required. (ii) Controllability over molecule−electrode contact: Because the SAMs in the ensemble molecular junctions are formed through an autonomous self-assembly process enabling covalent bond, the electronic functionality of the molecule may be quenched due to the strong coupling.[223,321,322] However, the strong molecular bond on an electrode is desired for better thermal stability of the molecular junction.[5,103] Therefore, it is crucial to be able to control the contact characteristics of the molecule−electrode interface in the molecular junction depending on one's purpose. (iii) Manufacturability in the form of practical products: Although the high-yield ensemble molecular junction fabrication techniques described in this review are generally compatible with the available semiconductor fabrication processes, postprocesses like packaging and wiring interconnects should be accompanied by the junction fabrication for commercial microelectronics applications. Thus, the yielded devices should also be compatible with those postmanufacturing processes. (iv) Operational stability in the daily life environment: The distinctive functionality of the functional molecular devices should maintain the features over a wide thermal range and harsh mechanical stress environment, especially for wearable electronics applications.

Starting from the attractive property of molecular self-assembly, which is an autonomous bottom-up fabrication methodology that includes up-scaled approaches, the research field of molecular electronics has made considerable progress in recent years. Although it is expected that molecular electronics would not ultimately replace the well-developed world of CMOS microelectronics in the near future, molecular electronic devices can complement silicon-based devices by involving hybrid circuits, thus providing distinctive functionalities and insights.[30,323] Finally, with the collective intelligence and creativity encouraged by researchers in this field worldwide, we believe that we can leap into a brighter future of molecular electronics from the research laboratory to real life applications.

AUTHOR INFORMATION

Corresponding Author

*E-mail: tlee@snu.ac.kr.

ORCID

Takhee Lee: 0000-0001-5988-5219

Notes

The authors declare no competing financial interest.

ACKNOWLEDGMENTS

This work was accomplished through the financial support from the National Creative Research Laboratory Program (grant no. 2012026372) provided by the National Research Foundation of Korea (NRF) grant.

VOCABULARY

molecular junction, a nanoscale junction that a single molecule or a bundle of molecules are captured between the electrodes; **functional molecular device**, a molecular junction exhibiting conventional solid-state electronic device features beyond a simple resistor such as diode, transistor, and memory *etc.*; **ensemble molecular junction**, a molecular junction that contains a bundle of molecules (> ∼1000) between the electrodes; **high device yield**, the percentage of devices that are functioning properly among all manufactured devices is high enough; **self-assembled monolayer**, spontaneously formed molecular assemblies on specific surfaces by adsorption which are packed into large ordered domain; **molecular diode**, molecular electronic devices that function as a conventional diode; **molecular switch**, molecular electronic devices that function as a conventional electronic switch; **molecular memory**, molecular electronic devices that function as a nonvolatile memory

REFERENCES

(1) Aviram, A.; Ratner, M. A. Molecular Rectifiers. *Chem. Phys. Lett.* **1974**, *29*, 277−283.

(2) Reed, M. A.; Zhou, C.; Muller, C. J.; Burgin, T. P.; Tour, J. M. Conductance of a Molecular Junction. *Science* **1997**, *278*, 252−254.

(3) Nitzan, A.; Ratner, M. A. Electron Transport in Molecular Wire Junctions. *Science* **2003**, *300*, 1384−1389.

(4) Collier, C. P.; Wong, E. W.; Belohradský, M.; Raymo, F. M.; Stoddart, J. F.; Kuekes, P. J.; Williams, R. S.; Heath, J. R. Electronically Configurable Molecular-Based Logic Gates. *Science* **1999**, *285*, 391−394.

(5) Love, J. C.; Estroff, L. A.; Kriebel, J. K.; Nuzzo, R. G.; Whitesides, G. M. Self-Assembled Monolayers of Thiolates on Metals as a Form of Nanotechnology. *Chem. Rev.* **2005**, *105*, 1103−1169.

(6) Metzger, R. M.; Chen, B.; Höpfner, U.; Lakshmikantham, M. V.; Vuillaume, D.; Kawai, T.; Wu, X.; Tachibana, H.; Hughes, T. V.; Sakurai, H.; et al. Unimolecular Electrical Rectification in Hexadecylquinolinium Tricyanoquinodimethanide. *J. Am. Chem. Soc.* **1997**, *119*, 10455−10466.

(7) Xiang, D.; Wang, X.; Jia, C.; Lee, T.; Guo, X. Molecular-Scale Electronics: from Concept to Function. *Chem. Rev.* **2016**, *116*, 4318−4440.

(8) Mann, B.; Kuhn, H. Tunneling through Fatty Acid Salt Monolayers. *J. Appl. Phys.* **1971**, *42*, 4398−4405.

(9) Wold, D. J.; Frisbie, C. D. Formation of Metal-Molecule-Metal Tunnel Junctions: Microcontacts to Alkanethiol Monolayers with a Conducting AFM Tip. *J. Am. Chem. Soc.* **2000**, *122*, 2970−2971.

(10) Engelkes, V. B.; Beebe, J. M.; Frisbie, C. D. Length-Dependent Transport in Molecular Junctions Based on SAMs of Alkanethiols and Alkanedithiols: Effect of Metal Work Function and Applied Bias on Tunneling Efficiency and Contact Resistance. *J. Am. Chem. Soc.* **2004**, *126*, 14287−14296.

(11) Beebe, J. M.; Kim, B. S.; Frisbie, C. D.; Kushmerick, J. G. Measuring Relative Barrier Heights in Molecular Electronic Junctions with Transition Voltage Spectroscopy. *ACS Nano* **2008**, *2*, 827−832.

(12) Kaun, C. C.; Guo, H. Resistance of Alkanethiol Molecular Wires. *Nano Lett.* **2003**, *3*, 1521−1525.

(13) Porter, M. D.; Bright, T. B.; Allara, D. L.; Chidsey, C. E. D. Spontaneously Organized Molecular Assemblies. 4. Structural Characterization of n-Alkyl Thiol Monolayers on Gold by Optical

DOI: 10.1021/acsnano.7b02967
ACS Nano 2017, 11, 6511−6548

Ellipsometry, Infrared Spectroscopy, and Electrochemistry. *J. Am. Chem. Soc.* **1987**, *109*, 3559−3568.
(14) Vericat, C.; Vela, M. E.; Benitez, G. A.; Martin Gago, J. A.; Torrelles, X.; Salvarezza, R. C. Surface Characterization of Sulfur and Alkanethiol Self-Assembled Monolayers on Au(111). *J. Phys.: Condens. Matter* **2006**, *18*, R867−R900.
(15) Salomon, A.; Cahen, D.; Lindsay, S.; Tomfohr, J.; Engelkes, V. B.; Frisbie, C. D. Comparison of Electronic Transport Measurements on Organic Molecules. *Adv. Mater.* **2003**, *15*, 1881−1890.
(16) Tomfohr, J. K.; Sankey, O. F. Complex Band Structure, Decay Lengths, and Fermi Level Alignment in Simple Molecular Electronic Systems. *Phys. Rev. B: Condens. Matter Mater. Phys.* **2002**, *65*, 245105.
(17) Kim, Y.; Hellmuth, T. J.; Sysoiev, D.; Pauly, F.; Pietsch, T.; Wolf, J.; Erbe, A.; Huhn, T.; Groth, U.; Steiner, U. E.; et al. Charge Transport Characteristics of Diarylethene Photoswitching Single-Molecule Junctions. *Nano Lett.* **2012**, *12*, 3736−3742.
(18) McCreery, R. L.; Wu, J.; Prasad Kalakodimi, R. Electron Transport and Redox Reactions in Carbon-Based Molecular Electronic Junctions. *Phys. Chem. Chem. Phys.* **2006**, *8*, 2572−2590.
(19) McCreery, R. L.; Dieringer, J.; Solak, A. O.; Snyder, B.; Nowak, A. M.; McGovern, W. R.; DuVall, S. Molecular Rectification and Conductance Switching in Carbon-Based Molecular Junctions by Structural Rearrangement Accompanying Electron Injection. *J. Am. Chem. Soc.* **2003**, *125*, 10748−10758.
(20) Gorman, C. B.; Carroll, R. L.; Fuierer, R. R. Negative Differential Resistance in Patterned Electroactive Self-Assembled Monolayers. *Langmuir* **2001**, *17*, 6923−6930.
(21) Russew, M. M.; Hecht, S. Photoswitches: from Molecules to Materials. *Adv. Mater.* **2010**, *22*, 3348−3360.
(22) Jung, U.; Filinova, O.; Kuhn, S.; Zargarani, D.; Bornholdt, C.; Herges, R.; Magnussen, O. Photoswitching Behavior of Azobenzene-Containing Alkanethiol Self-Assembled Monolayers on Au Surfaces. *Langmuir* **2010**, *26*, 13913−13923.
(23) Derosa, P. A.; Guda, S.; Seminario, J. M. A Programmable Molecular Diode Driven by Charge-Induced Conformational Changes. *J. Am. Chem. Soc.* **2003**, *125*, 14240−14241.
(24) Kronemeijer, A. J.; Akkerman, H. B.; Kudernac, T.; van Wees, B. J.; Feringa, B. L.; Blom, P. W. M.; De Boer, B. Reversible Conductance Switching in Molecular Devices. *Adv. Mater.* **2008**, *20*, 1467−1473.
(25) Haick, H.; Cahen, D. Contacting Organic Molecules by Soft Methods: Towards Molecule-Based Electronic Devices. *Acc. Chem. Res.* **2008**, *41*, 359−366.
(26) Akkerman, H. B.; de Boer, B. Electrical Conduction through Single Molecules and Self-Assembled Monolayers. *J. Phys.: Condens. Matter* **2008**, *20*, 013001.
(27) Wang, G.; Kim, T. W.; Lee, T. Electrical Transport Characteristics through Molecular Layers. *J. Mater. Chem.* **2011**, *21*, 18117−18136.
(28) Ulgut, B.; Abruña, H. D. Electron Transfer through Molecules and Assemblies at Electrode Surfaces. *Chem. Rev.* **2008**, *108*, 2721−2736.
(29) Xiang, D.; Jeong, H.; Lee, T.; Mayer, D. Mechanically Controllable Break Junctions for Molecular Electronics. *Adv. Mater.* **2013**, *25*, 4845−4867.
(30) Son, J. Y.; Song, H. Molecular Scale Electronic Devices Using Single Molecules and Molecular Monolayers. *Curr. Appl. Phys.* **2013**, *13*, 1157−1171.
(31) McCreery, R. L.; Bergren, A. J. Progress with Molecular Electronic Junctions: Meeting Experimental Challenges in Design and Fabrication. *Adv. Mater.* **2009**, *21*, 4303−4322.
(32) Song, H.; Reed, M. A.; Lee, T. Single Molecule Electronic Devices. *Adv. Mater.* **2011**, *23*, 1583−1608.
(33) Zhang, J.; Kuznetsov, A. M.; Medvedev, I. G.; Chi, Q.; Albrecht, T.; Jensen, P. S.; Ulstrup, J. Single-Molecule Electron Transfer in Electrochemical Environments. *Chem. Rev.* **2008**, *108*, 2737−2791.
(34) Sun, L.; Diaz-Fernandez, Y. A.; Gschneidtner, T. A.; Westerlund, F.; Lara-Avila, S.; Moth-Poulsen, K. Single-Molecule Electronics: from Chemical Design to Functional Devices. *Chem. Soc. Rev.* **2014**, *43*, 7378−7411.
(35) Zhou, C.; Deshpande, M. R.; Reed, M. A.; Jones, L.; Tour, J. M. Nanoscale Metal Self-Assembled Monolayer Metal Heterostructures. *Appl. Phys. Lett.* **1997**, *71*, 611−613.
(36) Chen, J.; Reed, M. A.; Rawlett, A. M.; Tour, J. M. Large on-off Ratios and Negative Differential Resistance in a Molecular Electronic Device. *Science* **1999**, *286*, 1550−1552.
(37) Majumdar, N.; Gergel, N.; Routenberg, D.; Bean, J. C.; Harriott, L. R.; Li, B.; Pu, L.; Yao, Y.; Tour, J. M. Nanowell Device for the Electrical Characterization of Metal-Molecule-Metal Junctions. *J. Vac. Sci. Technol., B: Microelectron. Process. Phenom.* **2005**, *23*, 1417−1421.
(38) Wang, W. Y.; Lee, T.; Reed, M. A. Mechanism of Electron Conduction in Self-Assembled Alkanethiol Monolayer Devices. *Phys. Rev. B: Condens. Matter Mater. Phys.* **2003**, *68*, 035416.
(39) Wang, W. Y.; Lee, T.; Reed, M. A. Electronic Transport in Self-Assembled Alkanethiol Monolayers. *Phys. E* **2003**, *19*, 117−125.
(40) Wang, W. Y.; Lee, T.; Kretzschmar, I.; Reed, M. A. Inelastic Electron Tunneling Spectroscopy of an Alkanedithiol Self-Assembled Monolayer. *Nano Lett.* **2004**, *4*, 643−646.
(41) Wang, W. Y.; Lee, T.; Reed, M. A. Electron Tunnelling in Self-Assembled Monolayers. *Rep. Prog. Phys.* **2005**, *68*, 523−544.
(42) Hwang, G. J.; Jeng, P. R.; Lien, C.; Chen, C. S.; Tsao, Y. S.; Hwang, H. S.; Xu, S. Q.; Hong, T. M.; Chou, Y. C. Field Effects on Electron Conduction through Self-Assembled Monolayers. *Appl. Phys. Lett.* **2006**, *89*, 133120.
(43) Wang, W.; Lee, T.; Kamdar, M.; Reed, M. A.; Stewart, M. P.; Hwang, J. J.; Tour, J. M. Electrical Characterization of Metal-Molecule-Silicon Junctions. *Superlattices Microstruct.* **2003**, *33*, 217−226.
(44) Song, H.; Lee, T.; Choi, N. J.; Lee, H. A Statistical Method for Determining Intrinsic Electronic Transport Properties of Self-Assembled Alkanethiol Monolayer Devices. *Appl. Phys. Lett.* **2007**, *91*, 253116.
(45) Kim, T. W.; Wang, G. N.; Lee, H.; Lee, T. Statistical Analysis of Electronic Properties of Alkanethiols in Metal-Molecule-Metal Junctions. *Nanotechnology* **2007**, *18*, 315204.
(46) Wang, G.; Kim, T. W.; Lee, H.; Lee, T. Influence of Metal-Molecule Contacts on Decay Coefficients and Specific Contact Resistances in Molecular Junctions. *Phys. Rev. B: Condens. Matter Mater. Phys.* **2007**, *76*, 205320.
(47) Kim, T. W.; Wang, G.; Lee, T. Statistical Analysis of Electronic Transport through Chemisorbed *versus* Physisorbed Alkanethiol Self-Assembled Monolayers. *IEEE Trans. Nanotechnol.* **2008**, *7*, 140−144.
(48) Wang, G.; Kim, T. W.; Jang, Y. H.; Lee, T. Effects of Metal-Molecule Contact and Molecular Structure on Molecular Electronic Conduction in Nonresonant Tunneling Regime: Alkyl *versus* Conjugated Molecules. *J. Phys. Chem. C* **2008**, *112*, 13010−13016.
(49) Fisher, G. L.; Walker, A. V.; Hooper, A. E.; Tighe, T. B.; Bahnck, K. B.; Skriba, H. T.; Reinard, M. D.; Haynie, B. C.; Opila, R. L.; Winograd, N.; et al. Bond Insertion, Complexation, and Penetration Pathways of Vapor-Deposited Aluminum Atoms with HO- and CH_3O-Terminated Organic Monolayers. *J. Am. Chem. Soc.* **2002**, *124*, 5528−5541.
(50) Haynie, B. C.; Walker, A. V.; Tighe, T. B.; Allara, D. L.; Winograd, N. Adventures in Molecular Electronics: How to Attach Wires to Molecules. *Appl. Surf. Sci.* **2003**, *203*, 433−436.
(51) de Boer, B.; Frank, M. M.; Chabal, Y. J.; Jiang, W. R.; Garfunkel, E.; Bao, Z. Metallic Contact Formation for Molecular Electronics: Interactions between Vapor-Deposited Metals and Self-Assembled Monolayers of Conjugated Mono- and Dithiols. *Langmuir* **2004**, *20*, 1539−1542.
(52) Walker, A. V.; Tighe, T. B.; Cabarcos, O. M.; Reinard, M. D.; Haynie, B. C.; Uppili, S.; Winograd, N.; Allara, D. L. The Dynamics of Noble Metal Atom Penetration through Methoxy-Terminated Alkanethiolate Monolayers. *J. Am. Chem. Soc.* **2004**, *126*, 3954−3963.
(53) Haick, H.; Ghabboun, J.; Cahen, D. Pd *versus* Au as Evaporated Metal Contacts to Molecules. *Appl. Phys. Lett.* **2005**, *86*, 042113.
(54) Haick, H.; Niitsoo, O.; Ghabboun, J.; Cahen, D. Electrical Contacts to Organic Molecular Films by Metal Evaporation: Effect of Contacting Details. *J. Phys. Chem. C* **2007**, *111*, 2318−2329.

DOI: 10.1021/acsnano.7b02967
ACS Nano 2017, 11, 6511−6548

(55) Xu, T.; Morris, T. A.; Szulczewski, G. J.; Metzger, R. M.; Szablewski, M. Current-Voltage Characteristics of an LB Monolayer of Didecylammonium Tricyanoquinodimethanide Measured between Macroscopic Gold Electrodes. *J. Mater. Chem.* **2002**, *12*, 3167−3171.
(56) Bolotin, K. I.; Kuemmeth, F.; Pasupathy, A. N.; Ralph, D. C. Metal-Nanoparticle Single-Electron Transistors Fabricated Using Electromigration. *Appl. Phys. Lett.* **2004**, *84*, 3154−3156.
(57) Amlani, I.; Rawlett, A. M.; Nagahara, L. A.; Tsui, R. K. An Approach to Transport Measurements of Electronic Molecules. *Appl. Phys. Lett.* **2002**, *80*, 2761−2763.
(58) Chu, C. W.; Na, J. S.; Parsons, G. N. Conductivity in Alkylamine/Gold and Alkanethiol/Gold Molecular Junctions Measured in Molecule/Nanoparticle/Molecule Bridges and Conducting Probe Structures. *J. Am. Chem. Soc.* **2007**, *129*, 2287−2296.
(59) Long, D. P.; Patterson, C. H.; Moore, M. H.; Seferos, D. S.; Bazan, G. C.; Kushmerick, J. G. Magnetic Directed Assembly of Molecular Junctions. *Appl. Phys. Lett.* **2005**, *86*, 153105.
(60) Long, D. P.; Lazorcik, J. L.; Mantooth, B. A.; Moore, M. H.; Ratner, M. A.; Troisi, A.; Yao, Y.; Ciszek, J. W.; Tour, J. M.; Shashidhar, R. Effects of Hydration on Molecular Junction Transport. *Nat. Mater.* **2006**, *5*, 901−908.
(61) Kushmerick, J. G.; Allara, D. L.; Mallouk, T. E.; Mayer, T. S. Electrical and Spectroscopic Characterization of Molecular Junctions. *MRS Bull.* **2004**, *29*, 396−402.
(62) Kushmerick, J. G.; Holt, D. B.; Pollack, S. K.; Ratner, M. A.; Yang, J. C.; Schull, T. L.; Naciri, J.; Moore, M. H.; Shashidhar, R. Effect of Bond-Length Alternation in Molecular Wires. *J. Am. Chem. Soc.* **2002**, *124*, 10654−10655.
(63) Kushmerick, J. G.; Holt, D. B.; Yang, J. C.; Naciri, J.; Moore, M. H.; Shashidhar, R. Metal-Molecule Contacts and Charge Transport across Monomolecular Layers: Measurement and Theory. *Phys. Rev. Lett.* **2002**, *89*, 086802.
(64) Kushmerick, J. G.; Naciri, J.; Yang, J. C.; Shashidhar, R. Conductance Scaling of Molecular Wires in Parallel. *Nano Lett.* **2003**, *3*, 897−900.
(65) Kushmerick, J. G.; Whitaker, C. M.; Pollack, S. K.; Schull, T. L.; Shashidhar, R. Tuning Current Rectification across Molecular Junctions. *Nanotechnology* **2004**, *15*, S489−S493.
(66) Beebe, J. M.; Kim, B.; Gadzuk, J. W.; Frisbie, C. D.; Kushmerick, J. G. Transition from Direct Tunneling to Field Emission in Metal-Molecule-Metal Junctions. *Phys. Rev. Lett.* **2006**, *97*, 026801.
(67) Beebe, J. M.; Kushmerick, J. G. Nanoscale Switch Elements from Self-Assembled Monolayers on Silver. *Appl. Phys. Lett.* **2007**, *90*, 083117.
(68) Blum, A. S.; Kushmerick, J. G.; Pollack, S. K.; Yang, J. C.; Moore, M.; Naciri, J.; Shashidhar, R.; Ratna, B. R. Charge Transport and Scaling in Molecular Wires. *J. Phys. Chem. B* **2004**, *108*, 18124−18128.
(69) Race, H. H.; Reynolds, S. I. Electrical Properties of Multimolecular Films. *J. Am. Chem. Soc.* **1939**, *61*, 1425−1432.
(70) Slowinski, K.; Chamberlain, R. V.; Miller, C. J.; Majda, M. Through-Bond and Chain-to-Chain Coupling. Two Pathways in Electron Tunneling through Liquid Alkanethiol Monolayers on Mercury Electrodes. *J. Am. Chem. Soc.* **1997**, *119*, 11910−11919.
(71) Rampi, M. A.; Schueller, O. J. A.; Whitesides, G. M. Alkanethiol Self-Assembled Monolayers as the Dielectric of Capacitors with Nanoscale Thickness. *Appl. Phys. Lett.* **1998**, *72*, 1781−1783.
(72) Haag, R.; Rampi, M. A.; Holmlin, R. E.; Whitesides, G. M. Electrical Breakdown of Aliphatic and Aromatic Self-Assembled Monolayers Used as Nanometer-Thick Organic Dielectrics. *J. Am. Chem. Soc.* **1999**, *121*, 7895−7906.
(73) Slowinski, K.; Fong, H. K. Y.; Majda, M. Mercury-Mercury Tunneling Junctions. 1. Electron Tunneling across Symmetric and Asymmetric Alkanethiolate Bilayers. *J. Am. Chem. Soc.* **1999**, *121*, 7257−7261.
(74) Holmlin, R. E.; Haag, R.; Chabinyc, M. L.; Ismagilov, R. F.; Cohen, A. E.; Terfort, A.; Rampi, M. A.; Whitesides, G. M. Electron Transport through Thin Organic Films in Metal-Insulator-Metal Junctions Based on Self-Assembled Monolayers. *J. Am. Chem. Soc.* **2001**, *123*, 5075−5085.
(75) Chabinyc, M. L.; Chen, X. X.; Holmlin, R. E.; Jacobs, H.; Skulason, H.; Frisbie, C. D.; Mujica, V.; Ratner, M. A.; Rampi, M. A.; Whitesides, G. M. Molecular Rectification in a Metal-Insulator-Metal Junction Based on Self-Assembled Monolayers. *J. Am. Chem. Soc.* **2002**, *124*, 11730−11736.
(76) Rampi, M. A.; Whitesides, G. M. A Versatile Experimental Approach for Understanding Electron Transport through Organic Materials. *Chem. Phys.* **2002**, *281*, 373−391.
(77) Grave, C.; Tran, E.; Samori, P.; Whitesides, G. M.; Rampi, M. A. Correlating Electrical Properties and Molecular Structure of SAMs Organized between Two Metal Surfaces. *Synth. Met.* **2004**, *147*, 11−18.
(78) Duati, M.; Grave, C.; Tcbeborateva, N.; Wu, J. S.; Mullen, K.; Shaporenko, A.; Zharnikov, M.; Kriebel, J. K.; Whitesides, G. M.; Rampi, M. A. Electron Transport across Hexa-Peri-Hexabenzocoronene Units in a Metal-Self-Assembled Monolayer-Metal Junction. *Adv. Mater.* **2006**, *18*, 329−333.
(79) Yaffe, O.; Scheres, L.; Puniredd, S. R.; Stein, N.; Biller, A.; Lavan, R. H.; Shpaisman, H.; Zuilhof, H.; Haick, H.; Cahen, D.; et al. Molecular Electronics at Metal/Semiconductor Junctions. Si Inversion by Sub-Nanometer Molecular Films. *Nano Lett.* **2009**, *9*, 2390−2394.
(80) Weiss, E. A.; Chiechi, R. C.; Kaufman, G. K.; Kriebel, J. K.; Li, Z. F.; Duati, M.; Rampi, M. A.; Whitesides, G. M. Influence of Defects on the Electrical Characteristics of Mercury-Drop Junctions: Self-Assembled Monolayers of n-Alkanethiolates on Rough and Smooth Silver. *J. Am. Chem. Soc.* **2007**, *129*, 4336−4349.
(81) Chiechi, R. C.; Weiss, E. A.; Dickey, M. D.; Whitesides, G. M. Eutectic Gallium-Indium (EGaIn): a Moldable Liquid Metal for Electrical Characterization of Self-Assembled Monolayers. *Angew. Chem., Int. Ed.* **2008**, *47*, 142−144.
(82) Ghosh, S.; Halimun, H.; Mahapatro, A. K.; Choi, J.; Lodha, S.; Janes, D. Device Structure for Electronic Transport through Individual Molecules Using Nanoelectrodes. *Appl. Phys. Lett.* **2005**, *87*, 233509.
(83) Sordan, R.; Balasubramanian, K.; Burghard, M.; Kern, K. Coulomb Blockade Phenomena in Electromigration Break Junctions. *Appl. Phys. Lett.* **2005**, *87*, 013106.
(84) Trouwborst, M. L.; van der Molen, S. J.; van Wees, B. J. The Role of Joule Heating in the Formation of Nanogaps by Electromigration. *J. Appl. Phys.* **2006**, *99*, 114316.
(85) Heersche, H. B.; Lientschnig, G.; O'Neill, K.; van der Zant, H. S. J. *in situ* Imaging of Electromigration-Induced Nanogap Formation by Transmission Electron Microscopy. *Appl. Phys. Lett.* **2007**, *91*, 072107.
(86) Dickey, M. D.; Chiechi, R. C.; Larsen, R. J.; Weiss, E. A.; Weitz, D. A.; Whitesides, G. M. Eutectic Gallium-Indium (EGaIn): a Liquid Metal Alloy for the Formation of Stable Structures in Microchannels at Room Temperature. *Adv. Funct. Mater.* **2008**, *18*, 1097−1104.
(87) Thuo, M. M.; Reus, W. F.; Nijhuis, C. A.; Barber, J. R.; Kim, C.; Schulz, M. D.; Whitesides, G. M. Odd-Even Effects in Charge Transport across Self-Assembled Monolayers. *J. Am. Chem. Soc.* **2011**, *133*, 2962−2975.
(88) Cademartiri, L.; Thuo, M. M.; Nijhuis, C. A.; Reus, W. F.; Tricard, S.; Barber, J. R.; Sodhi, R. N. S.; Brodersen, P.; Kim, C.; Chiechi, R. C.; et al. Electrical Resistance of Ag^{TS}-$S(CH_2)_{n-1}CH_3$//Ga_2O_3/EGaln Tunneling Junctions. *J. Phys. Chem. C* **2012**, *116*, 10848−10860.
(89) Reus, W. F.; Thuo, M. M.; Shapiro, N. D.; Nijhuis, C. A.; Whitesides, G. M. The SAM, Not the Electrodes, Dominates Charge Transport in Metal-Monolayer//Ga_2O_3/Gallium-Indium Eutectic Junctions. *ACS Nano* **2012**, *6*, 4806−4822.
(90) Fracasso, D.; Valkenier, H.; Hummelen, J. C.; Solomon, G. C.; Chiechi, R. C. Evidence for Quantum Interference in SAMs of Arylethynylene Thiolates in Tunneling Junctions with Eutectic Ga-In (EGaIn) Top-Contacts. *J. Am. Chem. Soc.* **2011**, *133*, 9556−9563.
(91) Thuo, M. M.; Reus, W. F.; Simeone, F. C.; Kim, C.; Schulz, M. D.; Yoon, H. J.; Whitesides, G. M. Replacing -CH_2CH_2- with -CONH- Does Not Significantly Change Rates of Charge Transport through

DOI: 10.1021/acsnano.7b02967
ACS Nano 2017, 11, 6511−6548

Ag^{TS}-SAM//Ga_2O_3/EGaIn Junctions. *J. Am. Chem. Soc.* **2012**, *134*, 10876−10884.
(92) Yoon, H. J.; Shapiro, N. D.; Park, K. M.; Thuo, M. M.; Soh, S.; Whitesides, G. M. The Rate of Charge Tunneling through Self-Assembled Monolayers is Insensitive to Many Functional Group Substitutions. *Angew. Chem., Int. Ed.* **2012**, *51*, 4658−4661.
(93) Fracasso, D.; Muglali, M. I.; Rohwerder, M.; Terfort, A.; Chiechi, R. C. Influence of an Atom in EGaIn/ Ga_2O_3 Tunneling Junctions Comprising Self-Assembled Monolayers. *J. Phys. Chem. C* **2013**, *117*, 11367−11376.
(94) Nerngchamnong, N.; Yuan, L.; Qi, D. C.; Li, J.; Thompson, D.; Nijhuis, C. A. The Role of van der Waals Forces in the Performance of Molecular Diodes. *Nat. Nanotechnol.* **2013**, *8*, 113−118.
(95) Jiang, L.; Yuan, L.; Cao, L.; Nijhuis, C. A. Controlling Leakage Currents: The Role of the Binding Group and Purity of the Precursors for Self-Assembled Monolayers in the Performance of Molecular Diodes. *J. Am. Chem. Soc.* **2014**, *136*, 1982−1991.
(96) Yuan, L.; Jiang, L.; Zhang, B.; Nijhuis, C. A. Dependency of the Tunneling Decay Coefficient in Molecular Tunneling Junctions on the Topography of the Bottom Electrodes. *Angew. Chem., Int. Ed.* **2014**, *53*, 3377−3381.
(97) Krapchetov, D. A.; Ma, H.; Jen, A. K. Y.; Fischer, D. A.; Loo, Y. L. Solvent-Dependent Assembly of Terphenyl- and Quaterphenyldithiol on Gold and Gallium Arsenide. *Langmuir* **2005**, *21*, 5887−5893.
(98) Wan, A.; Jiang, L.; Sangeeth, C. S. S.; Nijhuis, C. A. Reversible Soft Top-Contacts to Yield Molecular Junctions with Precise and Reproducible Electrical Characteristics. *Adv. Funct. Mater.* **2014**, *24*, 4442−4456.
(99) Mbindyo, J. K. N.; Mallouk, T. E.; Mattzela, J. B.; Kratochvilova, I.; Razavi, B.; Jackson, T. N.; Mayer, T. S. Template Synthesis of Metal Nanowires Containing Monolayer Molecular Junctions. *J. Am. Chem. Soc.* **2002**, *124*, 4020−4026.
(100) Akkerman, H. B.; Blom, P. W. M.; de Leeuw, D. M.; de Boer, B. Towards Molecular Electronics with Large-Area Molecular Junctions. *Nature* **2006**, *441*, 69−72.
(101) Neuhausen, A. B.; Hosseini, A.; Sulpizio, J. A.; Chidsey, C. E. D.; Goldhaber-Gordon, D. Molecular Junctions of Self-Assembled Monolayers with Conducting Polymer Contacts. *ACS Nano* **2012**, *6*, 9920−9931.
(102) Wang, G.; Kim, Y.; Choe, M.; Kim, T. W.; Lee, T. A New Approach for Molecular Electronic Junctions with a Multilayer Graphene Electrode. *Adv. Mater.* **2011**, *23*, 755−760.
(103) Najarian, A. M.; Szeto, B.; Tefashe, U. M.; McCreery, R. L. Robust All-Carbon Molecular Junctions on Flexible or Semi-Transparent Substrates Using "Process-Friendly" Fabrication. *ACS Nano* **2016**, *10*, 8918−8928.
(104) Akkerman, H. B.; Naber, R. C. G.; Jongbloed, B.; van Hal, P. A.; Blom, P. W. M.; de Leeuw, D. M.; de Boer, B. Electron Tunneling through Alkanedithiol Self-Assembled Monolayers in Large-Area Molecular Junctions. *Proc. Natl. Acad. Sci. U. S. A.* **2007**, *104*, 11161−11166.
(105) Akkerman, H. B.; Kronemeijer, A. J.; van Hal, P. A.; de Leeuw, D. M.; Blom, P. W. M.; de Boer, B. Self-Assembled-Monolayer Formation of Long Alkanedithiols in Molecular Junctions. *Small* **2008**, *4*, 100−104.
(106) van Hal, P. A.; Smits, E. C. P.; Geuns, T. C. T.; Akkerman, H. B.; De Brito, B. C.; Perissinotto, S.; Lanzani, G.; Kronemeijer, A. J.; Geskin, V.; Cornil, J.; et al. Upscaling, Integration and Electrical Characterization of Molecular Junctions. *Nat. Nanotechnol.* **2008**, *3*, 749−754.
(107) Jeong, H.; Kim, D.; Wang, G.; Park, S.; Lee, H.; Cho, K.; Hwang, W. T.; Yoon, M. H.; Jang, Y. H.; Song, H.; et al. Redox-Induced Asymmetric Electrical Characteristics of Ferrocene-Alkanethiolate Molecular Devices on Rigid and Flexible Substrates. *Adv. Funct. Mater.* **2014**, *24*, 2472−2480.
(108) Kim, D.; Jeong, H.; Lee, H.; Hwang, W. T.; Wolf, J.; Scheer, E.; Huhn, T.; Jeong, H.; Lee, T. Flexible Molecular-Scale Electronic Devices Composed of Diarylethene Photoswitching Molecules. *Adv. Mater.* **2014**, *26*, 3968−3973.
(109) Kim, D.; Jeong, H.; Hwang, W. T.; Jang, Y.; Sysoiev, D.; Scheer, E.; Huhn, T.; Min, M.; Lee, H.; Lee, T. Reversible Switching Phenomenon in Diarylethene Molecular Devices with Reduced Graphene Oxide Electrodes on Flexible Substrates. *Adv. Funct. Mater.* **2015**, *25*, 5918−5923.
(110) Jeong, H.; Jang, Y.; Kim, D.; Hwang, W. T.; Kim, J. W.; Lee, T. An in-Depth Study of Redox-Induced Conformational Changes in Charge Transport Characteristics of a Ferrocene-Alkanethiolate Molecular Electronic Junction: Temperature-Dependent Transition Voltage Spectroscopy Analysis. *J. Phys. Chem. C* **2016**, *120*, 3564−3572.
(111) Wang, G.; Yoo, H.; Na, S. I.; Kim, T. W.; Cho, B.; Kim, D. Y.; Lee, T. Electrical Conduction through Self-Assembled Monolayers in Molecular Junctions: Au/Molecules/Au *versus* Au/Molecule/PEDOT:PSS/Au. *Thin Solid Films* **2009**, *518*, 824−828.
(112) Pandolfo, A. G.; Hollenkamp, A. F. Carbon Properties and Their Role in Supercapacitors. *J. Power Sources* **2006**, *157*, 11−27.
(113) Frackowiak, E. Carbon Materials for Supercapacitor Application. *Phys. Chem. Chem. Phys.* **2007**, *9*, 1774−1785.
(114) Zhang, L. L.; Zhao, X. S. Carbon-Based Materials as Supercapacitor Electrodes. *Chem. Soc. Rev.* **2009**, *38*, 2520−2531.
(115) Geim, A. K.; Novoselov, K. S. The Rise of Graphene. *Nat. Mater.* **2007**, *6*, 183−191.
(116) Castro Neto, A. H.; Guinea, F.; Peres, N. M. R.; Novoselov, K. S.; Geim, A. K. The Electronic Properties of Graphene. *Rev. Mod. Phys.* **2009**, *81*, 109−162.
(117) Huang, X.; Yin, Z. Y.; Wu, S. X.; Qi, X. Y.; He, Q. Y.; Zhang, Q. C.; Yan, Q. Y.; Boey, F.; Zhang, H. Graphene-Based Materials: Synthesis, Characterization, Properties, and Applications. *Small* **2011**, *7*, 1876−1902.
(118) Georgakilas, V.; Otyepka, M.; Bourlinos, A. B.; Chandra, V.; Kim, N.; Kemp, K. C.; Hobza, P.; Zboril, R.; Kim, K. S. Functionalization of Graphene: Covalent and Non-Covalent Approaches, Derivatives and Applications. *Chem. Rev.* **2012**, *112*, 6156−6214.
(119) Jang, Y.; Jeong, H.; Kim, D.; Hwang, W. T.; Kim, J. W.; Jeong, I.; Song, H.; Yoon, J.; Yi, G. C.; Jeong, H.; Lee, T. Electrical Characterization of Benzenedithiolate Molecular Electronic Devices with Graphene Electrodes on Rigid and Flexible Substrates. *Nanotechnology* **2016**, *27*, 145301.
(120) Seo, S.; Min, M.; Lee, J.; Lee, T.; Choi, S. Y.; Lee, H. Solution-Processed Reduced Graphene Oxide Films as Electronic Contacts for Molecular Monolayer Junctions. *Angew. Chem., Int. Ed.* **2012**, *51*, 108−112.
(121) Min, M.; Seo, S.; Lee, S. M.; Lee, H. Voltage-Controlled Nonvolatile Molecular Memory of an Azobenzene Monolayer through Solution-Processed Reduced Graphene Oxide Contacts. *Adv. Mater.* **2013**, *25*, 7045−7050.
(122) Park, S.; An, J. H.; Jung, I. W.; Piner, R. D.; An, S. J.; Li, X. S.; Velamakanni, A.; Ruoff, R. S. Colloidal Suspensions of Highly Reduced Graphene Oxide in a Wide Variety of Organic Solvents. *Nano Lett.* **2009**, *9*, 1593−1597.
(123) Zhu, Y. W.; Murali, S.; Cai, W. W.; Li, X. S.; Suk, J. W.; Potts, J. R.; Ruoff, R. S. Graphene and Graphene Oxide: Synthesis, Properties, and Applications. *Adv. Mater.* **2010**, *22*, 3906−3924.
(124) Skakalova, V.; Kaiser, A. B.; Dettlaff-Weglikowska, U.; Hrncarikova, K.; Roth, S. Effect of Chemical Treatment on Electrical Conductivity, Infrared Absorption, and Raman Spectra of Single-Walled Carbon Nanotubes. *J. Phys. Chem. B* **2005**, *109*, 7174−7181.
(125) Li, D.; Muller, M. B.; Gilje, S.; Kaner, R. B.; Wallace, G. G. Processable Aqueous Dispersions of Graphene Nanosheets. *Nat. Nanotechnol.* **2008**, *3*, 101−105.
(126) Mattevi, C.; Eda, G.; Agnoli, S.; Miller, S.; Mkhoyan, K. A.; Celik, O.; Mastrogiovanni, D.; Granozzi, G.; Garfunkel, E.; Chhowalla, M. Evolution of Electrical, Chemical, and Structural Properties of Transparent and Conducting Chemically Derived Graphene Thin Films. *Adv. Funct. Mater.* **2009**, *19*, 2577−2583.

DOI: 10.1021/acsnano.7b02967
ACS Nano 2017, 11, 6511−6548

(127) Eda, G.; Chhowalla, M. Chemically Derived Graphene Oxide: Towards Large-Area Thin-Film Electronics and Optoelectronics. *Adv. Mater.* **2010**, *22*, 2392−2415.
(128) Eda, G.; Chhowalla, M. Graphene-based Composite Thin Films for Electronics. *Nano Lett.* **2009**, *9*, 814−818.
(129) Moon, I. K.; Lee, J.; Ruoff, R. S.; Lee, H. Reduced Graphene Oxide by Chemical Graphitization. *Nat. Commun.* **2010**, *1*, 73.
(130) Yan, H. J.; Bergren, A. J.; McCreery, R. L. All-Carbon Molecular Tunnel Junctions. *J. Am. Chem. Soc.* **2011**, *133*, 19168−19177.
(131) Sayed, S. Y.; Bayat, A.; Kondratenko, M.; Leroux, Y.; Hapiot, P.; McCreery, R. L. Bilayer Molecular Electronics: All-Carbon Electronic Junctions Containing Molecular Bilayers Made with "Click" Chemistry. *J. Am. Chem. Soc.* **2013**, *135*, 12972−12975.
(132) Bayat, A.; Lacroix, J. C.; McCreery, R. L. Control of Electronic Symmetry and Rectification through Energy Level Variations in Bilayer Molecular Junctions. *J. Am. Chem. Soc.* **2016**, *138*, 12287−12296.
(133) Bergren, A. J.; Zeer-Wanklyn, L.; Semple, M.; Pekas, N.; Szeto, B.; McCreery, R. L. Musical Molecules: the Molecular Junction as an Active Component in Audio Distortion Circuits. *J. Phys.: Condens. Matter* **2016**, *28*, 094011.
(134) Ivashenko, O.; Bergren, A. J.; McCreery, R. L. Monitoring of Energy Conservation and Losses in Molecular Junctions through Characterization of Light Emission. *Adv. Electron. Mater.* **2016**, *2*, 1600351.
(135) Ivashenko, O.; Bergren, A. J.; McCreery, R. L. Light Emission as a Probe of Energy Losses in Molecular Junctions. *J. Am. Chem. Soc.* **2016**, *138*, 722−725.
(136) Ranganathan, S.; McCreery, R. L.; Majji, S. M.; Madou, M. Photoresist-Derived Carbon for Microelectromechanical Systems and Electrochemical Applications. *J. Electrochem. Soc.* **2000**, *147*, 277−282.
(137) Ranganathan, S.; McCreery, R. L. Electroanalytical Performance of Carbon Films with near-Atomic Flatness. *Anal. Chem.* **2001**, *73*, 893−900.
(138) Ranganathan, S.; Steidel, I.; Anariba, F.; McCreery, R. L. Covalently Bonded Organic Monolayers on a Carbon Substrate: a New Paradigm for Molecular Electronics. *Nano Lett.* **2001**, *1*, 491−494.
(139) Ru, J.; Szeto, B.; Bonifas, A.; McCreery, R. L. Microfabrication and Integration of Diazonium-Based Aromatic Molecular Junctions. *ACS Appl. Mater. Interfaces* **2010**, *2*, 3693−3701.
(140) Mattson, J. S.; Smith, C. A. Optically Transparent Carbon-Film Electrodes for Infrared Spectroelectrochemistry. *Anal. Chem.* **1975**, *47*, 1122−1125.
(141) Loo, Y. L.; Willett, R. L.; Baldwin, K. W.; Rogers, J. A. Additive, Nanoscale Patterning of Metal Films with a Stamp and a Surface Chemistry Mediated Transfer Process: Applications in Plastic Electronics. *Appl. Phys. Lett.* **2002**, *81*, 562−564.
(142) Loo, Y. L.; Lang, D. V.; Rogers, J. A.; Hsu, J. W. P. Electrical Contacts to Molecular Layers by Nanotransfer Printing. *Nano Lett.* **2003**, *3*, 913−917.
(143) Xia, Y. N.; Whitesides, G. M. Soft Lithography. *Angew. Chem., Int. Ed.* **1998**, *37*, 550−575.
(144) Gates, B. D.; Xu, Q. B.; Stewart, M.; Ryan, D.; Willson, C. G.; Whitesides, G. M. New Approaches to Nanofabrication: Molding, Printing, and Other Techniques. *Chem. Rev.* **2005**, *105*, 1171−1196.
(145) Cui, X. D.; Primak, A.; Zarate, X.; Tomfohr, J.; Sankey, O. F.; Moore, A. L.; Moore, T. A.; Gust, D.; Harris, G.; Lindsay, S. M. Reproducible Measurement of Single-Molecule Conductivity. *Science* **2001**, *294*, 571−574.
(146) Losic, D.; Shapter, J. G.; Gooding, J. J. Influence of Surface Topography on Alkanethiol SAMs Assembled from Solution and by Microcontact Printing. *Langmuir* **2001**, *17*, 3307−3316.
(147) Xu, B. Q.; Tao, N. J. Measurement of Single-Molecule Resistance by Repeated Formation of Molecular Junctions. *Science* **2003**, *301*, 1221−1223.
(148) Hallback, A. S.; Oncel, N.; Huskens, J.; Zandvliet, H. J. W.; Poelsema, B. Inelastic Electron Tunneling Spectroscopy on Decanethiol at Elevated Temoeratures. *Nano Lett.* **2004**, *4*, 2393−2395.
(149) Seminario, J. M.; Yan, L. M. *ab initio* Analysis of Electron Currents in Thioalkanes. *Int. J. Quantum Chem.* **2005**, *102*, 711−723.
(150) Coll, M.; Miller, L. H.; Richter, L. J.; Hines, D. R.; Jurchescu, O. D.; Gergel-Hackett, N.; Richter, C. A.; Hacker, C. A. Formation of Silicon-Based Molecular Electronic Structures Using Flip-Chip Lamination. *J. Am. Chem. Soc.* **2009**, *131*, 12451−12457.
(151) Shimizu, K. T.; Fabbri, J. D.; Jelincic, J. J.; Melosh, N. A. Soft Deposition of Large-Area Metal Contacts for Molecular Electronics. *Adv. Mater.* **2006**, *18*, 1499−1504.
(152) Jeong, H.; Hwang, W. T.; Kim, P.; Kim, D.; Jang, Y.; Min, M.; Xiang, D.; Song, H.; Park, Y. D.; Jeong, H.; et al. Investigation of Inelastic Electron Tunneling Spectra of Metal-Molecule-Metal Junctions Fabricated Using Direct Metal Transfer Method. *Appl. Phys. Lett.* **2015**, *106*, 063110.
(153) Jeong, H.; Kim, D.; Kim, P.; Cho, M. R.; Hwang, W. T.; Jang, Y.; Cho, K.; Min, M.; Xiang, D.; Park, Y. D.; et al. A New Approach for High-Yield Metal-Molecule-Metal Junctions by Direct Metal Transfer Method. *Nanotechnology* **2015**, *26*, 025601.
(154) Vilan, A.; Cahen, D. Soft Contact Deposition onto Molecularly Modified GaAs. Thin Metal Film Flotation: Principles and Electrical Effects. *Adv. Funct. Mater.* **2002**, *12*, 795−807.
(155) Nijhuis, C. A.; Reus, W. F.; Barber, J. R.; Dickey, M. D.; Whitesides, G. M. Charge Transport and Rectification in Arrays of SAM-Based Tunneling Junctions. *Nano Lett.* **2010**, *10*, 3611−3619.
(156) Nijhuis, C. A.; Reus, W. F.; Barber, J. R.; Whitesides, G. M. Comparison of SAM-Based Junctions with Ga_2O_3/EGaIn Top Electrodes to Other Large-Area Tunneling Junctions. *J. Phys. Chem. C* **2012**, *116*, 14139−14150.
(157) Wan, A.; Sangeeth, C. S. S.; Wang, L. J.; Yuan, L.; Jiang, L.; Nijhuis, C. A. Arrays of High Quality SAM-Based Junctions and Their Application in Molecular Diode Based Logic. *Nanoscale* **2015**, *7*, 19547−19556.
(158) McDonald, J. C.; Whitesides, G. M. Poly(Dimethylsiloxane) as a Material for Fabricating Microfluidic Devices. *Acc. Chem. Res.* **2002**, *35*, 491−499.
(159) Bonifas, A. P.; McCreery, R. L. 'Soft' Au, Pt and Cu Contacts for Molecular Junctions through Surface-Diffusion-Mediated Deposition. *Nat. Nanotechnol.* **2010**, *5*, 612−617.
(160) Bonifas, A. P.; McCreery, R. L. Assembling Molecular Electronic Junctions One Molecule at a Time. *Nano Lett.* **2011**, *11*, 4725−4729.
(161) Kim, Y.; Wang, G.; Choe, M.; Kim, J.; Lee, S.; Park, S.; Kim, D. Y.; Lee, B. H.; Lee, T. Electronic Properties Associated with Conformational Changes in Azobenzene-Derivative Molecular Junctions. *Org. Electron.* **2011**, *12*, 2144−2150.
(162) McCreery, R. L. Molecular Electronic Junctions. *Chem. Mater.* **2004**, *16*, 4477−4496.
(163) Lindsay, S. M.; Ratner, M. A. Molecular Transport Junctions: Clearing Mists. *Adv. Mater.* **2007**, *19*, 23−31.
(164) Paddonrow, M. N.; Shephard, M. J.; Jordan, K. D. Predicted Weak Distance Dependence of through-Bond Mediated Electronic Coupling in n-Alkane Bridges - an *ab initio* Molecular-Orbital Study. *J. Phys. Chem.* **1993**, *97*, 1743−1745.
(165) Simmons, J. G. Generalized Formula for Electric Tunnel Effect between Similar Electrodes Separated by a Thin Insulating Film. *J. Appl. Phys.* **1963**, *34*, 1793−1803.
(166) Simmons, J. G. Electric Tunnel Effect between Dissimilar Electrodes Separated by a Thin Insulating Film. *J. Appl. Phys.* **1963**, *34*, 2581−2590.
(167) Cygan, M. T.; Dunbar, T. D.; Arnold, J. J.; Bumm, L. A.; Shedlock, N. F.; Burgin, T. P.; Jones, L.; Allara, D. L.; Tour, J. M.; Weiss, P. S. Insertion, Conductivity, and Structures of Conjugated Organic Oligomers in Self-Assembled Alkanethiol Monolayers on Au{111}. *J. Am. Chem. Soc.* **1998**, *120*, 2721−2732.
(168) Kokkoli, E.; Zukoski, C. F. Effect of Solvents on Interactions between Hydrophobic Self-Assembled Monolayers. *J. Colloid Interface Sci.* **1999**, *209*, 60−65.

DOI: 10.1021/acsnano.7b02967
ACS Nano 2017, 11, 6511−6548

(169) Lee, T.; Wang, W. Y.; Klemic, J. F.; Zhang, J. J.; Su, J.; Reed, M. A. Comparison of Electronic Transport Characterization Methods for Alkanethiol Self-Assembled Monolayers. *J. Phys. Chem. B* **2004**, *108*, 8742−8750.
(170) Kafer, D.; Witte, G.; Cyganik, P.; Terfort, A.; Woll, C. A Comprehensive Study of Self-Assembled Monolayers of Anthracenethiol on Gold: Solvent Effects, Structure, and Stability. *J. Am. Chem. Soc.* **2006**, *128*, 1723−1732.
(171) Ssenyange, S.; Yan, H. J.; McCreery, R. L. Redox-Driven Conductance Switching *via* Filament Formation and Dissolution in Carbon/Molecule/TiO_2/Ag Molecular Electronic Junctions. *Langmuir* **2006**, *22*, 10689−10696.
(172) Nijhuis, C. A.; Reus, W. F.; Whitesides, G. M. Mechanism of Rectification in Tunneling Junctions Based on Molecules with Asymmetric Potential Drops. *J. Am. Chem. Soc.* **2010**, *132*, 18386−18401.
(173) Reus, W. F.; Nijhuis, C. A.; Barber, J. R.; Thuo, M. M.; Tricard, S.; Whitesides, G. M. Statistical Tools for Analyzing Measurements of Charge Transport. *J. Phys. Chem. C* **2012**, *116*, 6714−6733.
(174) Venkataraman, L.; Klare, J. E.; Tam, I. W.; Nuckolls, C.; Hybertsen, M. S.; Steigerwald, M. L. Single-Molecule Circuits with Well-Defined Molecular Conductance. *Nano Lett.* **2006**, *6*, 458−462.
(175) Wang, G.; Kim, Y.; Na, S. I.; Kahng, Y. H.; Ku, J.; Park, S.; Jang, Y. H.; Kim, D. Y.; Lee, T. Investigation of the Transition Voltage Spectra of Molecular Junctions Considering Frontier Molecular Orbitals and the Asymmetric Coupling Effect. *J. Phys. Chem. C* **2011**, *115*, 17979−17985.
(176) Guest, P. G. *Numerical Methods of Curve Fitting*; Cambridge University Press: Cambridge, 2012; pp 1−438.
(177) Chen, F.; Li, X. L.; Hihath, J.; Huang, Z. F.; Tao, N. J. Effect of Anchoring Groups on Single-Molecule Conductance: Comparative Study of Thiol-, Amine-, and Carboxylic-Acid-Terminated Molecules. *J. Am. Chem. Soc.* **2006**, *128*, 15874−15881.
(178) Nardes, A. M.; Kemerink, M.; Janssen, R. A. J. Anisotropic Hopping Conduction in Spin-Coated PEDOT:PSS Thin Films. *Phys. Rev. B: Condens. Matter Mater. Phys.* **2007**, *76*, 085208.
(179) Jeong, H.; Kim, D.; Kwon, H.; Hwang, W. T.; Jang, Y.; Min, M.; Char, K.; Xiang, D.; Jeong, H.; Lee, T. Statistical Investigation of the Length-Dependent Deviations in the Electrical Characteristics of Molecular Electronic Junctions Fabricated Using the Direct Metal Transfer Method. *J. Phys.: Condens. Matter* **2016**, *28*, 094003.
(180) Engelkes, V. B.; Beebe, J. M.; Frisbie, C. D. Analysis of the Causes of Variance in Resistance Measurements on Metal-Molecule-Metal Junctions Formed by Conducting-Probe Atomic Force Microscopy. *J. Phys. Chem. B* **2005**, *109*, 16801−16810.
(181) Hu, Y. B.; Zhu, Y.; Gao, H. J.; Guo, H. Conductance of an Ensemble of Molecular Wires: a Statistical Analysis. *Phys. Rev. Lett.* **2005**, *95*, 156803.
(182) Lortscher, E.; Weber, H. B.; Riel, H. Statistical Approach to Investigating Transport through Single Molecules. *Phys. Rev. Lett.* **2007**, *98*, 176807.
(183) Song, H.; Lee, T.; Choi, N. J.; Lee, H. Statistical Representation of Intrinsic Electronic Tunneling Characteristics through Alkyl Self-Assembled Monolayers in Nanowell Device Structures. *J. Vac. Sci. Technol., B: Microelectron. Nanometer Struct.-Process., Meas., Phenom.* **2008**, *26*, 904−908.
(184) Rudnicki, W. R.; Lesyng, B.; Harvey, S. C. Lagrangian Molecular-Dynamics Using Selected Conformational Degrees of Freedom, with Application to the Pseudorotation Dynamics of Furanose Rings. *Biopolymers* **1994**, *34*, 383−392.
(185) Hihath, J.; Tao, N. J. Electron-Phonon Interactions in Atomic and Molecular Devices. *Prog. Surf. Sci.* **2012**, *87*, 189−208.
(186) Okabayashi, N.; Paulsson, M.; Komeda, T. Inelastic Electron Tunneling Process for Alkanethiol Self-Assembled Monolayers. *Prog. Surf. Sci.* **2013**, *88*, 1−38.
(187) Bayman, A.; Hansma, P. K.; Kaska, W. C. Shifts and Dips in Inelastic-Electron-Tunneling Spectra Due to the Tunnel-Junction Environment. *Phys. Rev. B: Condens. Matter Mater. Phys.* **1981**, *24*, 2449−2455.
(188) Galperin, M.; Ratner, M. A.; Nitzan, A. Inelastic Electron Tunneling Spectroscopy in Molecular Junctions: Peaks and Dips. *J. Chem. Phys.* **2004**, *121*, 11965−11979.
(189) Yu, L. H.; Zangmeister, C. D.; Kushmerick, J. G. Origin of Discrepancies in Inelastic Electron Tunneling Spectra of Molecular Junctions. *Phys. Rev. Lett.* **2007**, *98*, 206803.
(190) Wang, W. Y.; Richter, C. A. Spin-Polarized Inelastic Electron Tunneling Spectroscopy of a Molecular Magnetic Tunnel Junction. *Appl. Phys. Lett.* **2006**, *89*, 153105.
(191) Taniguchi, M.; Tsutsui, M.; Yokota, K.; Kawai, T. Inelastic Electron Tunneling Spectroscopy of Single-Molecule Junctions Using a Mechanically Controllable Break Junction. *Nanotechnology* **2009**, *20*, 434008.
(192) Troisi, A.; Ratner, M. A. Inelastic Insights for Molecular Tunneling Pathways: Bypassing the Terminal Groups. *Phys. Chem. Chem. Phys.* **2007**, *9*, 2421−2427.
(193) Kim, Y.; Song, H.; Strigl, F.; Pernau, H. F.; Lee, T.; Scheer, E. Conductance and Vibrational States of Single-Molecule Junctions Controlled by Mechanical Stretching and Material Variation. *Phys. Rev. Lett.* **2011**, *106*, 196804.
(194) Lin, L. L.; Wang, C. K.; Luo, Y. Inelastic Electron Tunneling Spectroscopy of Gold-Benzenedithiol-Gold Junctions: Accurate Determination of Molecular Conformation. *ACS Nano* **2011**, *5*, 2257−2263.
(195) Mii, T.; Tikhodeev, S. G.; Ueba, H. Spectral Features of Inelastic Electron Transport *via* a Localized State. *Phys. Rev. B: Condens. Matter Mater. Phys.* **2003**, *68*, 205406.
(196) Persson, B. N. J.; Baratoff, A. Inelastic Electron-Tunneling from a Metal Tip - the Contribution from Resonant Processes. *Phys. Rev. Lett.* **1987**, *59*, 339−342.
(197) Sze, S. M.; Ng, K. K. *Physics of Semiconductor Devices*; John Wiley & Sons, Inc.: Hoboken, NJ, 2007; pp 1−832.
(198) Joachim, C.; Gimzewski, J. K.; Aviram, A. Electronics Using Hybrid-Molecular and Mono-Molecular Devices. *Nature* **2000**, *408*, 541−548.
(199) Ohara, M.; Kim, Y.; Yanagisawa, S.; Morikawa, Y.; Kawai, M. Role of Molecular Orbitals near the Fermi Level in the Excitation of Vibrational Modes of a Single Molecule at a Scanning Tunneling Microscope Junction. *Phys. Rev. Lett.* **2008**, *100*, 136104.
(200) Reed, M. A.; Lee, T. *Molecular Nanoelectronics*; American Scientific Publishers: Valencia, CA, 2003; pp 1−411.
(201) Choi, H.; Mody, C. C. M. The Long History of Molecular Electronics: Microelectronics Origins of Nanotechnology. *Soc. Stud. Sci.* **2009**, *39*, 11−50.
(202) Capozzi, B.; Xia, J.; Adak, O.; Dell, E. J.; Liu, Z. F.; Taylor, J. C.; Neaton, J. B.; Campos, L. M.; Venkataraman, L. Single-Molecule Diodes with High Rectification Ratios through Environmental Control. *Nat. Nanotechnol.* **2015**, *10*, 522−527.
(203) Kornilovitch, P. E.; Bratkovsky, A. M.; Williams, R. S. Current Rectification by Molecules with Asymmetric Tunneling Barriers. *Phys. Rev. B: Condens. Matter Mater. Phys.* **2002**, *66*, 165436.
(204) Zahid, F.; Ghosh, A. W.; Paulsson, M.; Polizzi, E.; Datta, S. Charging-Induced Asymmetry in Molecular Conductors. *Phys. Rev. B: Condens. Matter Mater. Phys.* **2004**, *70*, 1−5.
(205) Lörtscher, E.; Gotsmann, B.; Lee, Y.; Yu, L.; Rettner, C.; Riel, H. Transport Properties of a Single-Molecule Diode. *ACS Nano* **2012**, *6*, 4931−4939.
(206) Nijhuis, C. A.; Reus, W. F.; Siegel, A. C.; Whitesides, G. M. A Molecular Half-Wave Rectifier. *J. Am. Chem. Soc.* **2011**, *133*, 15397−15411.
(207) Yuan, L.; Jiang, L.; Thompson, D.; Nijhuis, C. A. On the Remarkable Role of Surface Topography of the Bottom Electrodes in Blocking Leakage Currents in Molecular Diodes. *J. Am. Chem. Soc.* **2014**, *136*, 6554−6557.
(208) Yuan, L.; Breuer, R.; Jiang, L.; Schmittel, M.; Nijhuis, C. A. A Molecular Diode with a Statistically Robust Rectification Ratio of Three Orders of Magnitude. *Nano Lett.* **2015**, *15*, 5506−5512.
(209) Ye, S.; Sato, Y.; Uosaki, K. Redox-Induced Orientation Change of a Self-Assembled Monolayer of 11-Ferrocenyl-1-Undecanethiol on a

DOI: 10.1021/acsnano.7b02967
ACS Nano 2017, 11, 6511−6548

Gold Electrode Studied by *in situ* FT-IRRAS. *Langmuir* **1997**, *13*, 3157−3161.
(210) Sayed, S. Y.; Fereiro, J. A.; Yan, H.; McCreery, R. L.; Bergren, A. J. Charge Transport in Molecular Electronic Junctions: Compression of the Molecular Tunnel Barrier in the Strong Coupling Regime. *Proc. Natl. Acad. Sci. U. S. A.* **2012**, *109*, 11498−11503.
(211) Krumbein, S. J. Metallic Electromigration Phenomena. *IEEE Trans. Compon., Hybrids, Manuf. Technol.* **1988**, *11*, 5−15.
(212) Pierce, D. G.; Brusius, P. G. Electromigration: a Review. *Microelectron. Reliab.* **1997**, *37*, 1053−1072.
(213) Weiss, E. A.; Kaufman, G. K.; Kriebel, J. K.; Li, Z.; Schalek, R.; Whitesides, G. M. Si/SiO_2-Templated Formation of Ultraflat Metal Surfaces on Glass, Polymer, and Solder Supports: Their Use as Substrates for Self-Assembled Monolayers. *Langmuir* **2007**, *23*, 9686−9694.
(214) Jiang, L.; Wang, T.; Nijhuis, C. A. Fabrication of Ultra-Flat Silver Surfaces with Sub-Micro-Meter Scale Grains. *Thin Solid Films* **2015**, *593*, 26−39.
(215) Floyd, T. L. *Digital Fundamentals*; Prentice-Hall International Inc.: Upper Saddle River, NJ, 2014; pp 1−912.
(216) Huang, Y.; Duan, X.; Cui, Y.; Lauhon, L. J.; Kim, K. H.; Lieber, C. M. Logic Gates and Computation from Assembled Nanowire Building Blocks. *Science* **2001**, *294*, 1313−1317.
(217) De Ruiter, G.; van der Boom, M. E. Surface-Confined Assemblies and Polymers for Molecular Logic. *Acc. Chem. Res.* **2011**, *44*, 563−573.
(218) Green, J. E.; Choi, J. W.; Boukai, A.; Bunimovich, Y.; Johnston-Halperin, E.; Deionno, E.; Luo, Y.; Sheriff, B. A.; Xu, K.; Shin, Y. S.; et al. A 160-Kilobit Molecular Electronic Memory Patterned at 10^{11} Bits Per Square Centimetre. *Nature* **2007**, *445*, 414−417.
(219) Lee, J.; Chang, H.; Kim, S.; Bang, G. S.; Lee, H. Molecular Monolayer Nonvolatile Memory with Tunable Molecules. *Angew. Chem., Int. Ed.* **2009**, *48*, 8501−8504.
(220) Seo, S.; Lee, J.; Choi, S. Y.; Lee, H. Multilevel Conductance Switching for a Monolayer of Redox-Active Metal Complexes through Various Metallic Contacts. *J. Mater. Chem.* **2012**, *22*, 1868−1875.
(221) Sanvito, S.; Rocha, A. R. Molecular-Spintronics: the Art of Driving Spin through Molecules. *J. Comput. Theor. Nanosci.* **2006**, *3*, 624−642.
(222) Sanvito, S. Molecular Spintronics. *Chem. Soc. Rev.* **2011**, *40*, 3336−3355.
(223) Dulić, D.; van der Molen, S. J.; Kudernac, T.; Jonkman, H. T.; De Jong, J. J. D.; Bowden, T. N.; van Esch, J.; Feringa, B. L.; van Wees, B. J. One-Way Optoelectronic Switching of Photochromic Molecules on Gold. *Phys. Rev. Lett.* **2003**, *91*, 207402.
(224) Katsonis, N.; Kudernac, T.; Walko, M.; van der Molen, S. J.; van Wees, B. J.; Feringa, B. L. Reversible Conductance Switching of Single Diarylethenes on a Gold Surface. *Adv. Mater.* **2006**, *18*, 1397−1400.
(225) Whalley, A. C.; Steigerwald, M. L.; Guo, X.; Nuckolls, C. Reversible Switching in Molecular Electronic Devices. *J. Am. Chem. Soc.* **2007**, *129*, 12590−12591.
(226) Mativetsky, J. M.; Pace, G.; Elbing, M.; Rampi, M. A.; Mayor, M.; Samorì, P. Azobenzenes as Light-Controlled Molecular Electronic Switches in Nanoscale Metal-Molecule-Metal Junctions. *J. Am. Chem. Soc.* **2008**, *130*, 9192−9193.
(227) Smaali, K.; Lenfant, S.; Karpe, S.; Oçafrain, M.; Blanchard, P.; Deresmes, D.; Godey, S.; Rochefort, A.; Roncali, J.; Vuillaume, D. High on-off Conductance Switching Ratio in Optically-Driven Self-Assembled Conjugated Molecular Systems. *ACS Nano* **2010**, *4*, 2411−2421.
(228) Jia, C.; Wang, J.; Yao, C.; Cao, Y.; Zhong, Y.; Liu, Z.; Liu, Z.; Guo, X. Conductance Switching and Mechanisms in Single-Molecule Junctions. *Angew. Chem., Int. Ed.* **2013**, *52*, 8666−8670.
(229) Seo, S.; Min, M.; Lee, S. M.; Lee, H. Photo-Switchable Molecular Monolayer Anchored between Highly Transparent and Flexible Graphene Electrodes. *Nat. Commun.* **2013**, *4*, 1920.
(230) Darwish, N.; Díez-Pérez, I.; Da Silva, P.; Tao, N.; Gooding, J. J.; Paddon-Row, M. N. Observation of Electrochemically Controlled Quantum Interference in a Single Anthraquinone-Based Norbornylogous Bridge Molecule. *Angew. Chem., Int. Ed.* **2012**, *51*, 3203−3206.
(231) Kay, N. J.; Higgins, S. J.; Jeppesen, J. O.; Leary, E.; Lycoops, J.; Ulstrup, J.; Nichols, R. J. Single-Molecule Electrochemical Gating in Ionic Liquids. *J. Am. Chem. Soc.* **2012**, *134*, 16817−16826.
(232) Henzl, J.; Mehlhorn, M.; Gawronski, H.; Rieder, K.; Morgenstern, K. Reversible *cis-trans* Isomerization of a Single Azobenzene Molecule. *Angew. Chem., Int. Ed.* **2006**, *45*, 603−606.
(233) Saremi, F.; Tieke, B. Photoinduced Switching in Self-Assembled Multilayers of an Azobenzene Bolaamphiphile and Polyelectrolytes. *Adv. Mater.* **1998**, *10*, 388−391.
(234) Liu, Y. C.; McCreery, R. L. Reactions of Organic Monolayers on Carbon Surfaces Observed with Unenhanced Raman Spectroscopy. *J. Am. Chem. Soc.* **1995**, *117*, 11254−11259.
(235) Bekyarova, E.; Itkis, M. E.; Ramesh, P.; Berger, C.; Sprinkle, M.; De Heer, W. A.; Haddon, R. C. Chemical Modification of Epitaxial Graphene: Spontaneous Grafting of Aryl Groups. *J. Am. Chem. Soc.* **2009**, *131*, 1336−1337.
(236) Browne, W. R.; De Jong, J. J. D.; Kudernac, T.; Walko, M.; Lucas, L. N.; Uchida, K.; van Esch, J. H.; Feringa, B. L. Oxidative Electrochemical Switching in Dithienylcyclopentenes, Part 1: Effect of Electronic Perturbation on the Efficiency and Direction of Molecular Switching. *Chem. - Eur. J.* **2005**, *11*, 6414−6429.
(237) Choi, B. Y.; Kahng, S. J.; Kim, S.; Kim, H.; Kim, H. W.; Song, Y. J.; Ihm, J.; Kuk, Y. Conformational Molecular Switch of the Azobenzene Molecule: a Scanning Tunneling Microscopy Study. *Phys. Rev. Lett.* **2006**, *96*, 156106.
(238) He, J.; Chen, F.; Liddell, P. A.; Andréasson, J.; Straight, S. D.; Gust, D.; Moore, T. A.; Moore, A. L.; Li, J.; Sankey, O. F.; et al. Switching of a Photochromic Molecule on Gold Electrodes: Single-Molecule Measurements. *Nanotechnology* **2005**, *16*, 695−702.
(239) Ikeda, M.; Tanifuji, N.; Yamaguchi, H.; Irie, M.; Matsuda, K. Photoswitching of Conductance of Diarylethene-Au Nanoparticle Network. *Chem. Commun.* **2007**, 1355−1357.
(240) Flood, A. H.; Stoddart, J. F.; Steuernnan, D. W.; Heath, J. R. Whence Molecular Electronics? *Science* **2004**, *306*, 2055−2056.
(241) Shipway, A. N.; Katz, E.; Willner, I. Molecular Memory and Processing Devices in Solution and on Surfaces. In *Molecular Machines and Motors*; Springer: Heidelberg, 2001; pp 237−281.
(242) Luo, Y.; Collier, C. P.; Jeppesen, J. O.; Nielsen, K. A.; DeIonno, E.; Ho, G.; Perkins, J.; Tseng, H. R.; Yamamoto, T.; Stoddart, J. F.; Heath, J. R. Two-Dimensional Molecular Electronics Circuits. *ChemPhysChem* **2002**, *3*, 519−525.
(243) Phoa, K.; Neaton, J. B.; Subramanian, V. First-Principles Studies of the Dynamics of [2]Rotaxane Molecular Switches. *Nano Lett.* **2009**, *9*, 3225−3229.
(244) Stan, M. R.; Franzon, P. D.; Goldstein, S. C.; Lach, J. C.; Ziegler, M. M. Molecular Electronics: from Devices and Interconnect to Circuits and Architecture. *Proc. IEEE* **2003**, *91*, 1940−1957.
(245) Lee, M. H.; Kim, Y. K.; Choi, Y. H. A Defect-Tolerant Memory Architecture for Molecular Electronics. *IEEE Trans. Nanotechnol.* **2004**, *3*, 152−157.
(246) DeHon, A.; Goldstein, S. C.; Kuekes, P. J.; Lincoln, P. Nonphotolithographic Nanoscale Memory Density Prospects. *IEEE Trans. Nanotechnol.* **2005**, *4*, 215−228.
(247) DeHon, A.; Naeimi, H. Seven Strategies for Tolerating Highly Defective Fabrication. *IEEE Des. Test.* **2005**, *22*, 306−315.
(248) Snider, G.; Kuekes, P.; Hogg, T.; Williams, R. S. Nano-electronic Architectures. *Appl. Phys. A: Mater. Sci. Process.* **2005**, *80*, 1183−1195.
(249) Pan, F.; Gao, S.; Chen, C.; Song, C.; Zeng, F. Recent Progress in Resistive Random Access Memories: Materials, Switching Mechanisms, and Performance. *Mater. Sci. Eng., R* **2014**, *83*, 1−59.
(250) Messer, B.; Song, J. H.; Yang, P. Microchannel Networks for Nanowire Patterning. *J. Am. Chem. Soc.* **2000**, *122*, 10232−10233.
(251) Martin, B. R.; Furnange, D. C.; Jackson, T. N.; Mallouk, T. E.; Mayer, T. S. Self-Alignment of Patterned Wafers Using Capillary Forces at a Water-Air Interface. *Adv. Funct. Mater.* **2001**, *11*, 381−386.

DOI: 10.1021/acsnano.7b02967
ACS Nano 2017, 11, 6511−6548

(252) Zhang, Y.; Chang, A.; Cao, J.; Wang, Q.; Kim, W.; Li, Y.; Morris, N.; Yenilmez, E.; Kong, J.; Dai, H. Electric-Field-Directed Growth of Aligned Single-Walled Carbon Nanotubes. *Appl. Phys. Lett.* **2001**, *79*, 3155−3157.
(253) Kuekes, P. J.; Williams, R. S. Demultiplexer for a Molecular Wire Crossbar Network, US Patent 6256767, July 3, 2001.
(254) Chen, Y.; Jung, G. Y.; Ohlberg, D. A. A.; Li, X.; Stewart, D. R.; Jeppesen, J. O.; Nielsen, K. A.; Stoddart, J. F.; Williams, R. S. Nanoscale Molecular-Switch Crossbar Circuits. *Nanotechnology* **2003**, *14*, 462−468.
(255) Alemani, M.; Peters, M. V.; Hecht, S.; Rieder, K. H.; Moresco, F.; Grill, L. Electric Field-Induced Isomerization of Azobenzene by STM. *J. Am. Chem. Soc.* **2006**, *128*, 14446−14447.
(256) Ferri, V.; Elbing, M.; Pace, G.; Dickey, M. D.; Zharnikov, M.; Samor, P.; Mayor, M.; Rampi, M. A. Light-Powered Electrical Switch Based on Cargo-Lifting Azobenzene Monolayers. *Angew. Chem., Int. Ed.* **2008**, *47*, 3407−3409.
(257) Min, M.; Bang, G. S.; Lee, H.; Yu, B. C. A Photoswitchable Methylene-Spaced Fluorinated Aryl Azobenzene Monolayer Grafted on Silicon. *Chem. Commun. (Cambridge, U. K.)* **2010**, *46*, 5232−5234.
(258) Mahapatro, A. K.; Ying, J.; Ren, T.; Janes, D. B. Electronic Transport through Ruthenium-Based Redox-Active Molecules in Metal-Molecule-Metal Nanogap Junctions. *Nano Lett.* **2008**, *8*, 2131−2136.
(259) Pradhan, B.; Das, S. Role of New Bis(2,2′-Bipyridyl)(Triazolopyridyl)Ruthenium(II) Complex in the Organic Bistable Memory Application. *Chem. Mater.* **2008**, *20*, 1209−1211.
(260) Seo, K.; Konchenko, A. V.; Lee, J.; Gyeong, S. B.; Lee, H. Molecular Conductance Switch-on of Single Ruthenium Complex Molecules. *J. Am. Chem. Soc.* **2008**, *130*, 2553−2559.
(261) Seo, K.; Konchenko, A. V.; Lee, J.; Bang, G. S.; Lee, H. Electron Transport Processes in on/off States of a Single Alkyl-Tailed Metal Complex Molecular Switch. *J. Mater. Chem.* **2009**, *19*, 7617−7624.
(262) Baghernejad, M.; Zhao, X.; Baruël Ørnsø, K.; Füeg, M.; Moreno-García, P.; Rudnev, A. V.; Kaliginedi, V.; Vesztergom, S.; Huang, C.; Hong, W.; et al. Electrochemical Control of Single-Molecule Conductance by Fermi-Level Tuning and Conjugation Switching. *J. Am. Chem. Soc.* **2014**, *136*, 17922−17925.
(263) Li, Z.; Li, H.; Chen, S.; Froehlich, T.; Yi, C.; Schönenberger, C.; Calame, M.; Decurtins, S.; Liu, S. X.; Borguet, E. Regulating a Benzodifuran Single Molecule Redox Switch *via* Electrochemical Gating and Optimization of Molecule/Electrode Coupling. *J. Am. Chem. Soc.* **2014**, *136*, 8867−8870.
(264) Behin-Aein, B.; Datta, D.; Salahuddin, S.; Datta, S. Proposal for an All-Spin Logic Device with Built-in Memory. *Nat. Nanotechnol.* **2010**, *5*, 266−270.
(265) Joo, N.; Renaudineau, S.; Delapierre, G.; Bidan, G.; Chamoreau, L. M.; Thouvenot, R.; Gouzerh, P.; Proust, A. Organosilyl/-Germyl Polyoxotungstate Hybrids for Covalent Grafting Onto Silicon Surfaces: Towards Molecular Memories. *Chem. - Eur. J.* **2010**, *16*, 5043−5051.
(266) Wassel, R. A.; Credo, G. M.; Fuierer, R. R.; Feldheim, D. L.; Gorman, C. B. Attenuating Negative Differential Resistance in an Electroactive Self-Assembled Monolayer-Based Junction. *J. Am. Chem. Soc.* **2004**, *126*, 295−300.
(267) He, J.; Fu, Q.; Lindsay, S.; Ciszek, J. W.; Tour, J. M. Electrochemical Origin of Voltage-Controlled Molecular Conductance Switching. *J. Am. Chem. Soc.* **2006**, *128*, 14828−14835.
(268) Kim, T. W.; Choi, H.; Oh, S. H.; Wang, G.; Kim, D. Y.; Hwang, H.; Lee, T. One Transistor-One Resistor Devices for Polymer Non-Volatile Memory Applications. *Adv. Mater.* **2009**, *21*, 2497−2500.
(269) Ji, Y.; Cho, B.; Song, S.; Kim, T. W.; Choe, M.; Kahng, Y. H.; Lee, T. Stable Switching Characteristics of Organic Nonvolatile Memory on a Bent Flexible Substrate. *Adv. Mater.* **2010**, *22*, 3071−3075.
(270) Kim, D. H.; Lu, N.; Ma, R.; Kim, Y. S.; Kim, R. H.; Wang, S.; Wu, J.; Won, S. M.; Tao, H.; Islam, A.; et al. Epidermal Electronics. *Science* **2011**, *333*, 838−843.
(271) Akinwande, D.; Petrone, N.; Hone, J. Two-Dimensional Flexible Nanoelectronics. *Nat. Commun.* **2014**, *5*, 5678.
(272) Gustafsson, G.; Cao, Y.; Treacy, G. M.; Klavetter, F.; Colaneri, N.; Heeger, A. J. Flexible Light-Emitting Diodes Made from Soluble Conducting Polymers. *Nature* **1992**, *357*, 477−479.
(273) Klauk, H.; Zschieschang, U.; Pflaum, J.; Halik, M. Ultralow-Power Organic Complementary Circuits. *Nature* **2007**, *445*, 745−748.
(274) Sekitani, T.; Zschieschang, U.; Klauk, H.; Someya, T. Flexible Organic Transistors and Circuits with Extreme Bending Stability. *Nat. Mater.* **2010**, *9*, 1015−1022.
(275) Kim, S. J.; Lee, J. S. Flexible Organic Transistor Memory Devices. *Nano Lett.* **2010**, *10*, 2884−2890.
(276) Sekitani, T.; Yokota, T.; Zschieschang, U.; Klauk, H.; Bauer, S.; Takeuchi, K.; Takamiya, M.; Sakurai, T.; Someya, T. Organic Nonvolatile Memory Transistors for Flexible Sensor Arrays. *Science* **2009**, *326*, 1516−1519.
(277) Mannsfeld, S. C. B.; Tee, B. C. K.; Stoltenberg, R. M.; Chen, C. V. H. H.; Barman, S.; Muir, B. V. O.; Sokolov, A. N.; Reese, C.; Bao, Z. Highly Sensitive Flexible Pressure Sensors with Microstructured Rubber Dielectric Layers. *Nat. Mater.* **2010**, *9*, 859−864.
(278) Gelinck, G. H.; Huitema, H. E. A.; Veenendaal, E. V.; Cantatore, E.; Schrijnemakers, L.; van der Putten, J. B. P. H.; Geuns, T. C. T.; Beenhakkers, M.; Giesbers, J. B.; Huisman, B. H.; et al. Flexible Active-Matrix Displays and Shift Registers Based on Solution-Processed Organic Transistors. *Nat. Mater.* **2004**, *3*, 106−110.
(279) Sekitani, T.; Nakajima, H.; Maeda, H.; Fukushima, T.; Aida, T.; Hata, K.; Someya, T. Stretchable Active-Matrix Organic Light-Emitting Diode Display Using Printable Elastic Conductors. *Nat. Mater.* **2009**, *8*, 494−499.
(280) Gomez De Arco, L.; Zhang, Y.; Schlenker, C. W.; Ryu, K.; Thompson, M. E.; Zhou, C. Continuous, Highly Flexible, and Transparent Graphene Films by Chemical Vapor Deposition for Organic Photovoltaics. *ACS Nano* **2010**, *4*, 2865−2873.
(281) Kim, D. H.; Viventi, J.; Amsden, J. J.; Xiao, J.; Vigeland, L.; Kim, Y. S.; Blanco, J. A.; Panilaitis, B.; Frechette, E. S.; Contreras, D.; et al. Dissolvable Films of Silk Fibroin for Ultrathin Conformal Bio-Integrated Electronics. *Nat. Mater.* **2010**, *9*, 511−517.
(282) Park, S.; Wang, G.; Cho, B.; Kim, Y.; Song, S.; Ji, Y.; Yoon, M. H.; Lee, T. Flexible Molecular-Scale Electronic Devices. *Nat. Nanotechnol.* **2012**, *7*, 438−442.
(283) Cairns, D. R.; Crawford, G. P. Electromechanical Properties of Transparent Conducting Substrates for Flexible Electronic Displays. *Proc. IEEE* **2005**, *93*, 1451−1458.
(284) Kim, K. S.; Zhao, Y.; Jang, H.; Lee, S. Y.; Kim, J. M.; Kim, K. S.; Ahn, J. H.; Kim, P.; Choi, J. Y.; Hong, B. H. Large-Scale Pattern Growth of Graphene Films for Stretchable Transparent Electrodes. *Nature* **2009**, *457*, 706−710.
(285) Eda, G.; Fanchini, G.; Chhowalla, M. Large-Area Ultrathin Films of Reduced Graphene Oxide as a Transparent and Flexible Electronic Material. *Nat. Nanotechnol.* **2008**, *3*, 270−274.
(286) Robertson, J. Diamond-like Amorphous Carbon. *Mater. Sci. Eng., R* **2002**, *37*, 129−282.
(287) Du, W.; Wang, T.; Chu, H. S.; Wu, L.; Liu, R.; Sun, S.; Phua, W. K.; Wang, L.; Tomczak, N.; Nijhuis, C. A. On-Chip Molecular Electronic Plasmon Sources Based on Self-Assembled Monolayer Tunnel Junctions. *Nat. Photonics* **2016**, *10*, 274−280.
(288) Wang, T.; Nijhuis, C. A. Molecular Electronic Plasmonics. *Appl. Mater. Today* **2016**, *3*, 73−86.
(289) Barnes, W. L.; Dereux, A.; Ebbesen, T. W. Surface Plasmon Subwavelength Optics. *Nature* **2003**, *424*, 824−830.
(290) Gramotnev, D. K.; Bozhevolnyi, S. I. Plasmonics beyond the Diffraction Limit. *Nat. Photonics* **2010**, *4*, 83−91.
(291) Koller, D. M.; Hohenau, A.; Ditlbacher, H.; Galler, N.; Reil, F.; Aussenegg, F. R.; Leitner, A.; List, E. J. W.; Krenn, J. R. Organic Plasmon-Emitting Diode. *Nat. Photonics* **2008**, *2*, 684−687.
(292) Fan, P.; Colombo, C.; Huang, K. C. Y.; Krogstrup, P.; Nygård, J.; Fontcuberta I Morral, A.; Brongersma, M. L. An Electrically-Driven GaAs Nanowire Surface Plasmon Source. *Nano Lett.* **2012**, *12*, 4943−4947.

DOI: 10.1021/acsnano.7b02967
ACS Nano 2017, 11, 6511−6548

(293) Huang, K. C. Y.; Seo, M. K.; Sarmiento, T.; Huo, Y.; Harris, J. S.; Brongersma, M. L. Electrically Driven Subwavelength Optical Nanocircuits. *Nat. Photonics* **2014**, *8*, 244−249.
(294) Lambe, J.; McCarthy, S. L. Light Emission from Inelastic Electron Tunneling. *Phys. Rev. Lett.* **1976**, *37*, 923−925.
(295) Dawson, P.; Walmsley, D. G.; Quinn, H. A.; Ferguson, A. J. L. Observation and Explanation of Light-Emission Spectra from Statistically Rough Cu, Ag, and Au Tunnel Junctions. *Phys. Rev. B: Condens. Matter Mater. Phys.* **1984**, *30*, 3164−3178.
(296) Ushioda, S. Light Emission Associated with Tunneling Phenomena. *J. Lumin.* **1990**, *47*, 131−136.
(297) Berndt, R.; Gimzewski, J. K.; Johansson, P. Inelastic Tunneling Excitation of Tip-Induced Plasmon Modes on Noble-Metal Surfaces. *Phys. Rev. Lett.* **1991**, *67*, 3796−3799.
(298) Moth-Poulsen, K.; Bjørnholm, T. Molecular Electronics with Single Molecules in Solid-State Devices. *Nat. Nanotechnol.* **2009**, *4*, 551−556.
(299) Shen, Q.; Guo, X.; Steigerwald, M. L.; Nuckolls, C. Integrating Reaction Chemistry into Molecular Electronic Devices. *Chem. - Asian J.* **2010**, *5*, 1040−1057.
(300) Aradhya, S. V.; Venkataraman, L. Single-Molecule Junctions beyond Electronic Transport. *Nat. Nanotechnol.* **2013**, *8*, 399−410.
(301) Xiao, X.; Xu, B.; Tao, N. Changes in the Conductance of Single Peptide Molecules upon Metal-Ion Binding. *Angew. Chem., Int. Ed.* **2004**, *43*, 6148−6152.
(302) Andringa, A. M.; Spijkman, M. J.; Smits, E. C. P.; Mathijssen, S. G. J.; van Hal, P. A.; Setayesh, S.; Willard, N. P.; Borshchev, O. V.; Ponomarenko, S. A.; Blom, P. W. M.; et al. Gas Sensing with Self-Assembled Monolayer Field-Effect Transistors. *Org. Electron.* **2010**, *11*, 895−898.
(303) Liu, S.; Zhang, X.; Luo, W.; Wang, Z.; Guo, X.; Steigerwald, M. L.; Fang, X. Single-Molecule Detection of Proteins Using Aptamer-Functionalized Molecular Electronic Devices. *Angew. Chem., Int. Ed.* **2011**, *50*, 2496−2502.
(304) Gao, L.; Li, L. L.; Wang, X.; Wu, P.; Cao, Y.; Liang, B.; Li, X.; Lin, Y.; Lu, Y.; Guo, X. Graphene-DNAzyme Junctions: a Platform for Direct Metal Ion Detection with Ultrahigh Sensitivity. *Chem. Sci.* **2015**, *6*, 2469−2473.
(305) Smits, E. C. P.; Mathijssen, S. G. J.; van Hal, P. A.; Setayesh, S.; Geuns, T. C. T.; Mutsaers, K. A. H. A.; Cantatore, E.; Wondergem, H. J.; Werzer, O.; Resel, R.; et al. Bottom-up Organic Integrated Circuits. *Nature* **2008**, *455*, 956−959.
(306) Mathijssen, S. G. J.; Smits, E. C. P.; van Hal, P. A.; Wondergem, H. J.; Ponomarenko, S. A.; Moser, A.; Resel, R.; Bobbert, P. A.; Kemerink, M.; Janssen, R. A. J.; et al. Monolayer Coverage and Channel Length Set the Mobility in Self-Assembled Monolayer Field-Effect Transistors. *Nat. Nanotechnol.* **2009**, *4*, 674−680.
(307) Jäger, C. M.; Schmaltz, T.; Novak, M.; Khassanov, A.; Vorobiev, A.; Hennemann, M.; Krause, A.; Dietrich, H.; Zahn, D.; Hirsch, A.; et al. Improving the Charge Transport in Self-Assembled Monolayer Field-Effect Transistors: from Theory to Devices. *J. Am. Chem. Soc.* **2013**, *135*, 4893−4900.
(308) Schmaltz, T.; Amin, A. Y.; Khassanov, A.; Meyer-Friedrichsen, T.; Steinrück, H. G.; Magerl, A.; Segura, J. J.; Voitchovsky, K.; Stellacci, F.; Halik, M. Low-Voltage Self-Assembled Monolayer Field-Effect Transistors on Flexible Substrates. *Adv. Mater.* **2013**, *25*, 4511−4514.
(309) Kim, W. Y.; Kim, K. S. Tuning Molecular Orbitals in Molecular Electronics and Spintronics. *Acc. Chem. Res.* **2010**, *43*, 111−120.
(310) Marquardt, C. W.; Grunder, S.; Błaszczyk, A.; Dehm, S.; Hennrich, F.; Löhneysen, H. V.; Mayor, M.; Krupke, R. Electroluminescence from a Single Nanotube-Molecule-Nanotube Junction. *Nat. Nanotechnol.* **2010**, *5*, 863−867.
(311) Seldenthuis, J. S.; van der Zant, H. S. J.; Ratner, M. A.; Thijssen, J. M. Electroluminescence Spectra in Weakly Coupled Single-Molecule Junctions. *Phys. Rev. B: Condens. Matter Mater. Phys.* **2010**, *81*, 205430.
(312) Reecht, G.; Scheurer, F.; Speisser, V.; Dappe, Y. J.; Mathevet, F.; Schull, G. Electroluminescence of a Polythiophene Molecular Wire Suspended between a Metallic Surface and the Tip of a Scanning Tunneling Microscope. *Phys. Rev. Lett.* **2014**, *112*, 047403.
(313) Chong, M. C.; Sosa-Vargas, L.; Bulou, H.; Boeglin, A.; Scheurer, F.; Mathevet, F.; Schull, G. Ordinary and Hot Electroluminescence from Single-Molecule Devices: Controlling the Emission Color by Chemical Engineering. *Nano Lett.* **2016**, *16*, 6480−6484.
(314) Cho, Y.; Kim, W. Y.; Kim, K. S. Effect of Electrodes on Electronic Transport of Molecular Electronic Devices. *J. Phys. Chem. A* **2009**, *113*, 4100−4104.
(315) Min, S. K.; Kim, W. Y.; Cho, Y.; Kim, K. S. Fast DNA Sequencing with a Graphene-Based Nanochannel Device. *Nat. Nanotechnol.* **2011**, *6*, 162−165.
(316) Rajan, A. C.; Rezapour, M. R.; Yun, J.; Cho, Y.; Cho, W. J.; Min, S. K.; Lee, G.; Kim, K. S. Two Dimensional Molecular Electronics Spectroscopy for Molecular Fingerprinting, DNA Sequencing, and Cancerous DNA Recognition. *ACS Nano* **2014**, *8*, 1827−1833.
(317) Sangeeth, C. S. S.; Wan, A.; Nijhuis, C. A. Equivalent Circuits of a Self-Assembled Monolayer-Based Tunnel Junction Determined by Impedance Spectroscopy. *J. Am. Chem. Soc.* **2014**, *136*, 11134−11144.
(318) Sangeeth, C. S. S.; Wan, A.; Nijhuis, C. A. Probing the Nature and Resistance of the Molecule-Electrode Contact in SAM-Based Junctions. *Nanoscale* **2015**, *7*, 12061−12067.
(319) Song, P.; Sangeeth, C. S. S.; Thompson, D.; Du, W.; Loh, K. P.; Nijhuis, C. A. Noncovalent Self-Assembled Monolayers on Graphene as a Highly Stable Platform for Molecular Tunnel Junctions. *Adv. Mater.* **2016**, *28*, 631−639.
(320) Trasobares, J.; Vuillaume, D.; Théron, D.; Clément, N. A 17 GHz Molecular Rectifier. *Nat. Commun.* **2016**, *7*, 12850.
(321) Qiu, X. H.; Nazin, G. V.; Hot, W. Vibrationally Resolved Fluorescence Excited with Submolecular Precision. *Science* **2003**, *299*, 542−546.
(322) Ballmann, S.; Härtle, R.; Coto, P. B.; Elbing, M.; Mayor, M.; Bryce, M. R.; Thoss, M.; Weber, H. B. Experimental Evidence for Quantum Interference and Vibrationally Induced Decoherence in Single-Molecule Junctions. *Phys. Rev. Lett.* **2012**, *109*, 056801.
(323) Kuhr, W. G. Integration of Molecular Components into Silicon Memory Devices. *Electrochem. Soc. Interface* **2004**, *13*, 34−38.

DOI: 10.1021/acsnano.7b02967
ACS Nano 2017, 11, 6511−6548